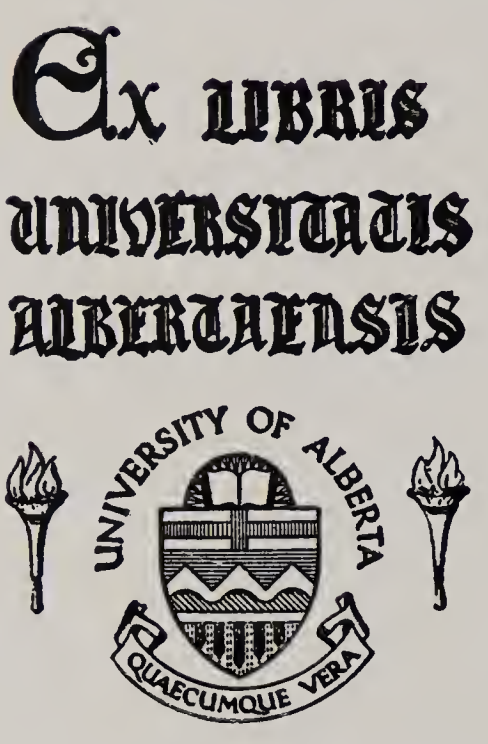

University of Alberta
Printing Department

UNIVERSITY OF ALBERTA
LIBRARY

Regulations Regarding Theses and Dissertations

Typescript copies of theses and dissertations for Master's and Doctor's degrees deposited in the University of Alberta Library, as the official Copy of the Faculty of Graduate Studies, may be consulted in the Reference Reading Room only.

A second copy is on deposit in the Department under whose supervision the work was done. Some Departments are willing to loan their copy to libraries, through the inter-library loan service of the University of Alberta Library.

These theses and dissertations are to be used only with due regard to the rights of the author. Written permission of the author and of the Department must be obtained through the University of Alberta Library when extended passages are copied. When permission has been granted, acknowledgement must appear in the published work.

This thesis or dissertation has been used in accordance with the above regulations by the persons listed below. The borrowing library is obligated to secure the signature of each user.

Please sign below:

Date	Signature	Institution

THE UNIVERSITY OF ALBERTA

STUDY OF THE LOW EXCITED STATES OF NA^{22} FROM THE REACTION $F^{19}(\alpha,n\gamma)$ NA^{22}

by

TOUSSAINT PAUL GEORGES CAROLA

A THESIS

SUBMITTED TO THE FACULTY OF GRADUATE STUDIES

IN PARTIAL FULFILMENT OF THE REQUIREMENTS FOR THE DEGREE

OF MASTER OF SCIENCE

DEPARTMENT OF PHYSICS

EDMONTON, ALBERTA

JUNE, 1965

THE UNIVERSITY OF ALBERTA

FACULTY OF GRADUATE STUDIES

The undersigned certify that they have read and recommend to the Faculty of Graduate Studies for acceptance a thesis entitled "STUDY OF THE LOW EXCITED STATES OF NA^{22} FROM THE REACTION $F^{19}(\alpha,n\gamma)$ NA^{22}", submitted by TOUSSAINT PAUL GEORGES CAROLA in partial fulfilment of the requirements for the degree of Master of Science.

Date: June 21st 1965

ABSTRACT

From the reaction $F^{19}(\alpha,n\gamma)Na^{22}$, the low excited states of Na^{22} have been studied using the method of triple angular correlations.

At a bombarding energy of 5.38 MeV, at which the yield of the radiation reaches a maximum, neutron gamma-ray correlation and gamma-ray distribution experiments were performed for the 587 kev and the 892 kev levels of Na^{22}. The beam-current was limited to a maximum value of 0.2 microamperes. Because of the low-coincidence counting rate, the investigation of the 1.532 MeV level has not been performed.

The previous probable assignment, 1^+, for the 892 kev level does not fit the experimental results which indicate rather a 2^+ assignment. The two unquantized parameters of the angular correlation formula have been measured. The population parameters ratio, $X^2 = \frac{P(1)}{P(0)}$, is 0.20 ± 0.20 and the quadrupole to dipole mixing ratio, δ is equal to 0.72 ± 0.31.

ACKNOWLEDGEMENTS

I am indebted to my supervisor, Dr. J. T. Sample, for suggesting this project and for his valuable guidance and helpful criticism throughout the experiment.

I would also like to thank Dr. W. C. Olsen for his assistance during the experiment, Dr. H. W. Taylor, Dr. K. Ramavataram and Dr. G. C. Neilson for many valuable discussions.

I wish to thank Dr. W. K. Dawson, W. G. Davies and T. B. Grandy who prepared the computer programs.

Special thanks are due to Mr. J. B. Elliott for operating the machine.

The technical assistance of Messrs. L. Holm, E. B. Cairns, C. F. Green and R. Gordon is greatly appreciated.

Thanks also to Mrs. P. Babet for her help in typing the manuscript.

En qualité d'étudiant étranger, je profite de cette occasion pour remercier tous ceux qui ont su m'apporter une aide fort appréciée, tant sur le plan universitaire que sur le plan humain.

TABLE OF CONTENTS

TABLE OF ILLUSTRATIONS

Page

LIST OF TABLES

CHAPTER I

1.1 Introduction

The knowledge of spectroscopic parameters like spin and parity of excited states or the multipole mixing ratio of decay radiation is very important for a better understanding of nuclear matter and more particularly of nuclear forces which are revealed indirectly through these parameters. Even-even nuclei have been investigated more and more in recent years, nuclear models describing these nuclei have been consequently refined and the matching between theoretical predictions and experimental results is improving. On the other hand, nuclei whose configuration is far from closed shells such as odd-odd nuclei are more difficult to compare with models proposed by the theoreticians. In a sense, this should excite the interest of experimentalists because some kind of "unified" model, allowing an understanding of all nuclear forces, may be expected when the amount of information garnered from all nuclei becomes sufficient.

The first aim of this experiment was to determine the spectroscopic parameters of the levels 892 kev and 1.532 Mev of Na^{22} from the reaction $F^{19}(\alpha, n\gamma)Na^{22}$ by the use of triple angular correlations as described by Litherland and Ferguson (Li 61). For reasons explained in detail later (section 2.2), the investigation of the 1.532 Mev state had to be given up.

The originality of the method proposed by Litherland and Ferguson lies in the fact that if a nuclear state is formed by absorption of unpolarized particles in the direction of the quantization axis followed by the emission of a second particle which is detected along this axis, then the magnetic quantum numbers of the substates which can be populated do not exceed the sum of the spins of the target nucleus and the incident and emergent particles.

In cases where the sum of spins does not exceed $\frac{1}{2}$, for instance in a reaction such as O^{18} $(\alpha, n\gamma)Ne^{21}$, the angular correlation of gamma rays emitted by deexcitation of Ne^{21*} is independent of the details of formation of the intermediate state and, for a given spin assignment, this angular correlation is a function of one parameter only, namely the multipole mixing ratio δ. Since angular correlation experiments generally yield the two values a_2/a_o and a_4/a_o, this is more than sufficient to determine unambiguously the spectroscopic parameters.

In a reaction such as F^{19} $(\alpha, n\gamma)Na^{22}$, the sum of spins is 1 and a second unquantized parameter is thus introduced in the angular correlation formulae, namely the ratio of two population parameters $P(1)/P(0)$. Since three parameters have to be determined now from experimental data, the analysis may not lead to a clear cut answer in some cases.

Moreover, because of the finite size of the neutron counter, higher magnetic substates can be populated as shown later and the chances of getting ambiguous results therefore increased.

Thus, before performing the experiment, it had to be borne in mind: first, that no theoretical graph of the possible angular correlation function could be plotted because of these two unquantized parameters; consequently, it would not be easy to evaluate the validity of the collected data; secondly, that it might not be possible to limit to one spin value only the assignment of the levels to be studied.

Actually, recent computing methods based on "χ^2 fitting programs", (some examples of which are given by Pronko (Pr 65)) allow these ambiguities to be removed, and it was known that as a last resort, it would be possible to have recourse to them.

1.2 TRIPLE ANGULAR CORRELATION

In the past few years, the theory of angular correlations has been simplified by the introduction of more powerful mathematical techniques and also by the tabulation of the coefficients involved in the calculation of the theoretical values.

This experiment shows one example of triple correlation as defined by Litherland and Ferguson (Li 61) (Li 64) and is so called because three directions are involved in the correlation: beam axis or axis of quantization (z-axis) and directions of the two different counters with respect to the beam axis.

After recalling briefly the general formalism of angular correlation theory, the theoretical formulae of triple angular correlation will be discussed and special application in the case of $F^{19}(\alpha, n\gamma)\ Na^{22}$ reaction will be introduced.

(a) General formalism of angular correlations for aligned nuclei.

Considering an electromagnetic radiation produced by deexcitation of an axially symmetric state with angular momentum a and emitted in the direction θ with respect to the quantization axis, the intensity of this radiation is given by:

$$W(\theta) = \text{trace } \underline{\rho}\,\underline{\epsilon} = \sum_{\substack{a \\ kn}} \rho_{kn}\, \epsilon_{kn} \qquad (2.1)$$

where $\underline{\rho}$ is the density matrix of the excited level and its elements are related to the population of the different magnetic sublevels.

$\underline{\epsilon}$ is an efficiency matrix so-called because it describes the actual efficiency of detection of the radiation in the direction θ.

Because the excited nucleus is considered here to be aligned (i.e., in an axially symmetric state) one can show that only the terms n = 0 are non vanishing and also that the density matrix is diagonal.

In many cases, it is better to deal with tensors rather than with matrices because tensors transform more simply than matrices under rotations. These tensors are related to the matrices by a general relationship which, for instance, in the case of density matrix yields the tensor parameters:

$$\rho_{kn}(a\ a') = \sum_{\alpha\ \alpha'} (-1)^{\alpha-\alpha'} (a\ a'\ \ \alpha-\alpha' \mid kn) \langle a\alpha \mid \rho \mid a'\alpha' \rangle \qquad (2.2)$$

where $(a\ a'\ \alpha\text{-}\alpha'\ |\ kn)$ is a Clebsch-Gordon coefficient. The notation used here is the notation of Devons and Goldfarb (De 57): the Greek letters represent the magnetic substates of the state tagged by the equivalent latin letter.

From the properties of the Clebsch-Gordon coefficients, it can be seen that:

$$|\ a - a'\ | \leqslant k \leqslant a + a'$$

and

$$n = \alpha - \alpha' \quad .$$

Devons and Goldfarb (De 57) show that, because of symmetry conditions, $n = 0$ is the only possible value; thus $\alpha = \alpha'$. Moreover, if the state has definite parity and if no polarization is present in the incident particle and target nucleus, the only non vanishing tensor parameters are those with $k = 0$ or k even. The eveness of k implies that the density matrix elements (population parameters) are equal for symmetrical magnetic sublevels; that is:

$$P(\alpha) = P(\alpha')$$

or $$< a\alpha\ |\ \rho\ |\ a'\alpha' > = <a\text{-}\alpha\ |\ \rho\ |\ a'\text{-}\alpha'> \qquad (2.3)$$

For each particular case, the angular correlation formulae may be derived by using, for instance, the properties of tensor products. An approximation introduced in the evaluation of the efficiency tensor parameters is to consider a plane wave propagating along the z-axis and detected by an ideal point detector. For a given angle θ, the rotation of the efficiency tensor is then performed and corrections for detectors of finite dimensions are made.

From an experimental point of view the angular correlation function is usually defined by:

$$W(\theta) = 1 + \frac{a_2}{a_o} P_2 (\cos \theta) + \frac{a_4}{a_o} P_4 (\cos \theta) + \ldots \quad (2.4)$$

In order to compute the different a coefficients by the method proposed by Litherland et al (Li 61), one has to calculate different coefficients tabulated by Sharp et al (Sh 61). By their structure these coefficients appear as products of different Clebsch-Gordon and Racah coefficients and a concrete example will be given in the case of the F^{19} $(\alpha n \gamma)$ Na^{22} reaction.

(b) Triple correlation.

As shown in the diagram hereafter, a particle of orbital angular momentum ℓ_1, and spin s_1, impinging on a

nucleus of spin a will create, when a reaction occurs, an intermediate state of spin b which will then deexcite by emission of a particle of orbital angular momentum ℓ_2 and spin s_2, feeding the magnetic sublevels of a state c which decays to the ground state by emission of an electromagnetic radiation of spins L_1, L_2 (when considering the usual case of two multipoles mixing).

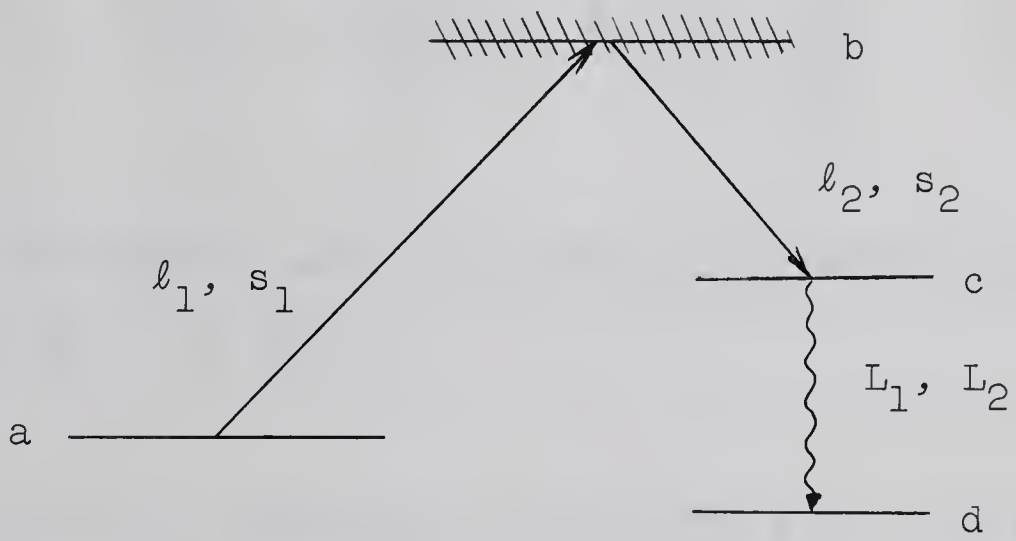

The counter detecting the emitted particle is placed at 0° or 180° with respect to the z-axis and is first assumed to be equivalent to an "ideal point detector." Then, strong limitations occur in the number of magnetic sublevels fed, as shown by Litherland (Li 61); because the orbital angular momenta of the incoming and outgoing particles are perpendicular to the z-axis, only the intrinsic spins of the various particles involved are contributing in population parameters.

The incoming and outgoing channel spins, respectively $\vec{S}_1$ and $\vec{S}_2$ are defined by:

$$\vec{S}_1 = \vec{a} + \vec{s}_1$$
$$\vec{S}_2 = \vec{c} + \vec{s}_2 \qquad (2.5)$$

The intermediate state although it has no sharp spin is determined by:

$$\vec{b} = \vec{S}_1 + \vec{\ell}_1 = \vec{S}_2 + \vec{\ell}_2 \qquad (2.6)$$

The density matrix for this intermediate state b is shown to be (Li 61):

$$\langle b\beta \mid \rho \mid b'\beta' \rangle = \sum_{\alpha\sigma_1} (a\ \alpha\ s_1\sigma_1 \mid S_1\ \beta)^2\ (S_1\ \beta\ \ell_1\ 0 \mid b\ \beta)$$
$$\times\ (S_1\beta\ell_1'0 \mid b'\ \beta)\ \langle a\alpha \mid \rho \mid a\alpha\rangle\ \langle s_1\sigma_1 \mid \rho \mid s_1\sigma_1\rangle$$
$$\langle \ell_1 0 \mid \rho \mid \ell_1'\ 0\rangle$$
$$\times\ \langle S_1\ \ell_1 \| V \| b\rangle^*\ \langle S_1\ell_1' \| V \| b'\rangle \qquad (2.7)$$

If the states are assumed to be unpolarized then:

$$\langle a\ \alpha \mid \rho \mid a\alpha \rangle = \frac{1}{a(a+1)} \tag{2.8}$$

$$\langle s_1 \sigma_1 \mid \rho \mid s_1 \sigma_1 \rangle = \frac{1}{s_1(s_1+1)} \tag{2.8'}$$

And by considering a plane wave propagating along the z-axis one can show that:

$$\langle \ell_1 0 \mid \rho \mid \ell_1' 0 \rangle = \frac{1}{\sqrt{\ell_1(\ell_1+1)}\ \sqrt{\ell_1'(\ell_1'+1)}} \tag{2.9}$$

The "double bar" or reduced matrix elements are introduced by the perturbing Hamiltonian in the description of the absorption causing the transition, as a perturbation.

From the properties of Clebsch Gordon coefficients, it is interesting to point out that:

$$\beta = \alpha + \sigma \tag{2.10}$$

Similarly the density matrix of the final state c is:

$$\langle c\gamma s_2\sigma_2\ell_2 0 \mid \rho \mid c\gamma s_2\sigma_2\ell'_2 0\rangle = \langle c\gamma \mid \rho \mid c\gamma\rangle \langle s_2\sigma_2 \mid \rho \mid s_2\sigma_2\rangle\langle \ell_2 0 \mid \rho \mid \ell'_2 0\rangle$$

$$= \sum_{bb'S_2S'_2} (S_2\beta\ell_2 0 \mid b\beta)\ (S'_2\beta\ell'_2 0 \mid b\beta)$$

$$x\ (c\gamma S_2\sigma_2 \mid S_2\beta)\ (c\gamma s_2\sigma_2 \mid S_2\ \beta)$$

$$x\ \langle b\beta \mid \beta \mid b'\beta\rangle\ x\ \langle S_2\ell_2 \| V \| b\rangle$$

$$\langle S'_2\ell'_2 \| V \| b\rangle^* \qquad (2.11)$$

From this equation, one can see that the density matrix of the final state is the product of three density matrices involving the non excited final state and the orbital and spin part of the particle exciting this state. Also, from the third Clebsch Gordon coefficient, one gets:

$$\beta = \gamma + \sigma_2 \qquad (2.12)$$

Now, from (2.10) and (2.12)

$$\beta = \alpha + \sigma_1 = \gamma + \sigma_2 \qquad (2.13)$$

thus, the maximum value of γ will be determined by:

$$\gamma_{max} = \max\ (\alpha + \sigma_1 + \sigma_2) = a + s_1 + s_2\ . \qquad (2.14)$$

This shows:

1) that the value of γ which is the magnetic quantum number of the final state c is independent of the spin b of the intermediate state and of the orbital angular momenta ℓ'_1, ℓ'_2.

2) that the formula for the angular distribution with respect to the beam of the electromagnetic radiation decaying from a state of spin c to a state of spin d, can be used for angular correlation, i.e., when the intermediate particle is actually detected in coincidence with the electromagnetic radiation. The main difference between the two ways of investigation comes from the limitation of γ_{max} when the intermediate particle is detected at 0° or 180°.

It must be pointed out that this is not coincidental, since basically angular distribution formalism and angular correlation formalism are similar. Consequently, the angular distribution or angular correlation of electromagnetic radiation issued from a state c, whose population parameters, $P(\gamma)$ are

$$P(\gamma) = \langle c\gamma \mid \rho \mid c\gamma \rangle$$

and leading to a state d, is given by:

$$W(\theta) = \Sigma \text{ (phase vector)(density matrix of state c)}$$

$$\text{x (efficiency matrix)} \qquad (2.15)$$

or

$$W(\theta) = \sum_{\gamma kp} (-1)^{f_6} \delta^P \left(P(\gamma)(c\gamma c-\gamma \mid k0)\right) \left(Z_1(L_1 c L_2 c, dk) Q_k P_k(\cos\theta)\right)$$

$$(2.16)$$

where

$$f_6 = d + \gamma + L_1 + L_2 + \frac{k}{2} \quad .$$

L_1 and L_2 are the mixing multipolarities of the electromagnetic radiation

δ is the multipole mixing ratio (see remark number (ii) hereafter)

Z_1 coefficient tabulated by Sharp et al (Sh 61)

p = 0, 1 or 2 (see case of $F^{19}(\alpha n\gamma)Na^{22}$)

Q_k is the attenuation factor due to the fact that the radiation is actually detected by finite size detectors. These values have been tabulated for different sizes of detectors and depend on the energy of the γ ray and the crystal-source distance.

Remarks:

i) In the case of angular correlation with detection of outgoing particles at 0° or 180°, it has been assumed that the detector is ideal (i.e., very small); actually, there is a finite size of detector which cannot be neglected. Litherland and Ferguson (Li 61) have shown that if the half angle subtended by the counter is ξ (in radians), the substates beyond γ_{max} are actually populated and the substates $(\gamma_{max} + n)$ are populated with a population proportional to ξ^{2n}. These calculations suppose that the detector is on the axis of the beam. When this is not the case, i.e. detector at 0° but its axis being perpendicular to the beam direction, it is reasonable to assume that these results are still valid although the definition of the angle ξ is less easy.

ii) If the angular correlation is being expressed as:

$$W(\theta) = W_{L_1 L_1}(\theta) + 2\delta\, W_{L_1 L_2}(\theta) + \delta^2\, W_{L_2 L_2}(\theta) \qquad L_1 < L_2$$

then δ is defined by:

$$\delta = \frac{\text{amplitude of } L_2}{\text{amplitude of } L_1} = \frac{\langle d \,\|L_2\|\, c\rangle}{\langle d \,\|L_1\|\, c\rangle}$$

where $\langle d \,\|L_2\|\, c\rangle$ and $\langle d \,\|L_1\|\, c\rangle$ are the reduced matrix elements of the multipole radiation.

iii) Since angular distribution and angular correlation are identical, an alternate method can be used in the case where neutrons are the outgoing particles. Effectively, when neutrons have a low energy, or in other words, when the state fed by neutrons is just above threshold, a limitation of γ_{max} is again possible since low energy neutrons have zero or low angular momentum. However, this method is only possible when a resonance occurs just above threshold.

(c) Application to F^{19} $(\alpha,n\gamma)Na^{22}$ reaction.

Due to the limitations brought by recent experiments (see section 1.3 c), the calculations for the unknown spins of the 2 states 892 kev and 1.532 Mev have been carried out assuming all possible values for the unknown spins between 1 and 4.

A very unlikely 0 spin because of high order multipolarity radiation would yield both angular distribution and angular correlation isotropic.

In the case of spin 1 the diagram of the reaction is the following:

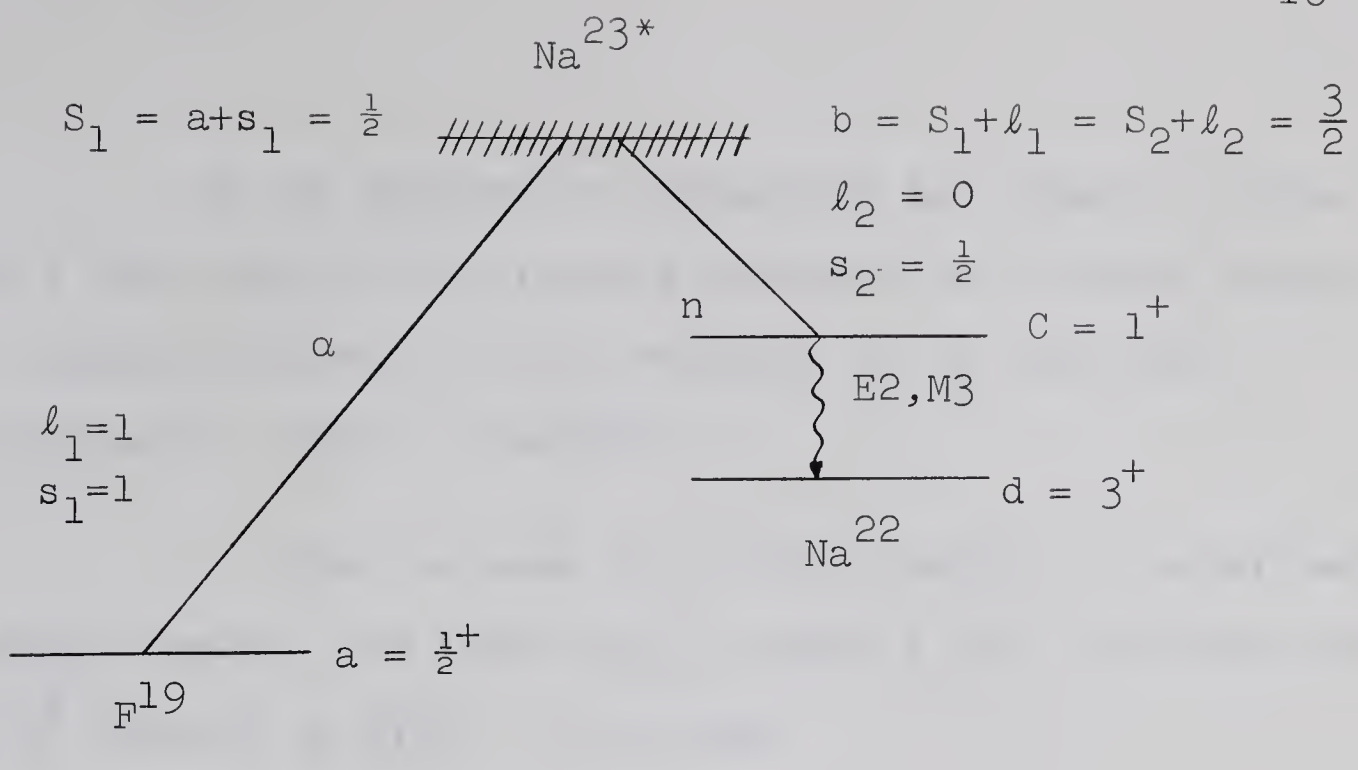

Since the parity is known, one should expect in this case a predominant E2 radiation with weak admixture of M3. As shown in section 1.3 c, the Weisskopf estimates give a ratio E_2/M_3 varying from 10^5 to 10^6 for the 2 states studied.

Using the formula (2.16), the calculations are then carried out for P(0) and P(1) since 0 and ±1 are the only magnetic sublevels which can be populated.

The complete expression of $W(\theta)$ results as follows:

$$W(\theta) = 1 + \frac{0.144\ \{P(0)-P(1)\} + 1.170\ \{P(0)-P(1)\}\delta - 0.250\{P(0)-P(1)\}\delta^2}{(1+\delta^2)\ \{P(0) + 2P(1)\}}$$

$$\times\ P_2\ (\cos\ \theta)$$

or

$$W(\theta) = 1 + \frac{0.144 + 1.170\,\delta - 0.250\,\delta^2}{(1 + \delta^2)\{P(0) + 2P(1)\}}\ \{P(0) - P(1)\}\ P_2\ (\cos\ \theta)$$

If the population parameters are equal, one can check that equally populated substates (or in other words, non aligned nuclei) will be revealed by an isotropic distribution $W(\theta)$ = constant.

In order to make the interpretation of experimental results easier, the graph a_2/a_o versus δ for different values of x^2 defined as $\frac{P(1)}{P(0)}$ is plotted.

This has been done for all the four possibilities and assuming s - wave neutrons (see appendix A1). As may be expected, some cases would lead to ambiguous results but in the most pessimistic case, the number of possible assignments should be reduced from 5 to 2, for instance a negative value of a_4/a_o would limit the possible spins to 2 and 3, a positive value to 2 and 4, etc. . . .

1.3 The Na^{22} nucleus.

a. Theoretical aspects.

Many models are available today, which try to describe nuclear structure. They are more or less successful in explaining the physical properties of nuclei and, although even-even nuclei and odd-even nuclei can often be understood theoretically, it appears that no theory adequately explains the physical properties of all odd-odd nuclei. In other words, closed shell nuclei or nuclei which can be described by a one particle state are the easiest to explain theoretically whereas nuclei such as odd-odd nuclei whose configuration is far from closed shells cannot be so easily comprehended.

Two main approaches have been taken into consideration by the theoreticians. The first one was logically introduced by the previous study of atomic structure: since atomic phenomena were satisfactorily explained by considering each electron separately, one tried to explain the nucleus considering it as an aggregate of nucleons obeying similar laws of quantization. This gave rise to the shell model which leads to a satisfactory matching with many experimental results, although it fails to account for the large nuclear quadrupole moments and spheroidal shape which many nuclei have. The second approach then, was to consider

the nucleus in two parts; a core whose shape would keep almost constant in time and some extracore nucleons. This second model is usually referred as the "collective model" although the terminology is not clear.

Finally, a kind of compromise was attained with the work of Nilsson and the Danish school: the Nilsson model, referred sometimes as the "unified model" could be defined as a more sophisticated shell model in which collective effects are taken into account. The energies of the single particle levels are function of the deformation parameter of the core. A comprehensive series of papers can be found in the Danish publications from 1950 to 1960, the most important of them being probably (Ni 55).

From the viewpoint of the shell model, Na^{22} has the configuration $p(1\ d_{5/2})^3\ n(1\ d_{5/2})^3$; in other words, outside the closed $p\frac{1}{2}$-proton shell, there are 3 protons in the $d_{5/2}$ shell and in order to complete this $1\ d_{5/2}$ shell, one would need to add 3 more protons. The situation is identical for the neutron shells. This also means that if the last filled shell limits an inert core, one would have to solve a six body problem to get the state function of the nucleus! However, under some simplifying assumptions, the shell model allows a satisfactory determination of some

physical constants like nuclear magnetic moments and ground state spin assignments even in such an extreme case. The Schmidt prediction for nuclear magnetic moments, although it deals with an extreme single particle model, can be applied to odd-odd nuclei and in the case of Na^{22} yields a value of 1.73 nuclear magnetons (Ra 57) which compares closely to the known experimental result: 1.75 nuclear magnetons. In order to determine the ground state spin of Na^{22}, Nordheim's rule as modified by Brennan and Bernstein (Br 60) can be applied. As shown by Brennan and Bernstein, the"weak rule" of Nordheim can be replaced by a stronger rule (R2). If J_1 and ℓ_1 (or J_2 and ℓ_2) are the single particle total and orbital angular momenta obtained from the adjacent odd A nuclei using standard shell model assignment, then the ground state spin J is given by:

$$J = | J_1 \pm J_2 | \quad \text{for} \quad J_1 = \ell_1 \pm \tfrac{1}{2}$$
$$\text{and} \quad J_2 = \ell_2 \pm \tfrac{1}{2}$$

Since Ne^{21} and Na^{23} both have ground state spin $\frac{3}{2}+$, this leads to two possible values for the ground state spin of Na^{22}, namely 3 and 0.

Before introducing the collective aspects of the nucleus, it may prove useful to point out that the formalism used hereafter is that introduced by the Danish school and can be recalled briefly by the following diagram:

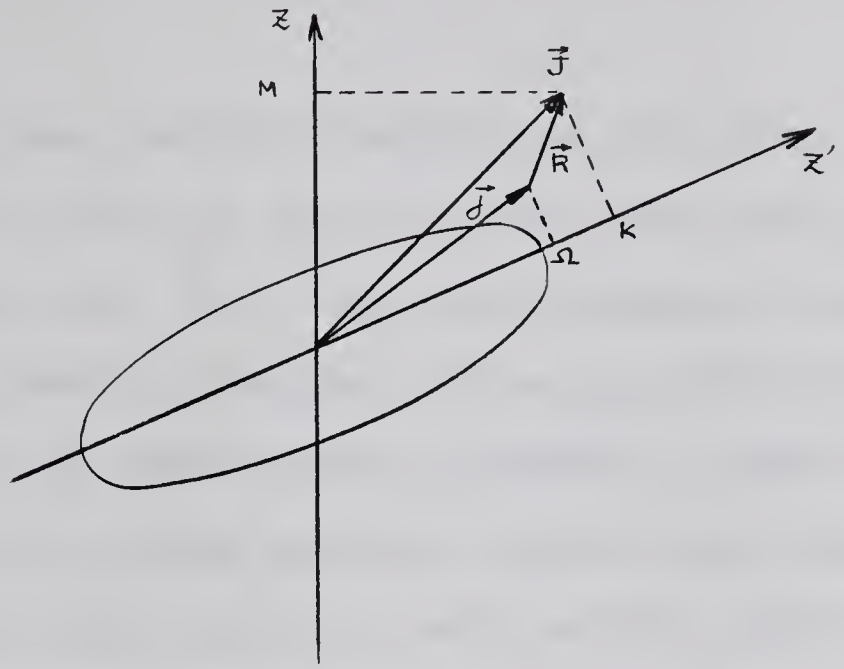

Fig. 1.3.1

where Z is the quantization axis and Z' an arbitrary axis

$\vec{J}$ is the total angular momentum of the nucleus, M and K its respective projections on the Z and Z' axes.

$\vec{R}$ is the total angular momentum of the core

$\vec{j}$ is the total angular momentum of the external particle(s) and Ω the projection of $\vec{j}$ on the Z' axis

In the case of axially symmetric nuclei, there is no contribution of the core angular momentum along Z' if Z' is symmetry axis; therefore $K = \Omega$. This can be shown from classical mechanics considerations (see e.g. (Pr 63) p. 237 and 256).

As seen earlier, both unpaired proton and neutron of Na^{22} are in the $d_{5/2}$ shell of the shell model representation. Nilsson (op. cit.) has shown that, by considering a non spherical shell potential, this $d_{5/2}$ level splits into 3 "orbits" as the deformation increases. These orbits corresponding to single particle states are labelled by the Nilsson number, the intrinsic spin value Ω and the parity of the state. According to this model, one should expect for the ground state of Na^{22} both odd neutron and proton in Nilsson orbit $7(\frac{3}{2}+)$,(Ar 65), hence two possible spin assignments corresponding to parallel and antiparallel coupling of the intrinsic spins:

$$J^{\pi} = \Omega_p + \Omega_n = 3^+$$

and

$$J^{\pi} = | \Omega_p - \Omega_n | = 0^+ .$$

It can be shown that parallel coupling is the most probable (Na 65) and this fact is confirmed by experiment as shown in table 1 of a paper by Rakavy (Ra 57). Experimentally, the ground state spin of Na^{22} is known to be 3^+.

Rakavy (op. cit.) has shown that Nilsson model could be more extensively applied in the region between A = 18 and A = 28. According to his calculations the deformation in the nuclei following O^{16} increases very rapidly and for A = 18 already attains a value characteristic of heavy nuclei revealing rotational spectra, i.e., for nuclei whose A varies from 160 to 180. The calculated deformation (which is known as δ or ϵ in the literature) reaches a maximum for Ne^{20} then stays almost constant until A = 25 is reached, then decreases. Evidence of the fact that rotational spectra are found in the region A = 18 to A = 28 is shown in a summary of pertinent work (Gov 60). Mottelson and Nilsson (Mo 59) pointed out that the deformation parameter δ decreases with increasing A because, in the model which is studied, the deformations are fundamentally of order $A^{-\frac{1}{3}}$. Commenting upon Rakavy's paper, Mottelson and Nilsson mention that the experimental data are not sufficiently complete to provide a very critical test of the coupling scheme as interpreted by Rakavy, although it does provide a satisfactory basis for interpreting most of the available evidence in this region (A = 18 to A = 28). Finally, it is interesting to point out that Varshalovich (Va 64) gives some evidence to support the fact that Na^{22} is probably strongly deformed, by studying the first two excited states of this nucleus.

As will be shown hereafter, only 3 states of Na^{22} have been assigned a definite spin value and it is therefore difficult to compare this nucleus to any model. However, for the reasons explained earlier, the rotational aspect of the nucleus seems to be the most applicable and will thus be taken into consideration.

b. A review of previous work on Na^{22}

At the present time, 23 excited states have been found for Na^{22} (Ar 65), but only three of them have been assigned a definite spin and parity whereas definite parity and probable values for spin have been assigned for the next two. (fig. 1.3.2.)

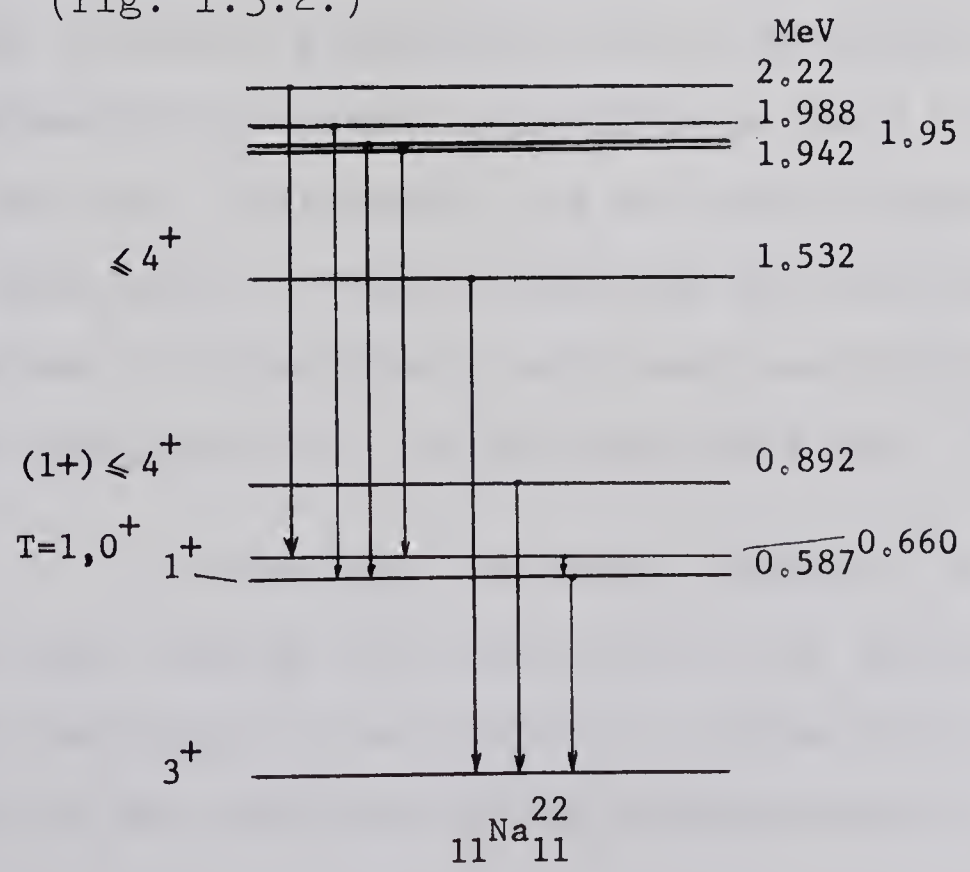

Fig. 1.3.2. Diagram illustrating the low-lying energy levels and gamma-ray branching in Na^{22} after Arnell and Wernbom-Selin (Ar 65).

By studying the pick-up reaction Na^{23} (d,t) Na^{22}, Vogelsang and McGruer (Vo 58) showed that the first three T = 0 excited levels have positive parity and that their spin value is limited to 4.

Temmer and Heydenberg (Te 58) found the first T = 1 state at 660 kev. This state is a 0^+ and decays to the ground via the 587 kev state.

Pellegrini (Pe 61) studied the Mg^{24} (d,α) Na^{22} reaction and tried to fit the angular distributions of alpha particles with D.W.B.A. theory and Butler theory. For the 1.532 Mev state the best fits were obtained with Butler calculations for $\ell = 0$ and $\ell = 4$, thus limiting the possible values of J^π to 1^+ or 3^+, 4^+, 5^+. For the 892 kev state, the best alpha particle distributions fit was obtained with D.W.B.A. calculations for $\ell = 0$. Since this fit was poor, Pellegrini did not give a possible assignment for this state. However Endt and Van der Leun (En 62) referred to Pellegrini's work and concluded that a probable spin assignment for the 892 kev state was (1^+).

In the past few years, research on Na^{22} was oriented much more towards the discovery of the second T = 1 state. As seen previously, the first T = 1 state is the 660 kev level which is the analogue of the ground state of Ne^{22} (T = 1, $J^\pi=0^+$).

Since the first excited state of Ne^{22} is the 1.28 Mev level, the second T = 1 state of Na^{22} is expected at an excitation energy of about 1.94 Mev. None of the three levels at 1.942, 1.95 and 1.988 MeV exhibits characteristic properties of a T = 1 state and the problem remains unsolved.

c. Predictions.

As seen earlier, Na^{22} can be considered as a strongly deformed nucleus exhibiting a pure rotational spectrum. Rakavy (Ra 57) gives 0.47 as the calculated equilibrium deformation and predicts a value of 1.78 n.m. for the nuclear magnetic moment, known to be 1.75 n.m. experimentally. Considering that there are 2 odd particles in the same Nilsson orbit $7(\frac{3}{2}+)$, three low lying bands can be expected according to Rakavy:

$K = 2\Omega = 3+$	with	$T = 0$ (the lowest level of this band is the ground state)
$K = 0^+$	with	$T = 0$ ($J^\pi = 1^+, 3^+, 5^+ \ldots$)
$K = 0^+$	with	$T = 1$ ($J^\pi = 0^+, 2^+, 4^+ \ldots$)

Paul (Pa 65) proposes a more complete level scheme by considering all the possible transitions for the two odd particles to higher Nilsson levels. He thus gets the different following combinations:

1) both proton and neutron in Nilsson orbit $7(\frac{3}{2}+)$. This gives bands of $K = 3^+$ and 0^+.

2) one particle in level $9(\frac{1}{2}+)$ and the other in level $7(\frac{3}{2}+)$, this gives four bands: two of $K=1^+$ and two of $K=2^+$.

3) one particle in level $5(\frac{5}{2}+)$ and the other in level $7(\frac{3}{2}+)$: two bands of $K=4^+$ and two of $K=1^+$.

Once more, it is necessary to point out that these predictions are rather speculative since the experimental investigations have not given enough information so far.

It has been seen that all the possible spin assignments for the states 892 kev and 1.532 MeV were limited to a maximum value of 4 with positive parity and that a probable spin assignment for the 892 kev state would be 1^+. If one considers the simple case of single particle transition, these possibilities lead to two different multipole radiation mixtures M1 and E2 for a transition 2^+ (3^+ or 4^+) to 3^+, M1 being predominant, E2 and M3 for a transition 1^+ to 3^+ E2 being predominant. As pointed out by many authors (see (Pr 63) p. 341 for instance), the Weisskopf estimates for single particle transitions may be off by a few orders of magnitude. However, these estimates generally give a basis for discussion and it may prove useful to calculate them.

For single particle transition, the mixing ratios of multipole radiation are given by:

$$\frac{M1}{E2} = \frac{2.8}{1.6} 10^5 \frac{1}{A^{4/3}} \frac{1}{E^2_\gamma}$$

for transition 2^+, 3^+, 4^+ to 3^+, and

$$\frac{E2}{M3} = \frac{1.8}{5} 10^7 \frac{1}{A^{4/3}} \frac{1}{E^2_\gamma}$$

for transition 1^+ to 3^+,

where A is the atomic number and E_γ the energy of the transition gamma-ray in MeV.

For the 1.532 MeV transition, one gets:

$$\frac{M1}{E2} = 1260$$

$$\frac{E2}{M3} = 6.5 \times 10^5$$

For the .892 MeV transition, one gets:

$$\frac{M1}{E2} = 3500$$

$$\frac{E2}{M3} = 1.8 \times 10^6$$

It is interesting to point out that, according to Morpurgo (Mo 63), E1 transitions are forbidden for the $\Delta T = 0$ transitions in self conjugate nuclei: $N = Z$ or $T_3 = 0$. Under the same conditions, M1 transitions are expected to be reduced by a factor 100 to 150. This rule does not affect E2 transitions. Experiments have shown, however, that electric quadrupole transitions are enhanced compared to the single particle approximation when the nucleus exhibits collective effects. (see (Mo 63) e.g.).

Thus in the case of transitions 2^+ (3^+ or 4^+) to 3^+, one can expect strong M1 E2 mixing in self conjugate nuclei. As shown by Morpurgo (op. cit.), the quadrupole transition may even become predominant in the case where $E_\gamma > 16/A^{2/3}$ (in MeV); this would correspond to $E_\gamma > 2$ MeV for Na^{22}.

CHAPTER II. EXPERIMENTAL ASPECTS

2.1 Experimental apparatus.

a. Correlation table.

The beam of alpha particles was accelerated by the 5.5 MV electrostatic accelerator* of the Nuclear Research Centre. The correlation table was the same as used by J. G. Pronko (Pr 65) but some changes have been introduced in the beam path (fig. 2.1) and the collimator has been adjusted to fit exactly the inside diameter of the tube.

The targets were prepared at the Nuclear Research Centre laboratory and consisted of a 0.002 inch thick platinum backing on which CaF_2 had been evaporated. In the first series of runs, a gold backing was added for the purpose of better heat transfer. For reasons explained later, this gold backing was removed in the second series of runs. The target was cooled by compressed air stream during the experiments.

* Model CN Van de Graaff, High Voltage Engineering Corporation, Burlington, Massachusetts, U. S. A.

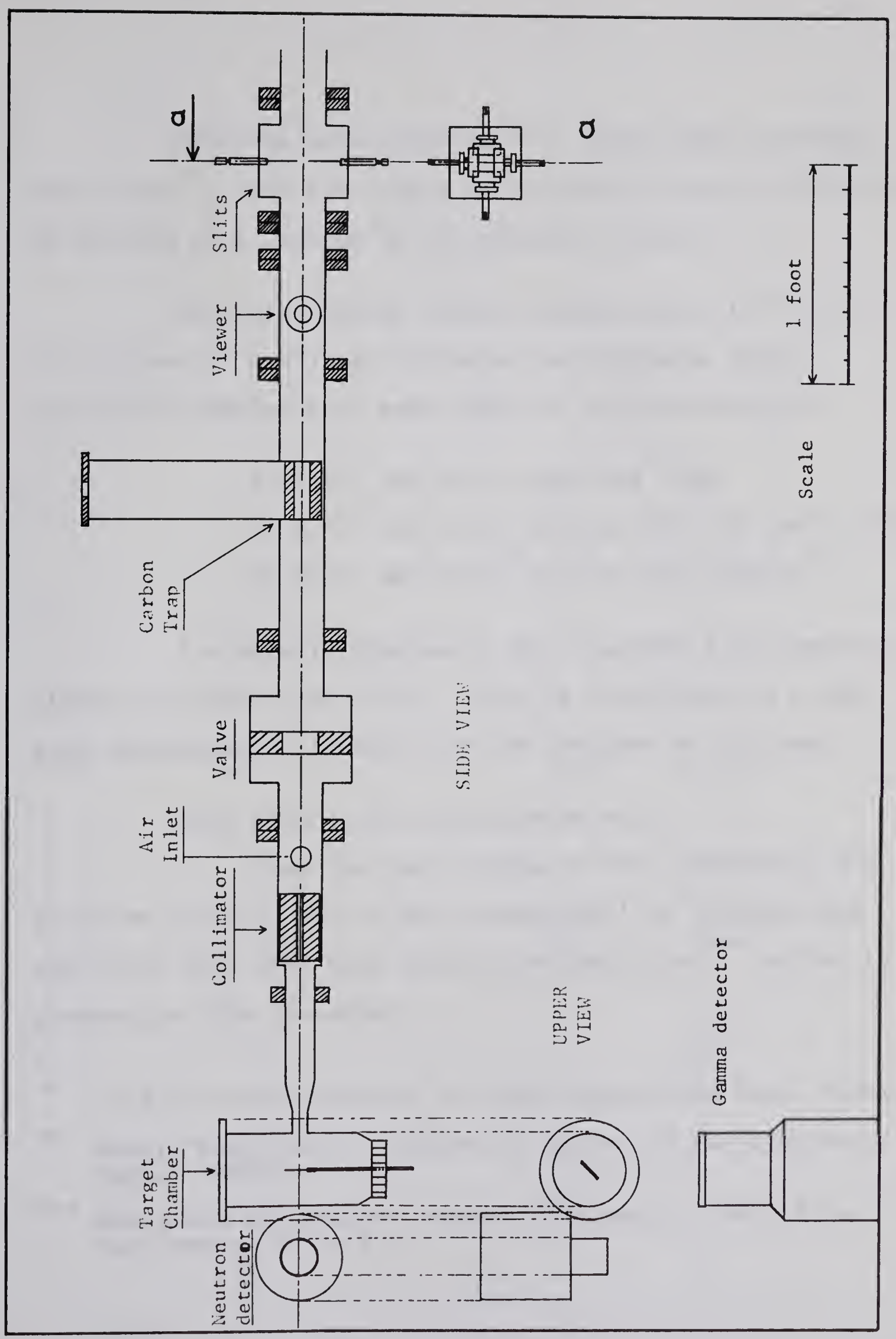

Fig 2.1: An illustration of the beam path.

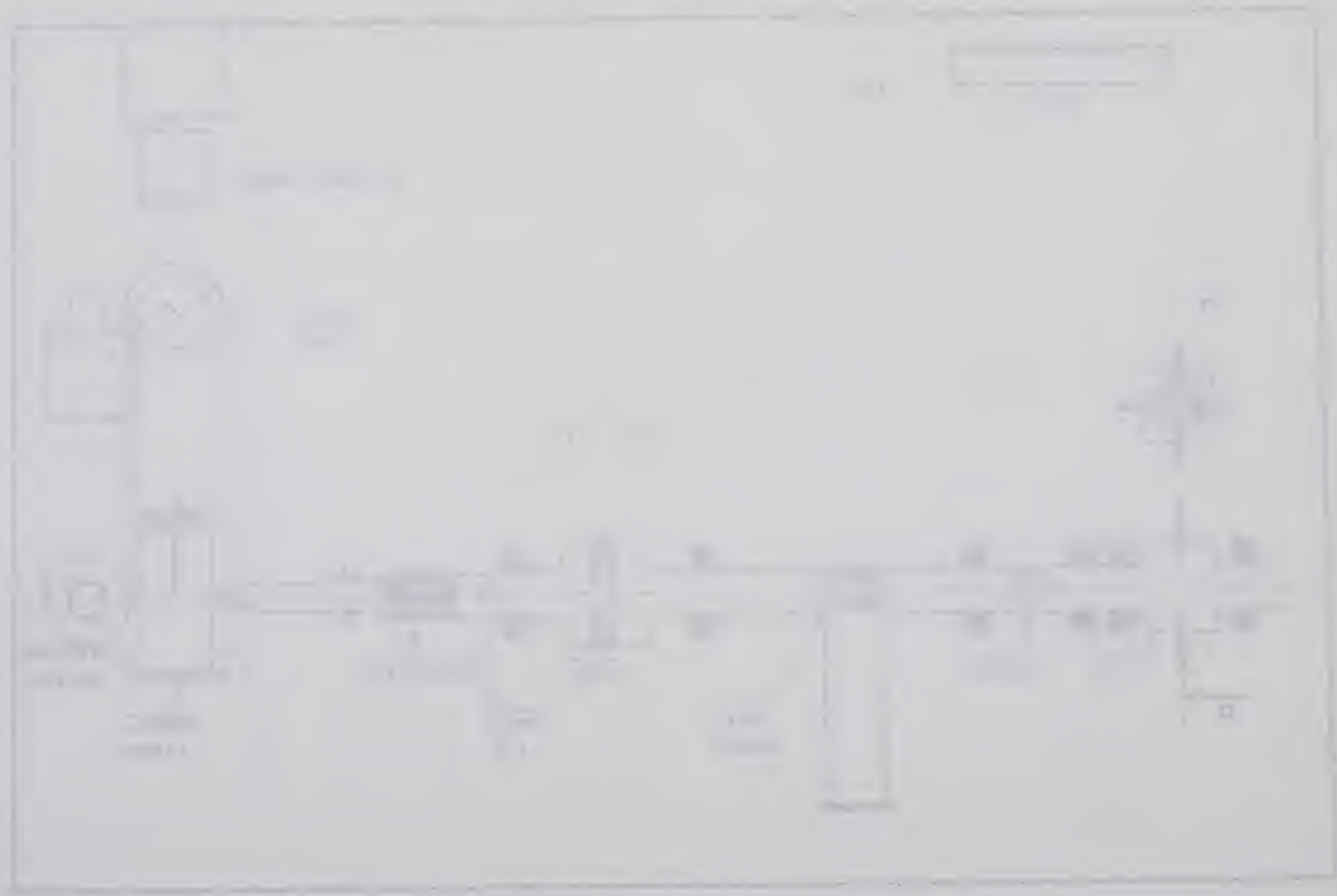

Neutrons were detected by a pulse shape discriminator probe*. The $1\frac{1}{2}$" long x $1\frac{1}{2}$" diameter liquid scintillator is mounted on a Philips 56 AVP photomultiplier.

Different sodium iodide crystal sizes (2" x 2", 3" x 3" and 4" x 4") and different scintillator photomultiplier combinations were used for the γ-detection:

4" x 4" NaI (Tl) with RCA 7046
4" x 4" NaI (Tl) with 58 AVP (XP 1040) Philips
3" x 3" NaI (Tl) with 54 AVP Philips**

A schematic diagram of the electronic equipment is given in illustration (2.2). This is equivalent to a fast-slow coincidence unit which can be analyzed as follows:

Fast side of the coincidence unit:

From the last dynode of the γ-detector, the positive pulse (2 volts, 60 microseconds) is limited then amplified by a wide band distributed amplifier*** before it enters the time converter.

* "P.S.D." Model NE 5553, Nuclear Enterprises Ltd., Winnipeg.

** Model "scintibloc". Quartz et silice, 8 rue d'Anjou, Paris, FRANCE.

*** Model 460 AR, Hewlett Packard Corporation, Palo Alto, California, U. S. A.

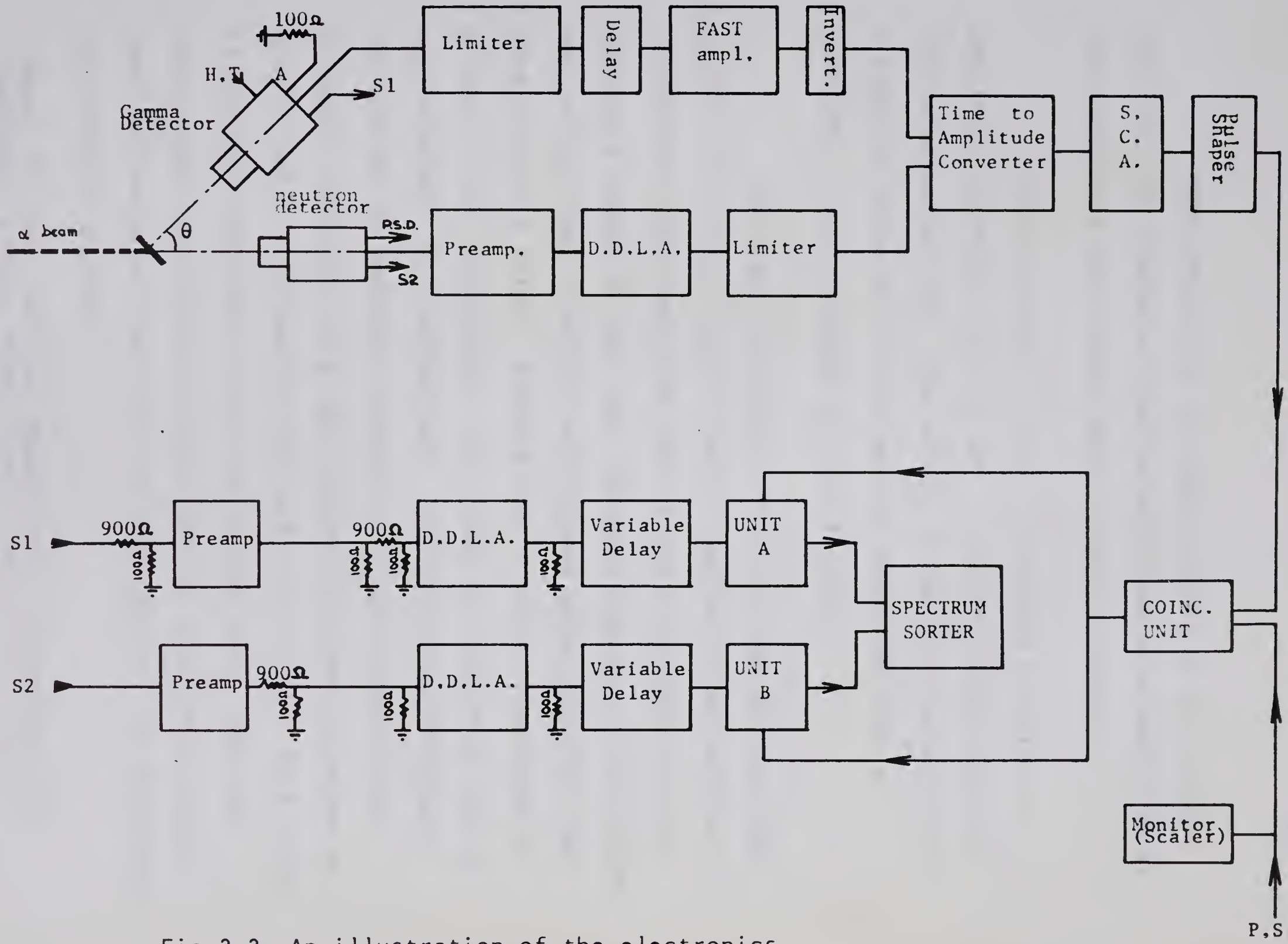

Fig 2.2: An illustration of the electronics.

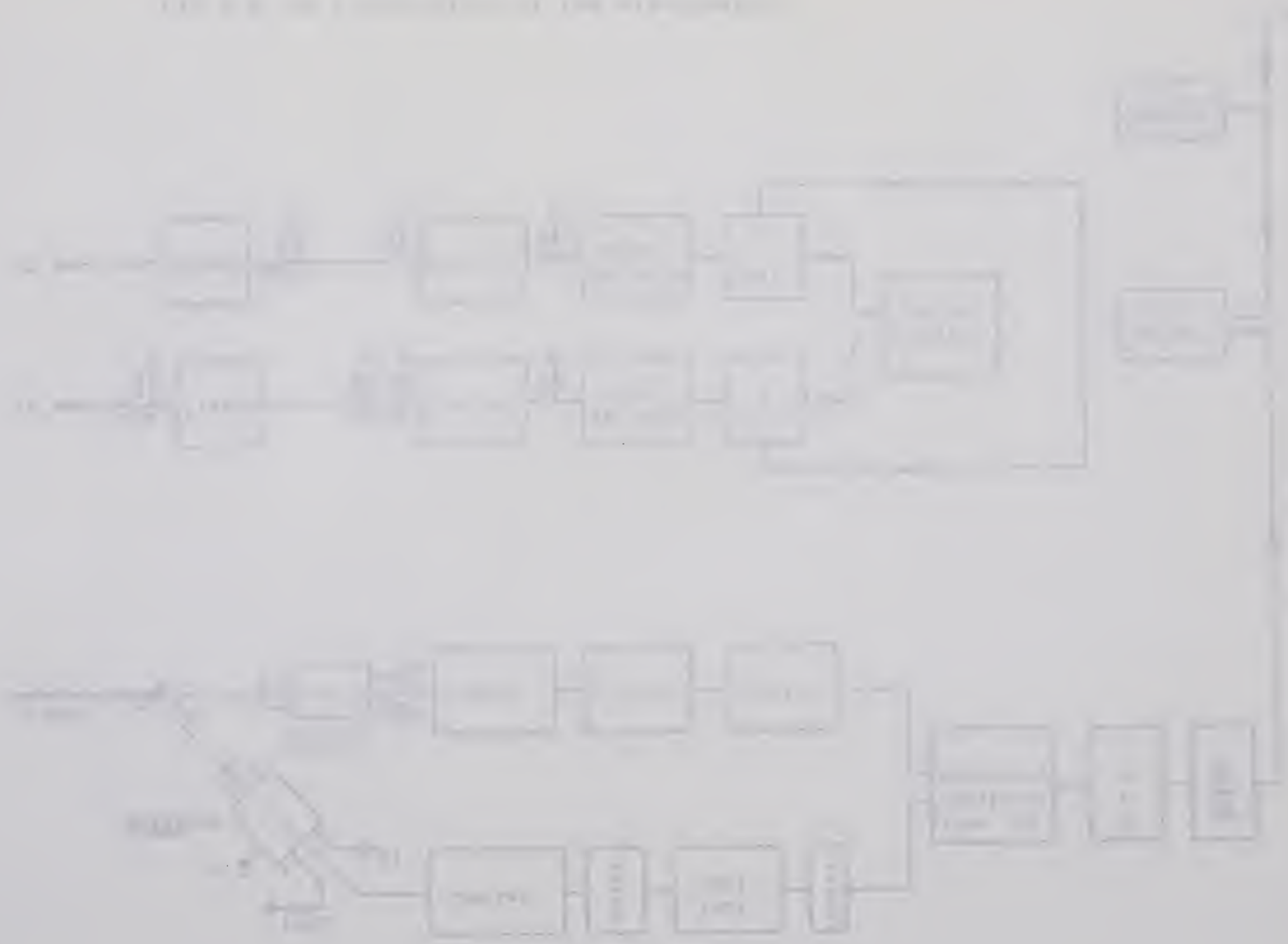

From the dynode 14 (fast output) of the neutron detector, the positive pulse is amplified by a double delay line amplifier and limited by a clipping circuit.

The two pulses (n and γ) entering the time to amplitude converter (Ne 60) are +5 volts in amplitude and 150 nanoseconds long. The output of the time converter is a negative pulse of 4 volts maximum amplitude with a risetime of approximately 100 nanoseconds.

This fast coincidence which is used as time base, is then fed into a single channel analyzer whose purpose is to determine the resolving time of the coincidence unit by setting a window on the time converted signals. This window was set in order to accept only pulses whose amplitude was greater than 3 volts. Knowing that 4 volts corresponds to a time of 150 nanoseconds, this fixes the resolving time at approximately 40 nanoseconds. The window was regularly checked and no apparent change in its width was noticed. A shaper following the single channel analyzer generates an output pulse 1 microsecond wide and 1 volt high. This pulse is put into coincidence with the neutron pulse from the pulse shape discriminator output and the coincident signal provides the gate pulses for the 1024 channel, two parameter, pulse height analyzer.*

* Model CN 1024, Technical Measurement Corporation, 441 Washington Avenue, North Haven, Connecticut, U.S.A.

Slow side of the coincidence unit:

The "slow" pulses from dynode 10 for the gamma-detector and for the linear output for the neutron detector are fed into separate lines including linear preamplifier (GO 60) and double delay line amplifier*. After amplification, the pulses traverse a variable delay box** before entering their respective inputs at the pulse height analyzer.

Delays are set in the different lines to cancel the difference in cable lengths and to match the arrival of slow and fast signals at the pulse height analyzer. In order to set these delays, a Na^{22} source is placed between the two detectors at 180^{o} one from the other and the simultaneous emission of the two annihilation gamma-rays is taken as time reference.

Singles spectra can be recorded by switching the input selectors of the pulse height analyzer to anticoincidence, thus ignoring the fast gating pulses.

* Transistor double delay line amplifier AEP 1436 Atomic Energy of Canada Limited, Chalk River, Ontario (cf. GO 60).

** Type 2011, AD-YU Electronics Limited, Passaic, New Jersey, U. S. A.

For monitoring purposes, the PSD output corresponding to neutron pulses is connected to a scaler. A gamma-ray monitor was also used during some runs. It consists of a 2" x 2" crystal and its associated photomultiplier, a preamplifier, a double delay line amplifier and a double channel analyzer before the scaler. The purpose of this second monitor was first to check the monitoring by neutrons and also to have a reliable normalization when the neutron detector was moved in order to determine its effect on the gamma-detector for small angles. (See "corrections" (section 2.4)).

2.2 Preliminary experimental results.

A test run was performed a few months before the experiment started. A previous study of $F^{19} + \alpha$ reaction by Freeman and Mani (Fr 64) has shown that the 1.532 MeV state of Na^{22} is excited at a resonance of 4.7 MeV bombarding energy. One of the spectra obtained during this test run is shown in fig. 2.3 and corresponds to a bombarding energy of approximately 4.7 MeV. As can be seen, three competing reactions are occurring: inelastic scattering $F^{19}(\alpha,\alpha')F^{19*}$, (α,p) reaction leading to Ne^{22*} (Q = 1.675 MeV) and finally (α,n) reaction leading to Na^{22*} (Q = - 1.942 MeV).

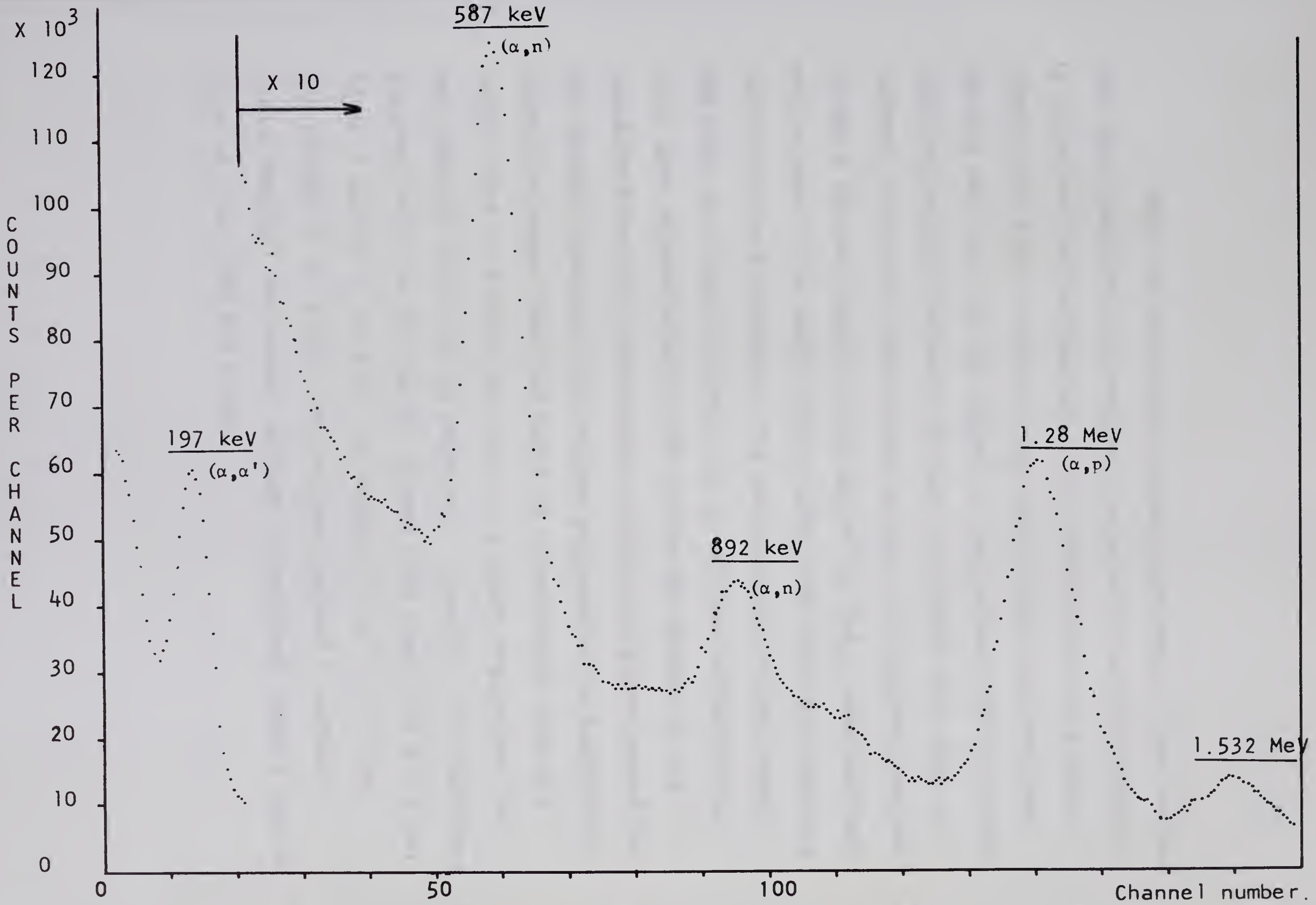

Fig. 2.3: Ungated spectrum for a bombarding energy of 4.7 MeV.

When the experiment actually started, it was noticed that both gamma-ray and neutron yields were high but apparently there was no overloading of the electronics for a beam current $\lesssim$ 0.5 μA. However, the target which had been used for the test run ($\simeq$ 100 μg/cm^2 of CaF_2 on a 0.002 inch thick platinum backing) appeared to burn out easily with such a current, although it was cooled by air. It was then decided to use a thicker target ($\simeq$ 300 μg/cm^2 of CaF_2, same backing) and to mount this target with a 1/32 inch thick gold backing for better heat transfer. The beam current on the target was kept at a value of about 0.5 μA and the corresponding yield gave approximately 5,500 counts per second in the gamma-detector and approximately 5,000 counts per second in the neutron detector, both values supposed to be acceptable. Since the target then was about 15 times thicker than the target used by Freeman and Mani, the sharp resonances they had observed could not be expected. Actually, the resonances observed with the 300 μg/cm^2 target were about 200 kev wide. After a series of runs in the region 4.5 MeV to 5.5 MeV, the energy of 4.79 MeV (from nuclear magnetic resonance field reading) was chosen because it produced maximum excitation of the 1.532 MeV state.

The main problem which had to be faced then was a large gain shift attaining maximum values of more than 30% per day. By feeding a pulse of constant amplitude into the gamma preamplifier, it was found that it was not the electronics but the detector itself which was faulty. Different detectors and different crystal-photomultiplier combinations were tried but they showed the same defect. However, since the gain shift was noticeably smaller with a 4" diameter x 4 " long crystal mounted on an XP 1040 photomultiplier, an angular correlation experiment was tried. It appeared that, although the coincidence spectra were well defined, the results were not reliable after all corrections had been applied. Moreover, these runs would only concern the 587 kev and 892 kev states since the statistics were too poor to investigate the 1.532 MeV state.

As shown in fig. 2.4, it had been noticed that for small angles (0° to 30°) two unidentified peaks appeared which corresponded to approximately 220 and 340 kev. The second peak at 340 kev disappeared almost completely (fig. 2.5) when a 2 inch thick piece of lithium doped paraffin was placed in front of the gamma detector, showing that this secondary effect was due to neutrons. Also, the sodium iodide crystal was getting activated by the high neutron yield.

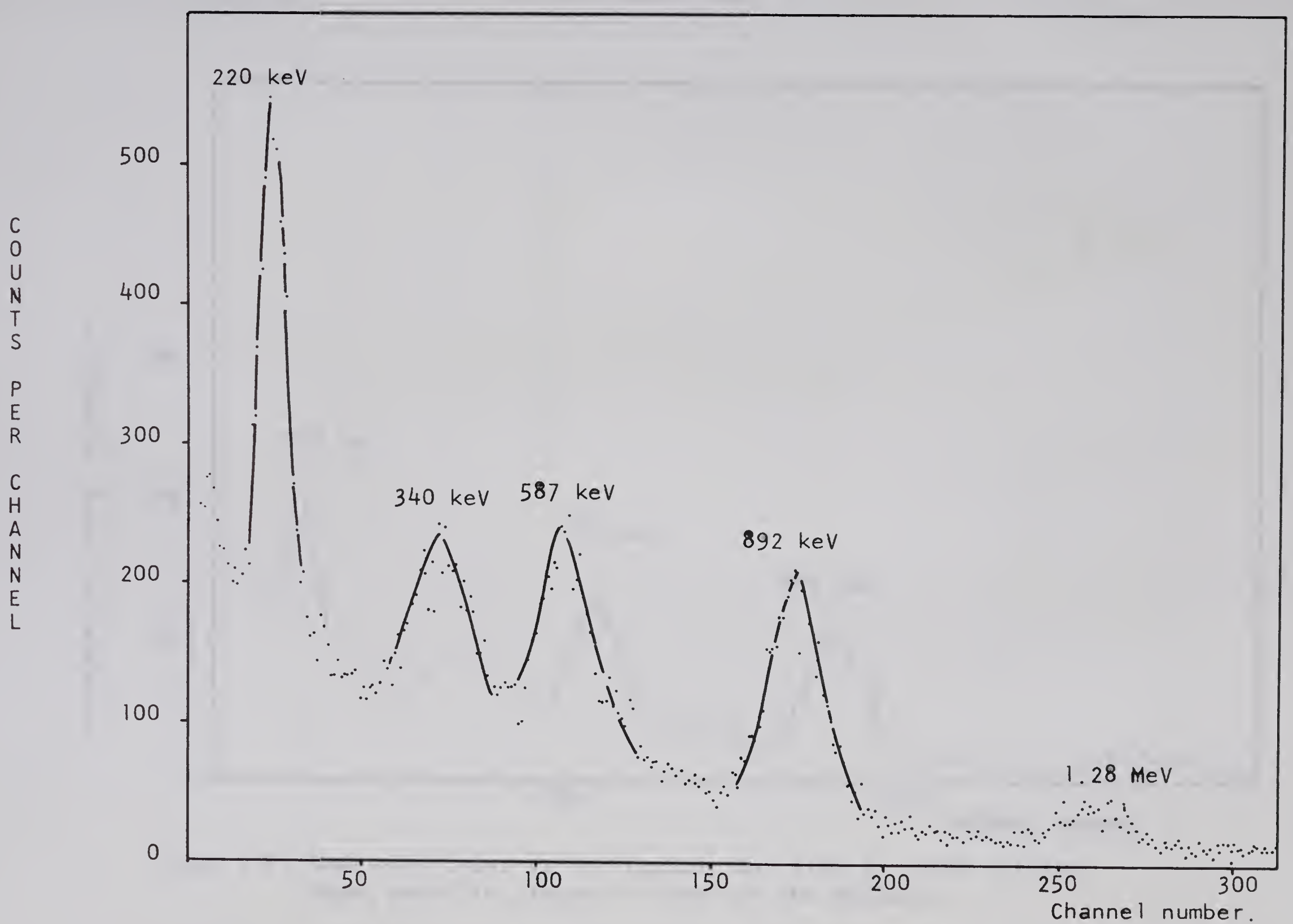

Fig. 2.4: Neutron gated spectrum for a bombarding energy of 5.01 MeV.
(4" x 4" crystal at 30 degrees from the beam axis)

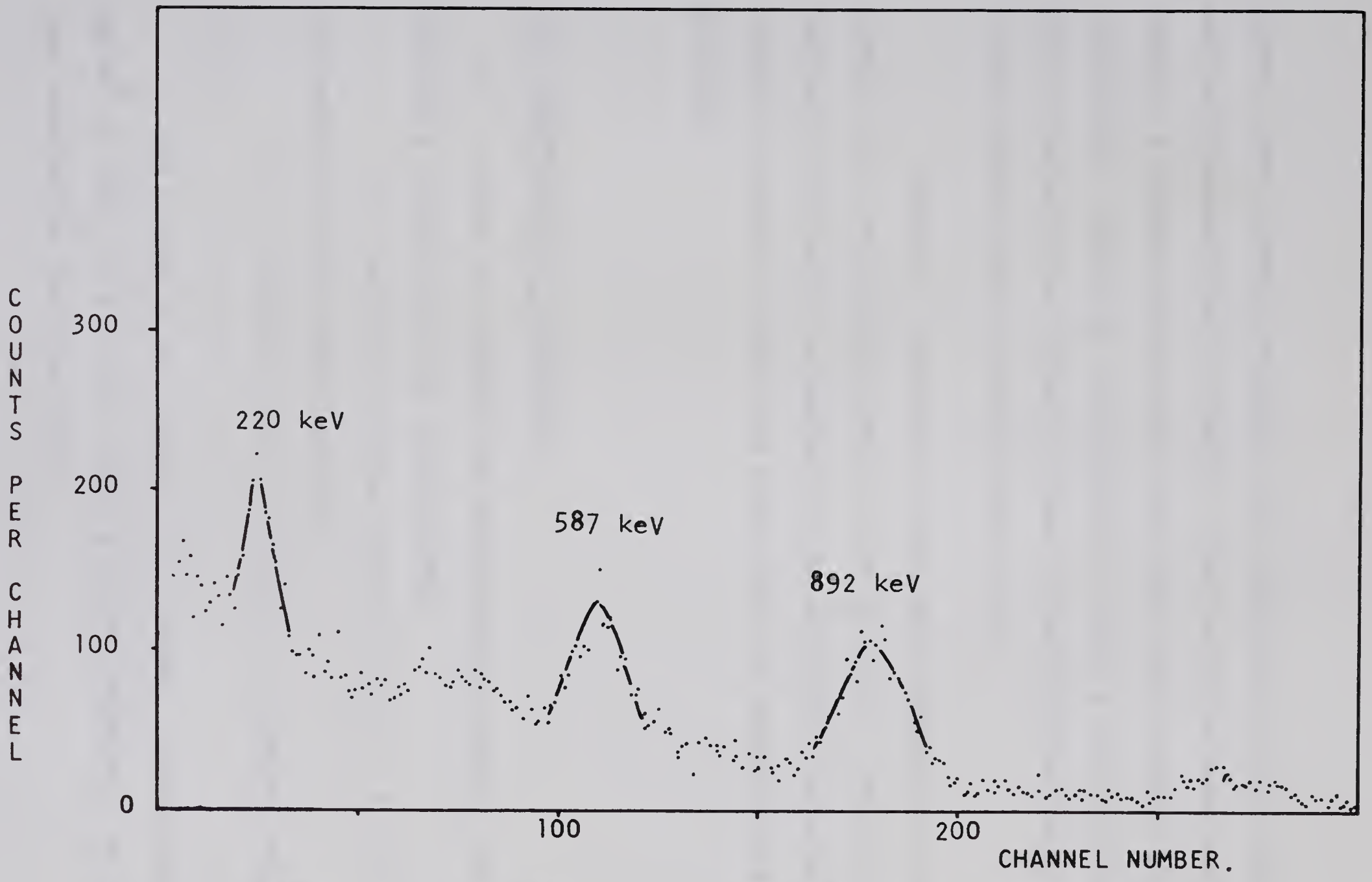

Fig. 2.5: Same conditions as in fig.2.4, but with 2" thick lithium doped paraffin placed in front of the detector.

After a few hours of running, the resolution of the detector was much poorer than initially. Then, with no beam on the target, a background spectrum was taken which showed high activation. Resuming the experiment after a few minutes with no beam on the target, it was found that the resolution of the detector had improved drastically.

Finally, a series of tests with radioactive sources showed that the counting rate of the 3" x 3" "scintibloc" had to be limited to a maximum value of 3,000 counts per second in order to limit the gain shift to less than 2% per day.

2.3 Experimental procedure.

a) In order to improve the experimental results, the following conditions were established:

i) limitation of the counting rate to 3×10^3 counts per second for the gamma detector.

ii) low beam current limited to a maximum value of 0.2 μA.

iii) use of an average thin target, approximately 100 $\mu g/cm^2$ of CaF_2 on a 0.002" thick platinum backing. No gold heat conducting back was used.

A 2.5" thick lithium doped paraffin cap was placed in front of the gamma detector to minimize the activation due to neutrons and also fulfill the condition (i) limiting the gamma counting rate. It was also decided to take one singles spectrum at 90^{o} after each run for checking and monitoring purposes.

b) Kinematics of the reaction.

The kinematic variables of the reaction were computed using a program written for the LGP 30 computer of the Nuclear Research Centre. From the results of the computations, the energy threshold for each excited state and the energy of neutrons emitted at 0^{o} for a given bombarding energy were obtained. The Q-value of the reaction is -1.949 MeV and the nuclear masses are as follows:

$$\left.\begin{aligned} M_1 &= 4.003876 \text{ amu} \\ M_2 &= 19.00444 \text{ amu} \end{aligned}\right\} \text{ input channel}$$

$$\left.\begin{aligned} M_3 &= 1.008986 \text{ amu} \\ M_4 &= 22.00143 \text{ amu} \end{aligned}\right\} \text{ output channel}$$

1 amu = 931.141 MeV

This resulted in the following table:

Level in Na^{22}	Threshold Energy	Level in Na^{22}	Threshold Energy
ground state	2.359 MeV	1.532 MeV	4.214 MeV
587 kev	3.070 MeV	1.942 MeV	4.711 MeV
660 kev	3.159 MeV	1.950 MeV	4.720 MeV
892 kev	3.439 MeV	1.988 MeV	4.766 MeV

Table 2.1 Threshold energies of the various levels of Na^{22}.

At three different bombarding energies, the neutrons feeding the various levels in Na^{22} have the following energies at 0^{o} .

Bombarding Energy	Neutron energy at 0^{o} for the various levels		
	ground state	587 Kev	892 kev
4.5 MeV	2.20 MeV	1.557 MeV	1.211 MeV
5 MeV	2.687 MeV	2.044 MeV	1.704 MeV
5.5 MeV	Not computed		2.192 MeV

Bombarding Energy	Neutron energy at 0^{o} for the various levels			
	1.532 MeV	1.94 MeV	1.95 MeV	1.988 MeV
4.5 MeV	0.436 MeV	Not excited		
5 MeV	0.966 MeV	0.453 MeV	0.442 MeV	0.390 MeV
5.5 MeV	1.470 MeV	0.989 MeV	0.979 MeV	0.933 MeV

Table 2.2 Energy of the neutrons feeding the various levels in Na^{22} and emitted at 0^{o} from the beam axis.

c) Neutron gamma discrimination

The neutron pulse shape discriminator was first tested with plutonium - beryllium and Co^{60} sources. With the discriminator level set at 0, it was checked that the rejection ratio was as high as claimed by the Nuclear Enterprises specifications (500:1). The results of this test are shown in fig. 2.6. The ungated spectrum corresponds to the linear output only, the gated spectrum to the linear output in coincidence with the pulse shape discriminator output. A second test was run with a thorium C source whose maximum gamma ray energy is 2.62 MeV. It showed that the discriminator level had to be set to 12 in order to get a comparable rejection ratio. Since the most energetic strong gamma ray from the reaction ($F^{19} + \alpha$) is the 2.1 MeV gamma ray corresponding to a transition from the second excited state in Ne^{22}, a discriminator level value of 9 was found to be optimum during testing with the beam. The results of this last test are illustrated by the fig. 2.7 and 2.8.

d) Yield curves for the 0.892 and 1.532 MeV states.

Yield curves were plotted for the 0.892 and 1.532 MeV gamma-rays from Na^{22} from 4.5 to 5.4 MeV. The energies were determined from nuclear magnetic resonance frequencies.

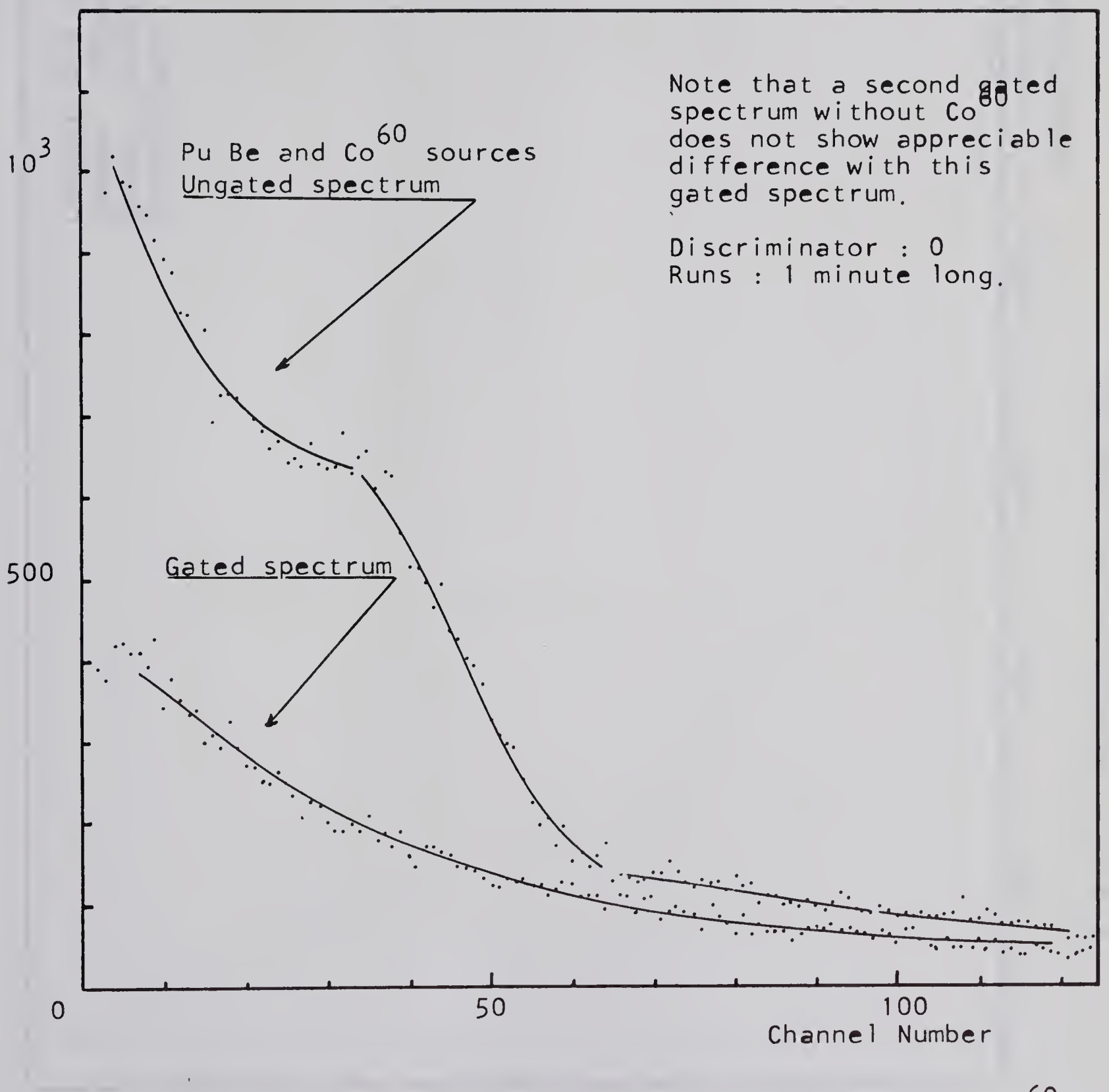

Fig 2.6: Gated and ungated neutron spectra for PuBe and Co^{60}

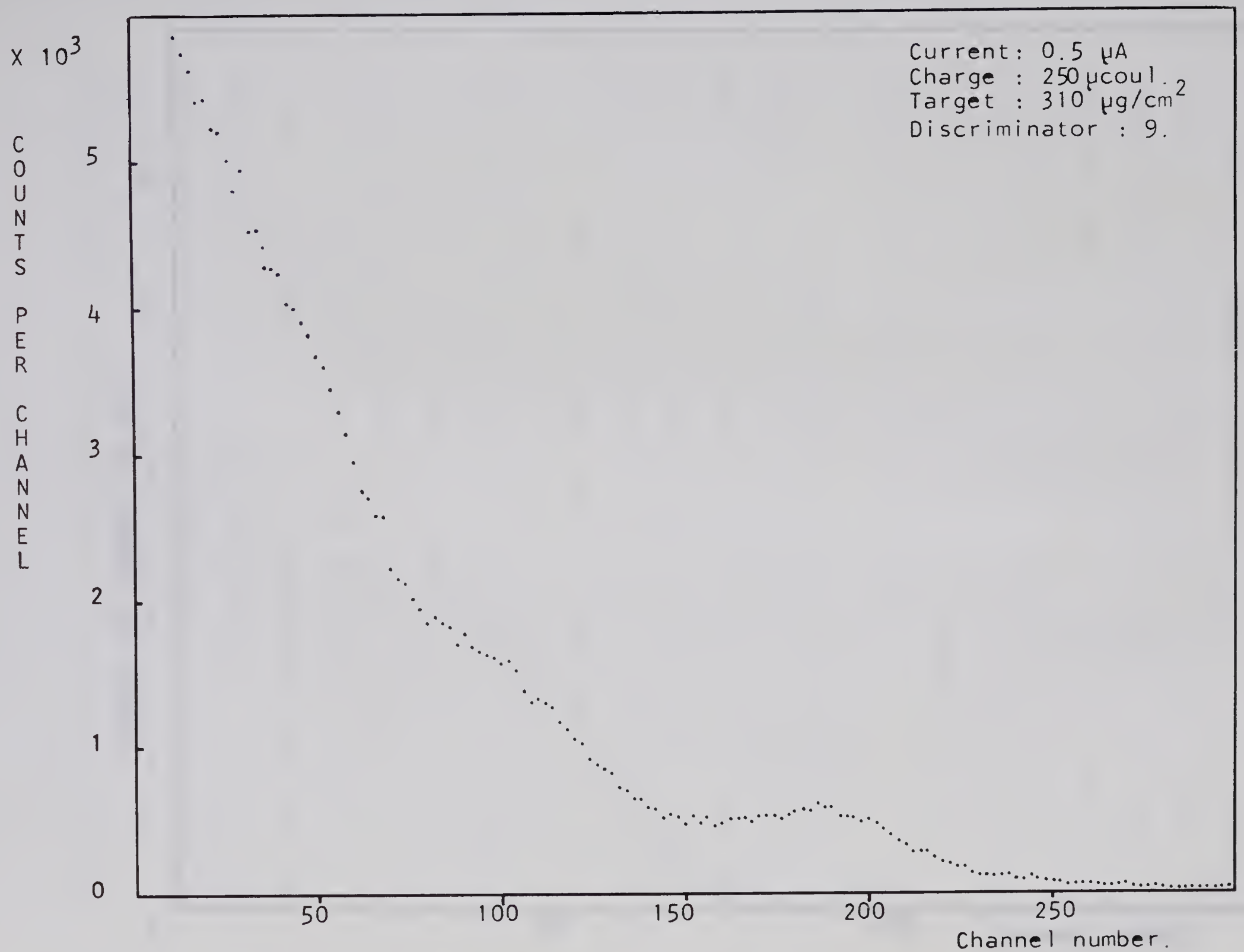

Fig. 2.7: Ungated neutron spectrum
Bombarding energy: 4.72MeV.

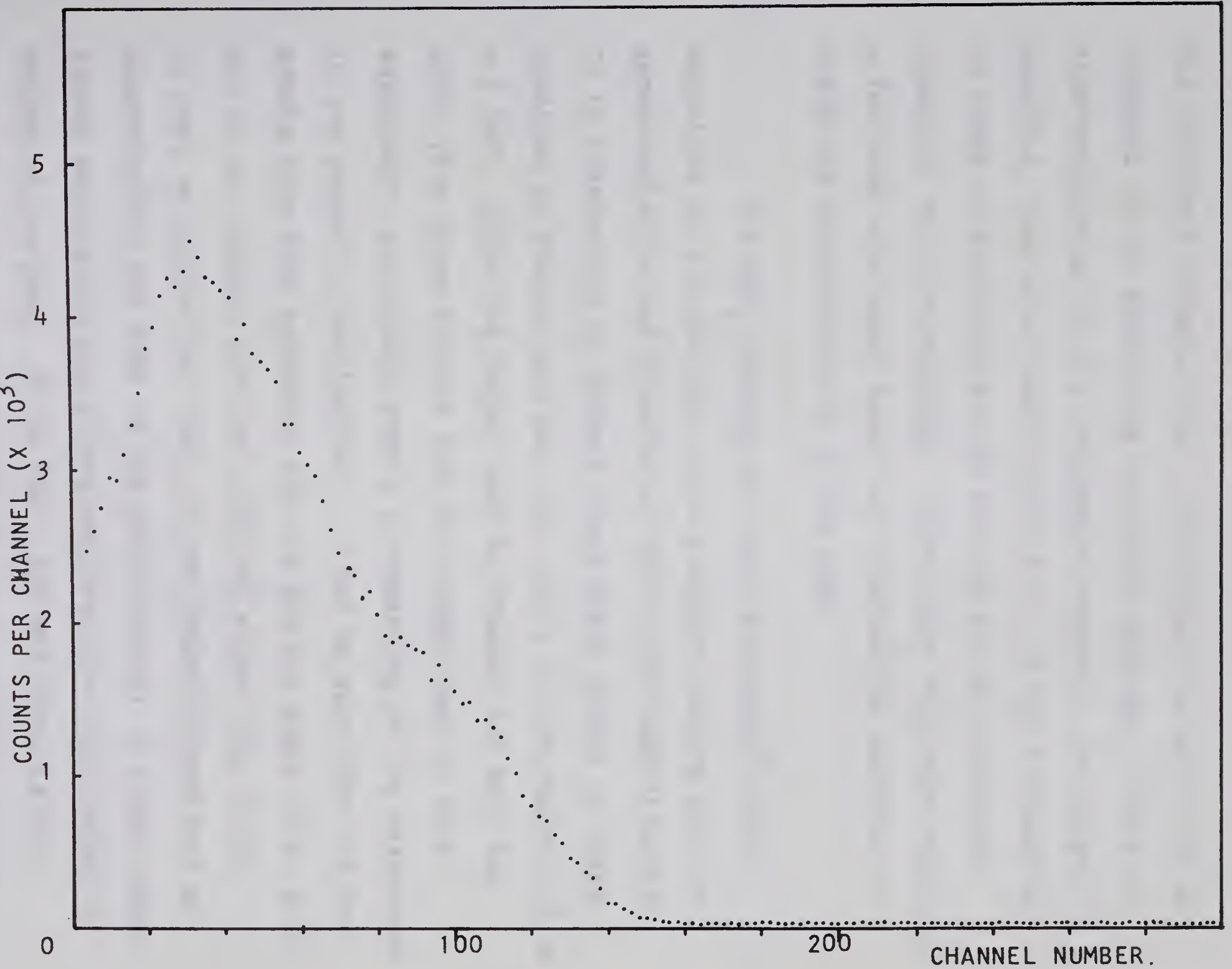

Fig. 2.8: Gated neutron spectrum.
(same conditions as in 2.7)

The corrected energies show a discrepancy of about 150 kev compared to the generating voltmeter readings. Since no other monitoring but the integrated charge on the target is possible, runs were taken from 4.5 to 5.4 MeV increasing by steps of approximately 20 kev and for an integrated charge of 50 microcoulombs. After these runs were completed a few runs were again taken for intermediate energies to check the reproducibility of the data.

The CaF_2 loading was about 100 $\mu g/cm^2$ thick deposited on a 0.002 inch thick platinum backing and the gamma-radiation was detected at 90° to the beam direction. It is interesting to compare these yield curves to those obtained by Freeman and Mani (op. cit), in the region 4.5 to 4.9 MeV. Since the target used by Freeman and Mani was about five times thinner than the target used in this experiment, one should expect a broadening of the resonances in the present investigation. It can be seen that the two graphs show some agreement for the 892 kev state (fig. 2.9) but do not compare for the 1.532 MeV state (fig. 2.10). It must be pointed out that, in the present experiment an approximation was made in the calculations: a linear background was assumed and subtracted from the total number of counts in the peak. Since the 1.532 MeV level is not strongly excited, this method may have partially affected

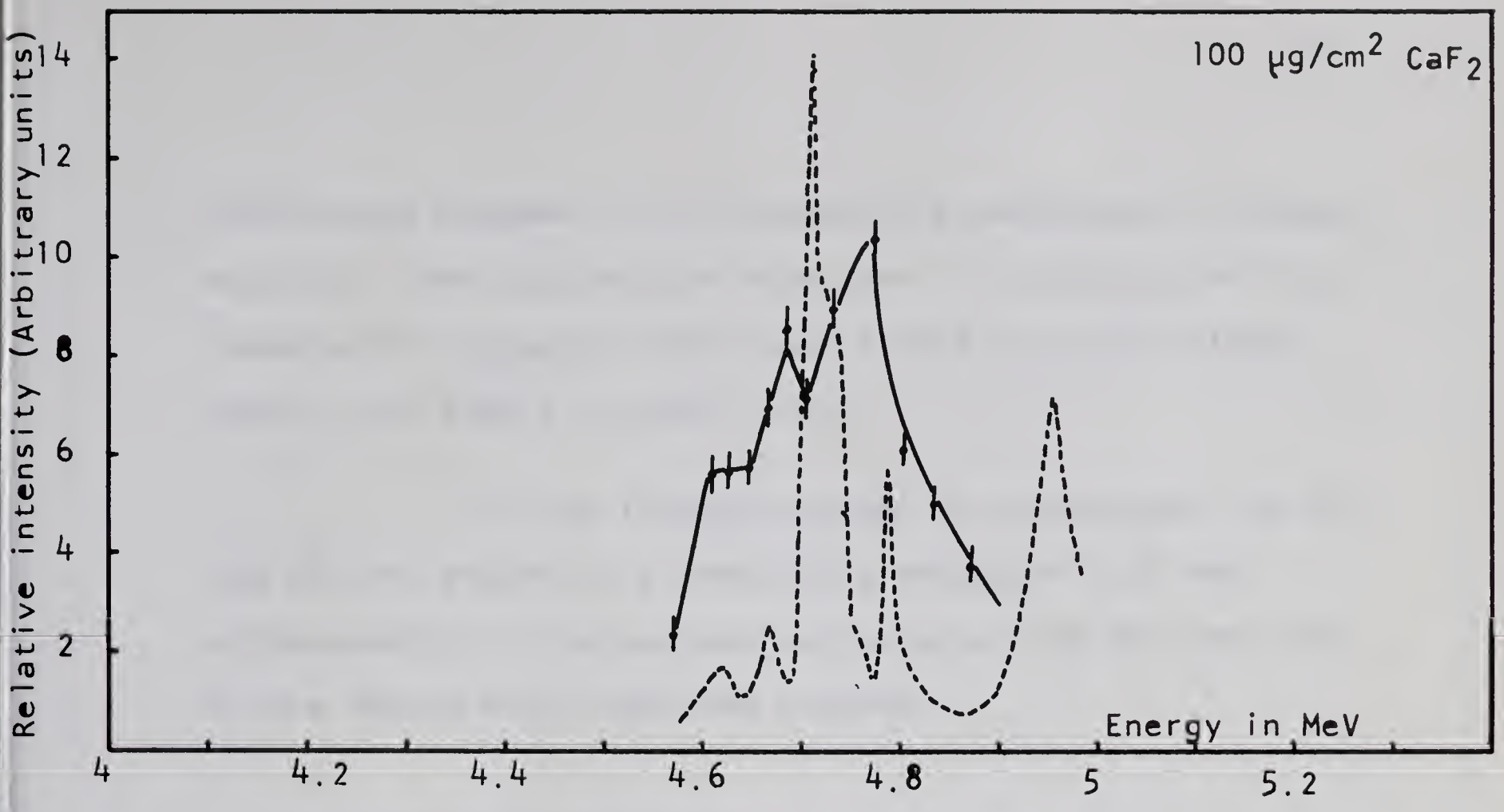

Fig. 2.10: Yield of the 1.532 MeV transition.

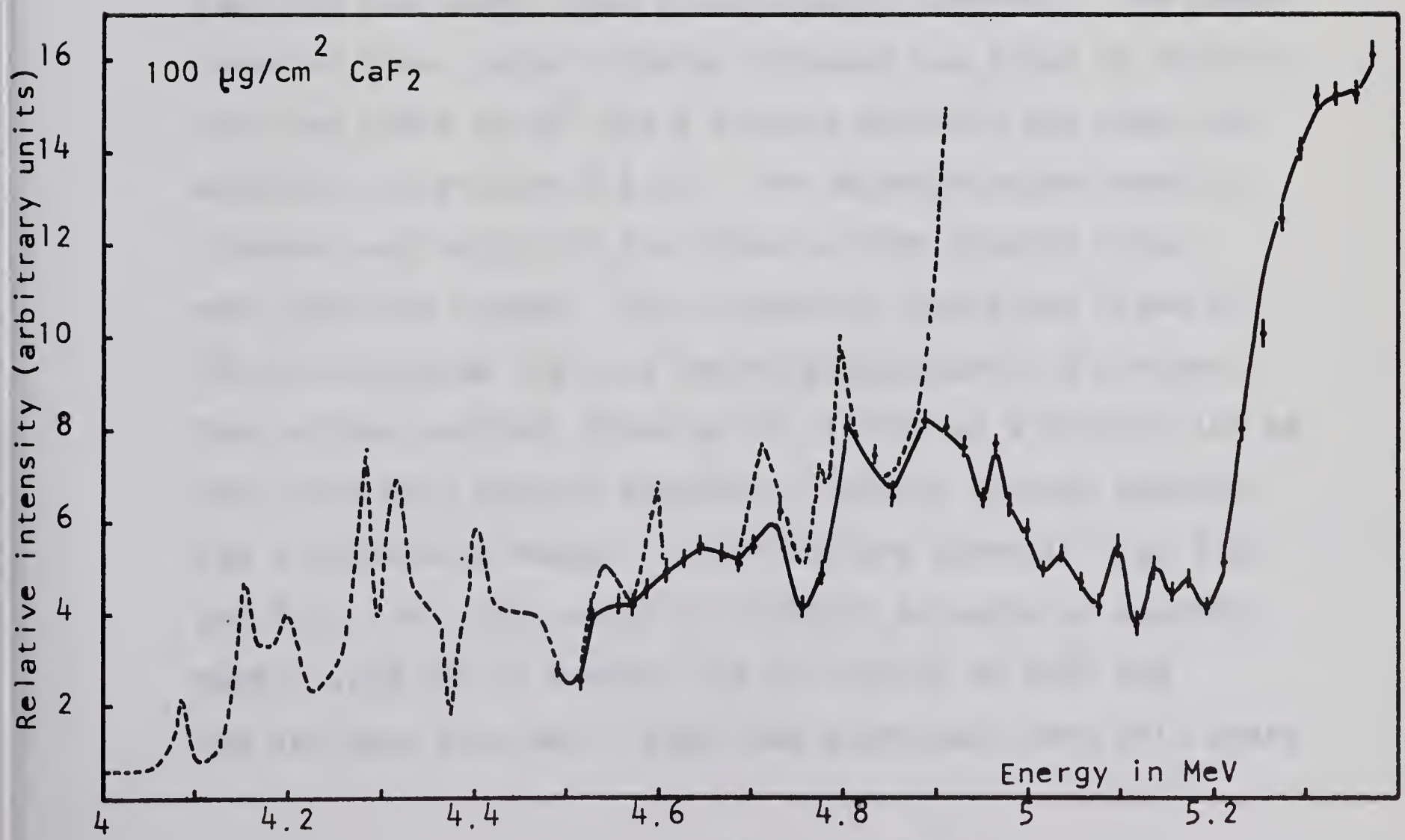

Fig. 2.9: Yield of the 892 keV transition.

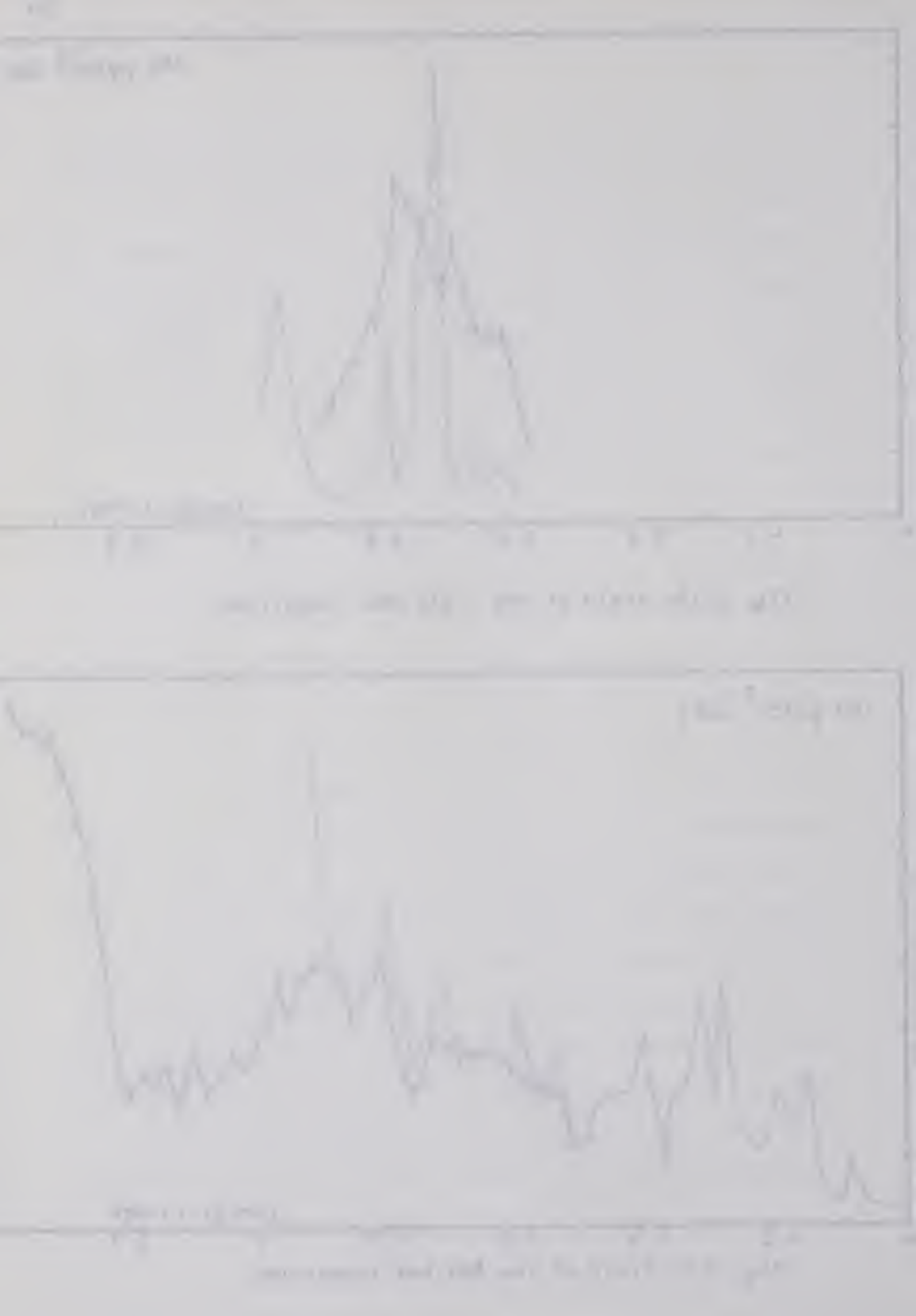

the results whereas, in the experiment performed by Freeman and Mani, the computations were done by a computer with a Gaussian fit program, which should lead to more reliable results for weakly excited levels.

It was finally decided to investigate the 587 and 892 kev states at a bombarding energy of 5.34 MeV corresponding to the maximum excitation of the 892 kev level in the region which had been studied.

e) Angular distributions.

For a given angle a singles (non-coincidence) spectrum was taken, then a coincidence spectrum. The gamma-detector whose target-crystal distance was fixed at 20.00 cm, was then moved to 90° and a singles spectrum was taken (as explained in section 2.3.a). The target chamber-detector distance and height of the detector were checked after each position change. The integrated charge was fixed at 250 microcoulombs and runs lasted approximately 2 minutes. The neutron counter, fixed at 0°, served as a monitor and as the coincident neutron detector. Typical singles spectra for a bombarding energy of 5.38 MeV are shown in fig. 2.11 and 2.12. At this energy the triplet situated at approximately 1.95 MeV is excited but the tables of Endt and van der Leun (op. cit.) show that gamma-rays from this state

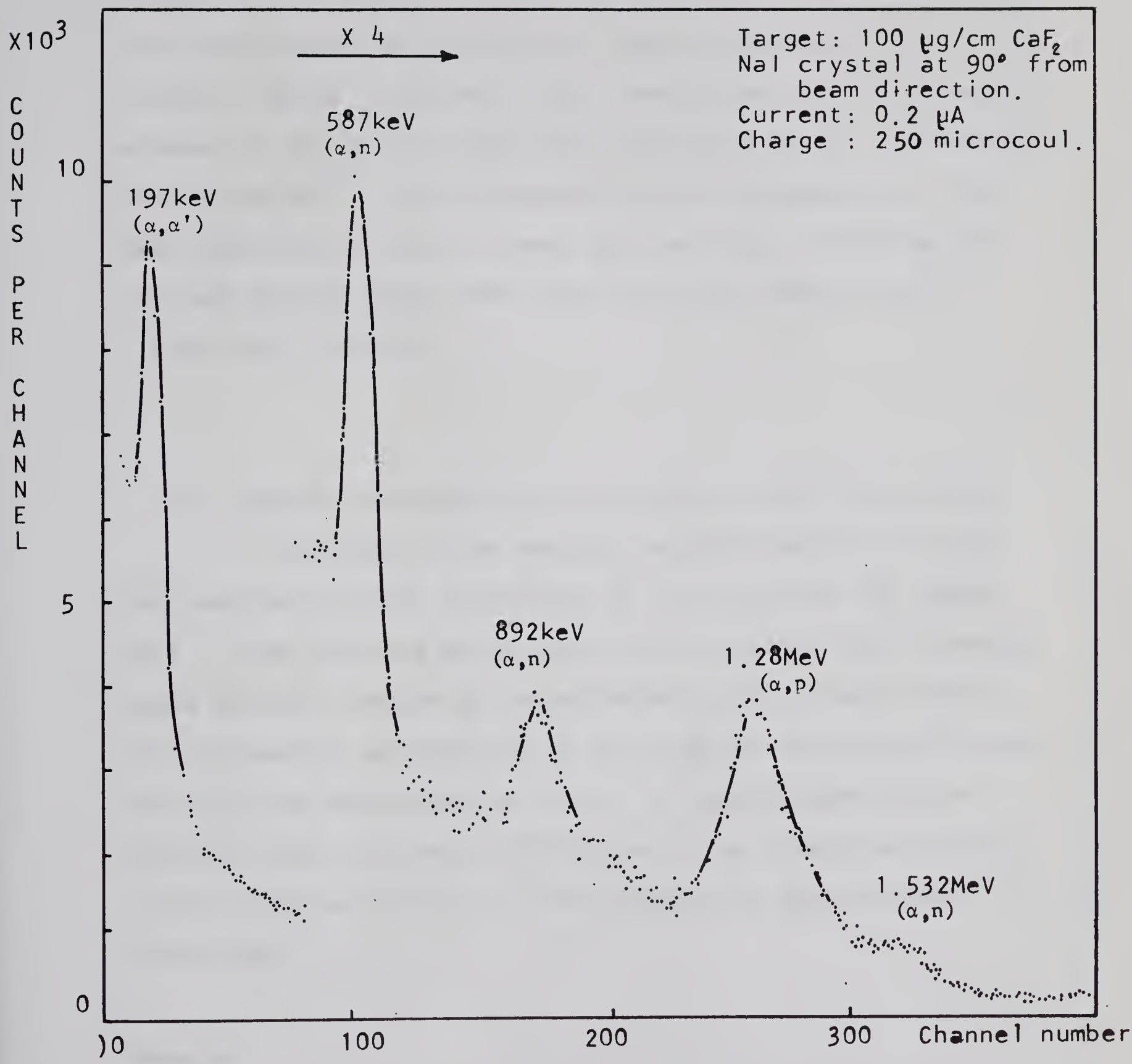

Fig 2.11: Ungated spectrum for a bombarding energy of 5.38 MeV.

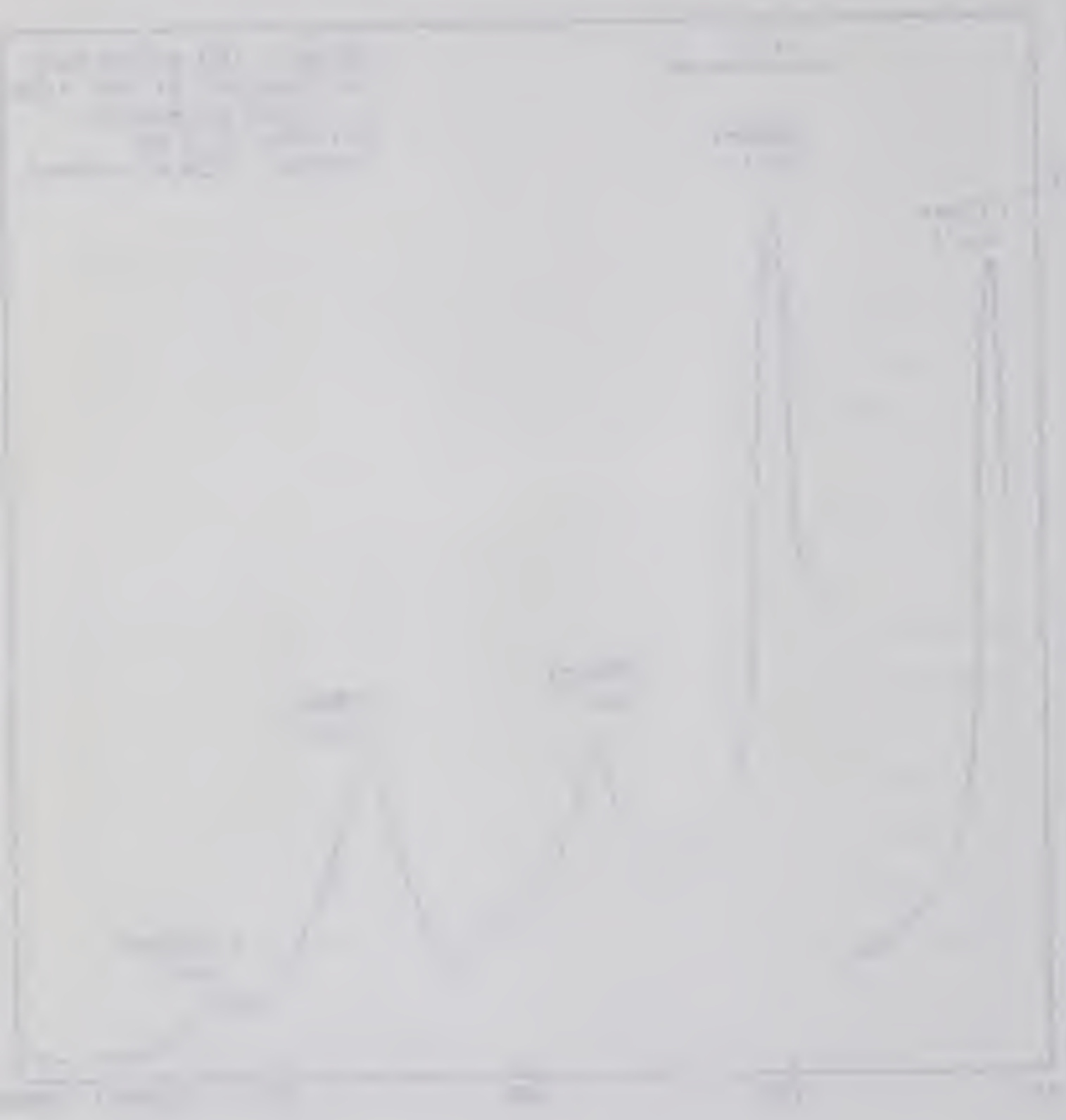

cascade to the ground via the 660 kev state. The transition from the triplet to the 660 kev state corresponds to an energy of about 1.290 MeV. This transition cannot be seen because of the strong competing transition of the 1.28 MeV level from Ne^{22}. The illustration 2.12 corresponds to the same spectrum but with a lower gain setting. It shows the two high energy gamma rays from the (α,p) reaction at 2.1 MeV and 3.35 MeV.

f) Angular correlations of the 587 and 892 kev states.

The axis of the neutron counter was at 90° from the beam axis and at a distance of 7.70 cm from the target axis. This destroys axial symmetry but allows runs at small gamma detector angles to be performed, and, as seen earlier, the fundamental assumptions of the angular correlation theory can still be considered as valid. A typical spectrum as shown in fig. 2.13 would correspond to an integrated charge of 250 microcoulombs and a running time of approximately 20 minutes.

Remarks:

1) The illustration 2.14 shows a background spectrum taken after the target had been used for about 24 hours. Three peaks can be seen which correspond to potassium 40 (1.46 MeV),

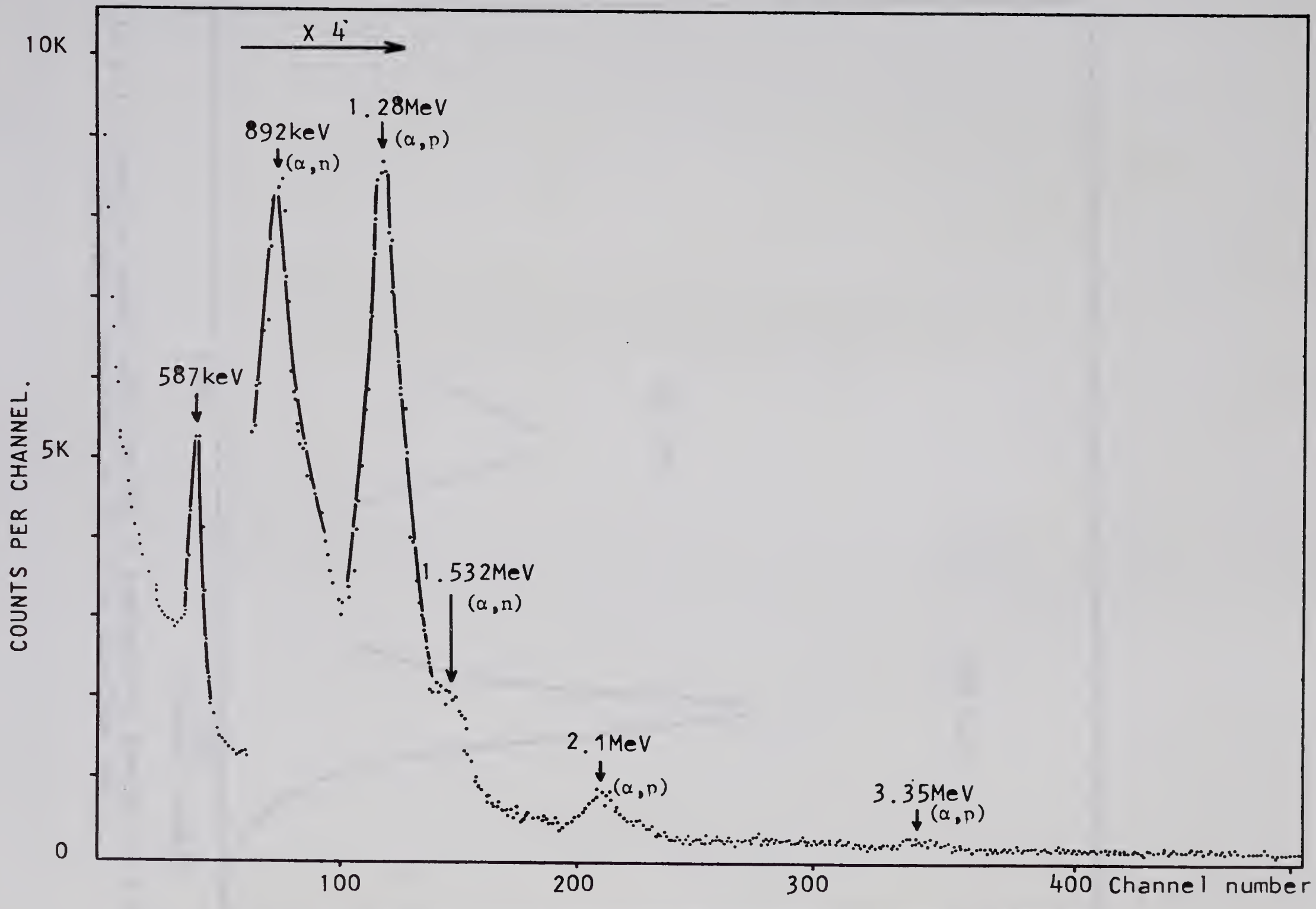

Fig 2.12: Same conditions as in fig 2.11, except for a gain setting divided by a factor of approximately 2.

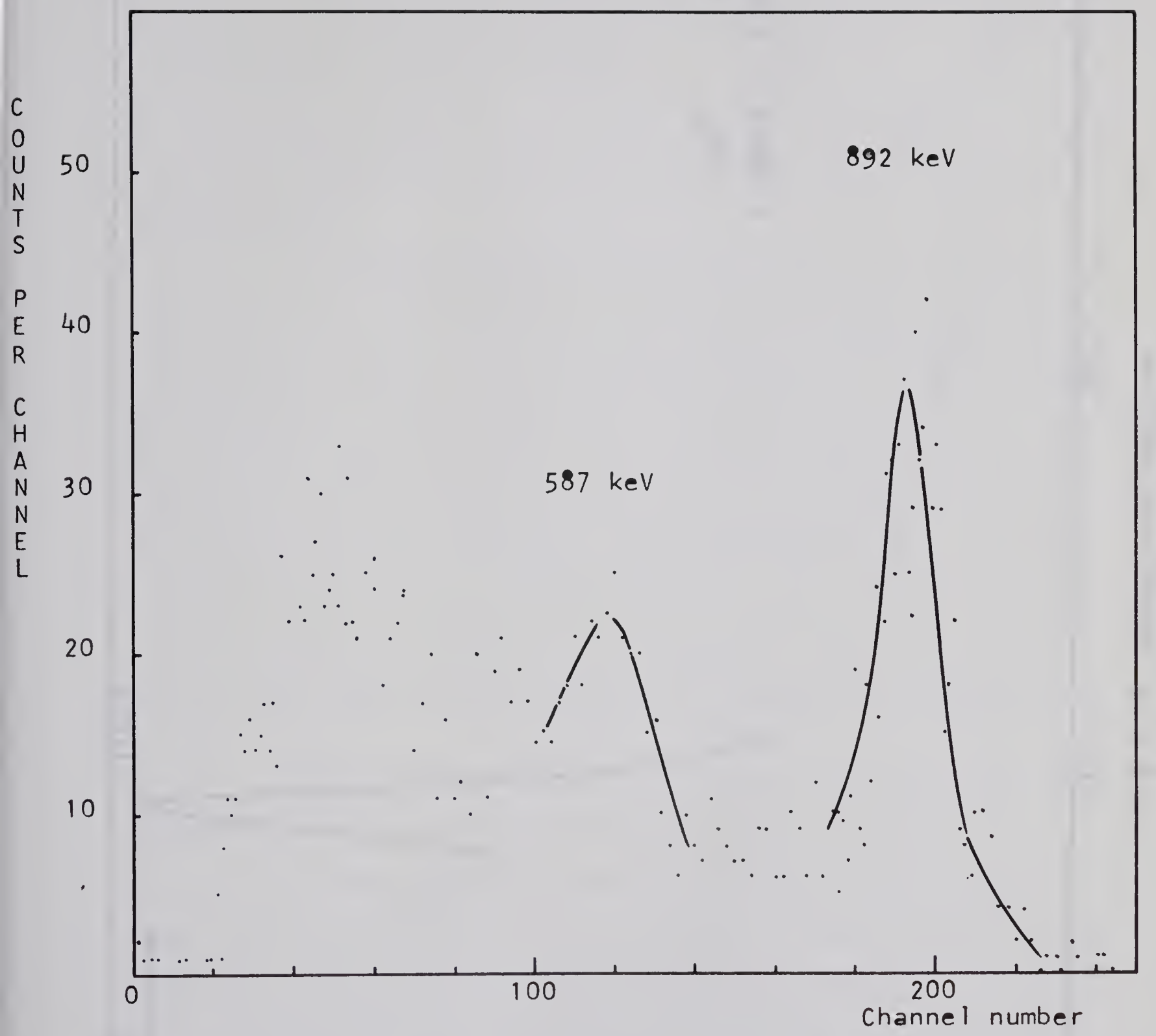

Fig 2.13: Neutron gated spectrum for a bombarding energy of 5.38MeV 3"x3" gamma-detector at 90 from the beam axis.

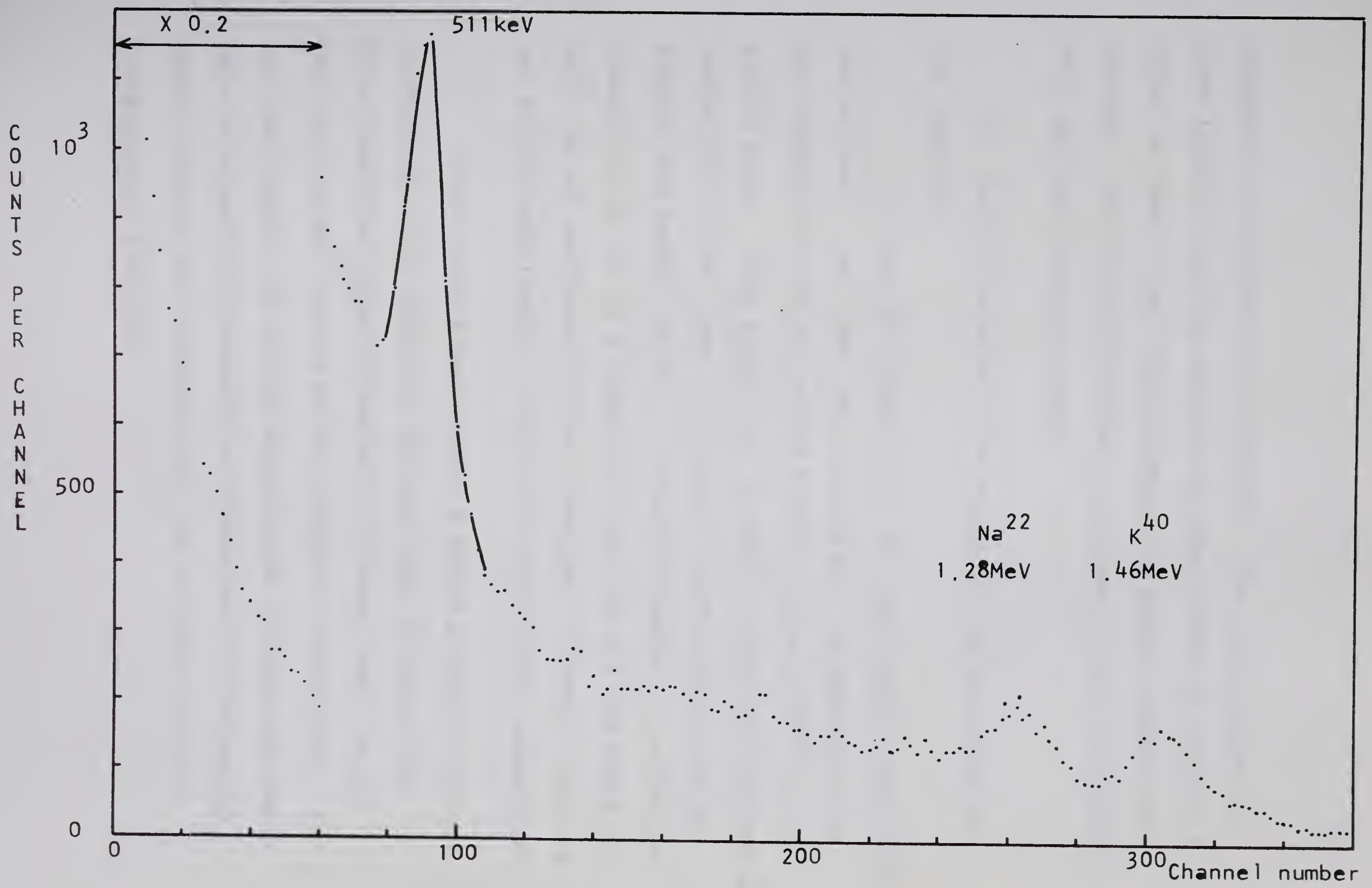

Fig 2.14: Background spectrum
Running time: 20 mn.

sodium 22 (1.28 MeV) and (511 kev). The sodium peaks had been induced from the reaction as was checked by placing a piece of lead 1 inch thick between the target chamber and counter. The potassium 40 activity comes from the environment and the detector itself.

2) Two points have to be mentioned from the study of the spectra:

i) From the figure 2.12, two high energy gamma-rays can be seen: the first one, at 3.35 MeV, is assumed to be the transition from the second excited state of Ne^{22} to the ground state. This transition is shown in Endt and Van der Leun tables (En 62) but does not appear in more recent work by Eswaran and Broude (Es 64). The second gamma-ray, which is assumed to be due to a transition from the 2.2 MeV state of Na^{22}, is not mentioned in the literature. However, there is not enough experimental evidence to verify these assumptions.

ii) In the gated spectra a peak is present which corresponds to an energy of 220 kev (fig. 2.4 and 2.5). This transition might correspond to a decay from the 2.2 MeV level in Na^{22} to one of the levels of the triplet. In this case again, not enough experimental evidence is available to support this assumption. Moreover, in the second series of runs, the yield was too low to make a further investigation possible.

2.4 Calculations and Corrections.

a. Area of the peaks.

The areas of the peaks were computed by the S.D.S. 920 computer from a Gaussian fit program written by W.G. Davies at the Nuclear Research Centre. The assumed nature of the function which fits the background is entered with the input data and may be linear, quadratic, exponential or a combination of these. After a few trials it appeared that best fits were obtained with a quadratic function describing the background. The normalization with respect to the neutron monitor was then applied. This normalization is tagged as "standard normalization." Independently, a second correction was applied which will be referred to as "correction for variations at 90^{o}" (see chapter III).

b. Correction for neutron counter.

As seen earlier, there is some absorption caused by the neutron counter for small angle positions. The absorption coefficients were determined by measuring the ratio of the intensities of the 587 kev and 892 kev peaks for neutron counter in and out, at a given position. The validity of the results shown in the next table, was verified by doing the same measurements with Na^{22} and Co^{60} sources and checking the continuity of the data.

Absorption coefficient	at	0°	15°	30°
for i) 587 kev		1.20	1.14	1.00
ii) 892 kev		1.15	1.08	1.00

Table 2.3 Correction factors for absorption in the neutron counter.

c. Correction for target thickness.

During the experiment, the target was either at 45° or 135° with respect to the beam axis.

For each position, the gamma-rays which are detected traverse a different thickness of the backing and this must be taken into account when corrections are applied. Details of calculations will be given in the appendix A 2 and results as follows for the two investigated gamma rays.

	Angle of detection defined with respect to the normal to the target (α).					
γ-ray energy	0°	15°	30°	45°	60°	75°
587 kev	0.997	0.997	0.9965	0.996	0.993	0.982
892 kev	0.998	0.998	0.998	0.9975	0.995	0.985

Table 2.4. Target thickness corrections for a 0.002" thick platinum backing. Gamma rays are detected at 20 cm from target.

d. Angular correlation and angular distribution fits.

The computation of the Legendre polynomial coefficients, A_k, was carried out by the nuclear research centre's LGP-30 computer from a program written by W. G. Davies. This program will accept any positive angle from 0° to 180° and will fit the data to any set of five A_k's from A_o to A_6 providing that there is one more data point than A_k's. For the analysis of experimental data, the fit was limited to fourth degree even Legendre polynomial coefficients, i.e. A_o, A_2 and A_4. For each set of data, two different kinds of analysis were performed:

i) analysis of the data corresponding to the ten measured positions from 0° to 135° by steps of 15°.

ii) analysis of the data corresponding to a set of seven angles from 0° to 90° and in which the data corresponding to positions symmetrical with respect to 90° had been averaged.

The output data are as follows:

i) best χ^2 fit for the experimental points

ii) unormalized coefficients A_o, A_2 and A_4

iii) coefficients A_2' and A_4' normalized with respect to A_o.

All the coefficients are given with their corresponding statistical and total errors.

e) Solid angle correction for gamma-ray detectors.

In section 1.2.b, it has been seen that the angular distribution may be expressed by:

$$W(\theta) = 1 + a'_2 P_2(\cos\theta) + a'_4 P_4(\cos\theta) + \ldots$$

where a'_2 and a'_4 are normalized with respect to a_o.

The a'_ks coefficients are related to the experimental coefficients, A'_ks, by:

$$a'_k \, Q_k = A'_k$$

where Q_k is the attenuation factor for the counter which detects the gamma rays and is defined by:

$$Q_k = \frac{J_k}{J_o} \quad .$$

and

$$J_k = \int_o^{\pi} \epsilon\,(\xi)\; P_k(\cos\ \xi)\, \sin\xi \; d\,\xi$$

$\epsilon(\xi)$ is the efficiency of the counter for a gamma-ray propagating in a direction at angle ξ to the axis of the counter.

Davisson (Da 64) has calculated and tabulated these coefficients, Q_k, for a 3" x 3" detector. But since these tables are limited to a maximum source to crystal face distance of 15 cm, the values of Q_k's had to be extrapolated for a distance of 20 cm.

Values of Q_k are equal for 587 kev and 892 kev gamma-rays and are given by:

$$Q_2 = 0.987$$

$$Q_4 = 0.950 \quad .$$

CHAPTER III.

Experimental results.

a. Validity of the different ways of analyzing the data.

Following the methods described in Chapter II, the angular distributions and the angular correlations have been analyzed. Figures 3.3 to 3.10 (inclusive) show the different angular correlation and distribution data and the calculated best fits.

It is interesting to compare the different ways the data have been analyzed for a given transition, namely:

i) by considering the neutron monitor normalization ("standard normalization") first fitting on 10 points and later on 7 points only.

ii) by applying a second correction monitored by the relative intensity of the peak from the ungated spectrum taken at 90° from the beam axis ("correction for variations at 90°").

The following two illustrations (fig. 3.1 and 3.2) give the results of the computations. The "a" coefficients are plotted with their errors corresponding to the larger of statistical and total errors*.

---

*Note: the total error as defined by Rose (Ro 53) is a comparison between the true coefficient a_{λ}^{0} and the least squares value a_{λ}. This error is shown to be defined by the product σX where σ(statistical error) is the root mean square deviation of the a_s' .

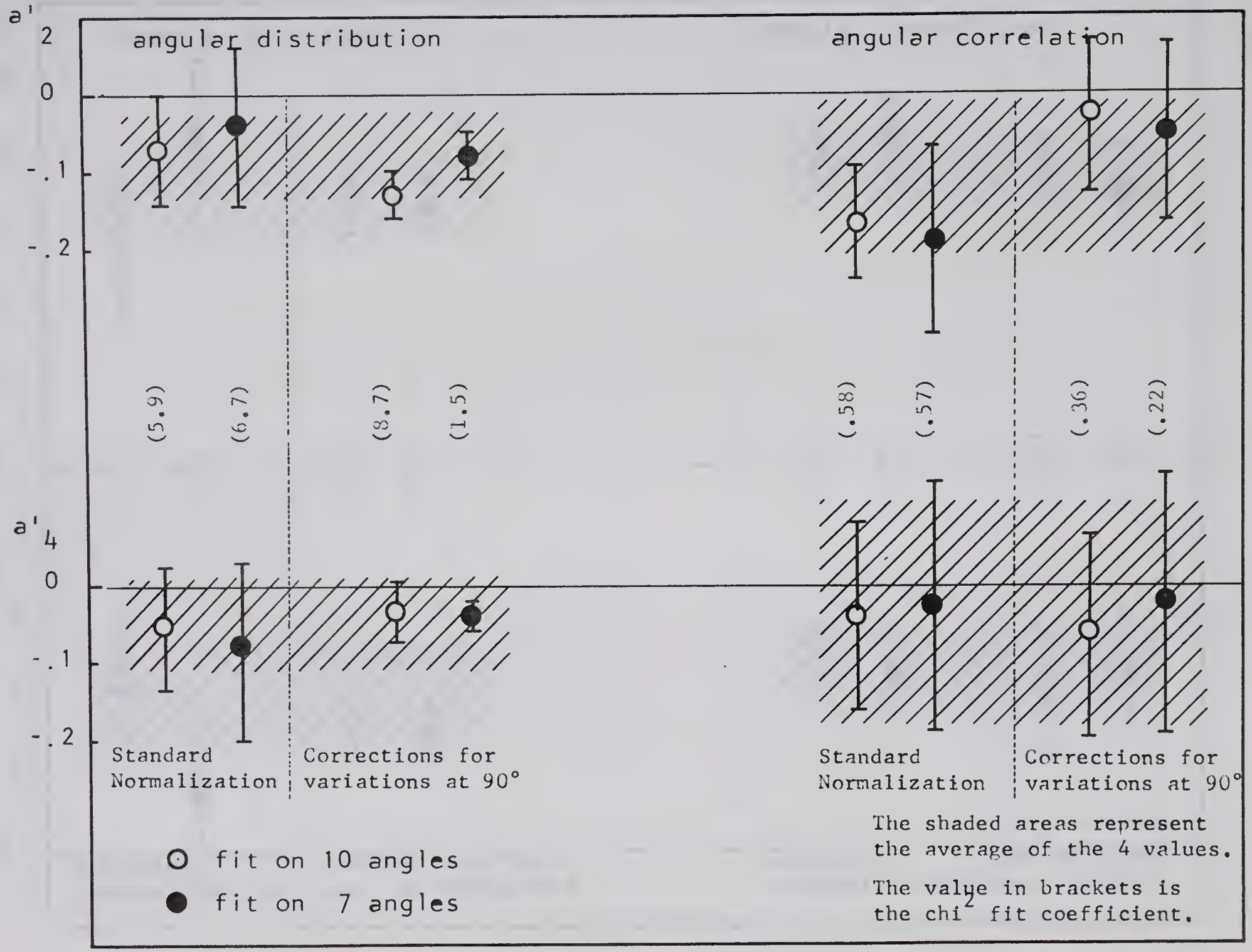

Fig 3.1: Comparison of angular distribution and angular correlation coefficients for the 587 keV state.

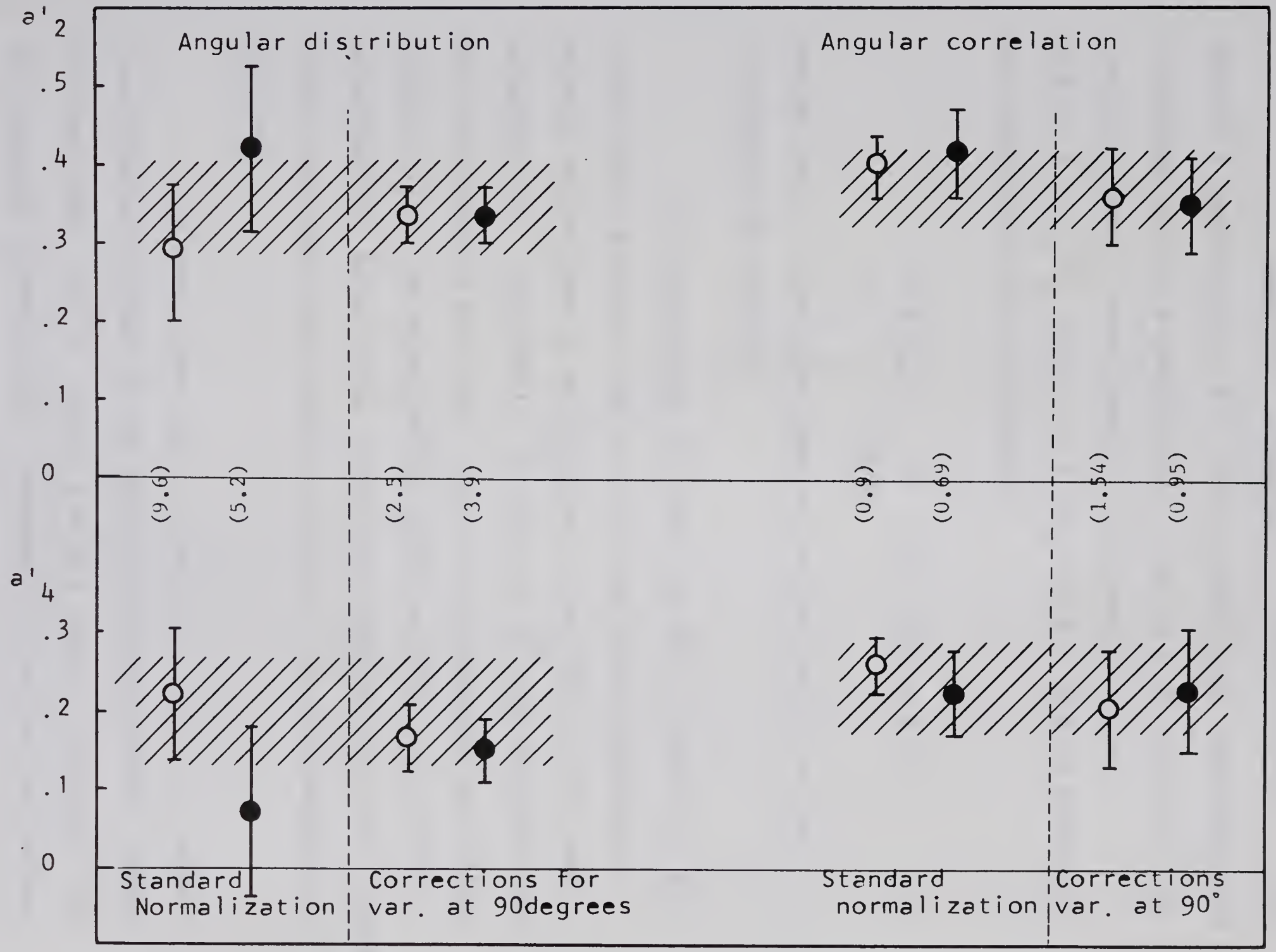

Fig 3.2: Comparison of angular distribution and angular correlation coefficients for the 892 keV state. (cf. previous plot)

An important parameter to consider first is the best fit coefficient, χ^2. This coefficient describes the closeness of the experimental curve to a function of the fourth order of even Legendre polynomials (i.e., $W(\theta) = 1 + a'_2 P_2 (\cos \theta) + a'_4 P_4 \cos \theta)$ and is given by the minimum of the expression:

$$\sum_i W_i \left(\mu_i - \sum_{\lambda_{even}}^{4} a_\lambda P_\lambda (\cos \theta_i)\right)^2$$

where the μ_i's are the observed values and w_i's the corresponding weights.

As pointed out by Rose (Ro 53), a value of χ^2 appreciably greater than one implies either systematic errors or the use of an incorrect function in the least squares fit. Conversely, a value of χ^2 much smaller than one indicates either that too many polynomials are introduced to fit the experimental graph or that one of the experimental data has an error much smaller than the others. (This smallest error is thus taken as the most significant weight).

As seen from fig. 3.1 and 3.2, the only cases of poor fits are those of the angular distributions. Except for one case, the χ^2 values are all smaller than one for the angular correlations. Because statistics are better

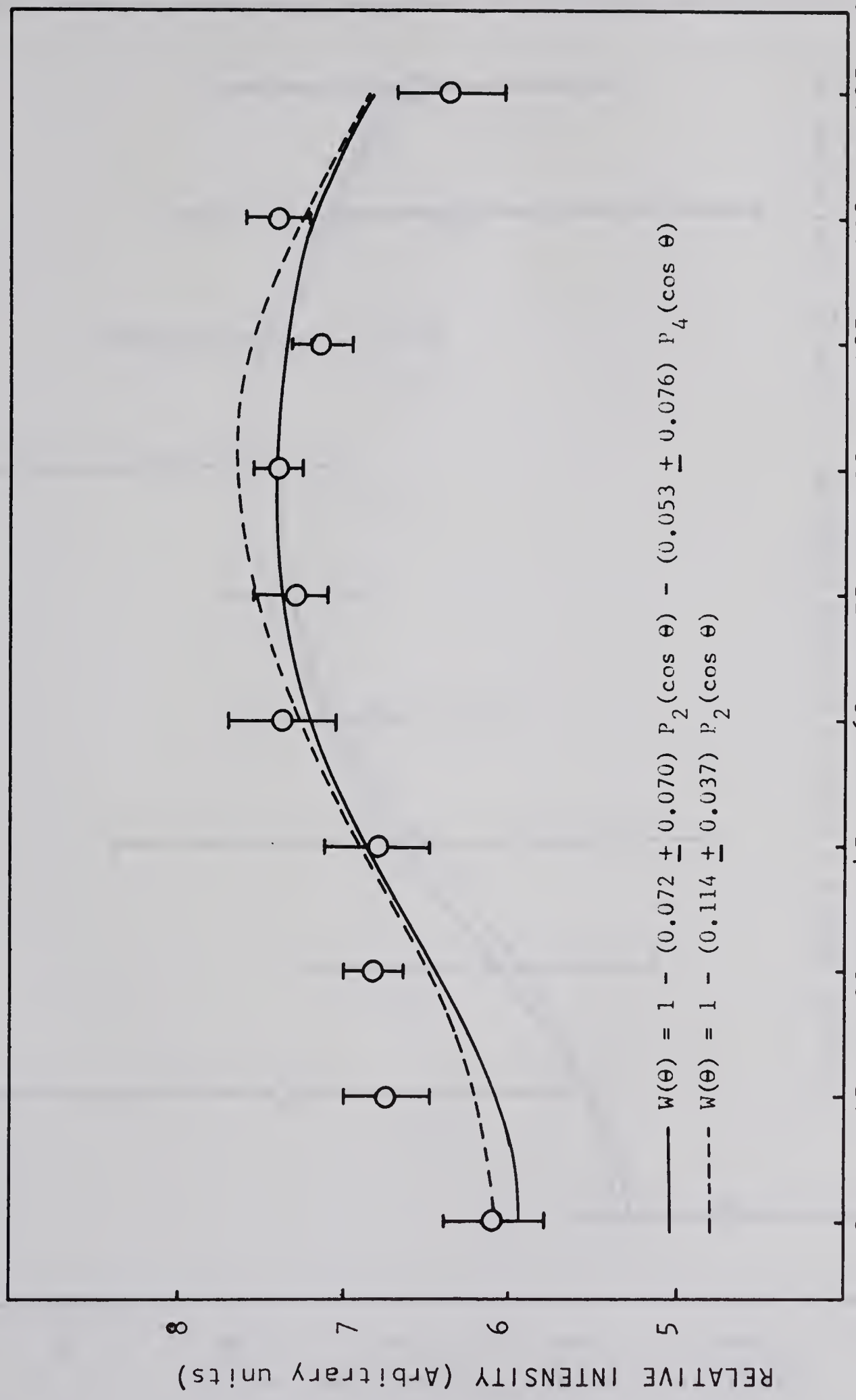

Fig 3.3: Measured gamma-ray distribution of the 587 keV state.
(Standard normalization)

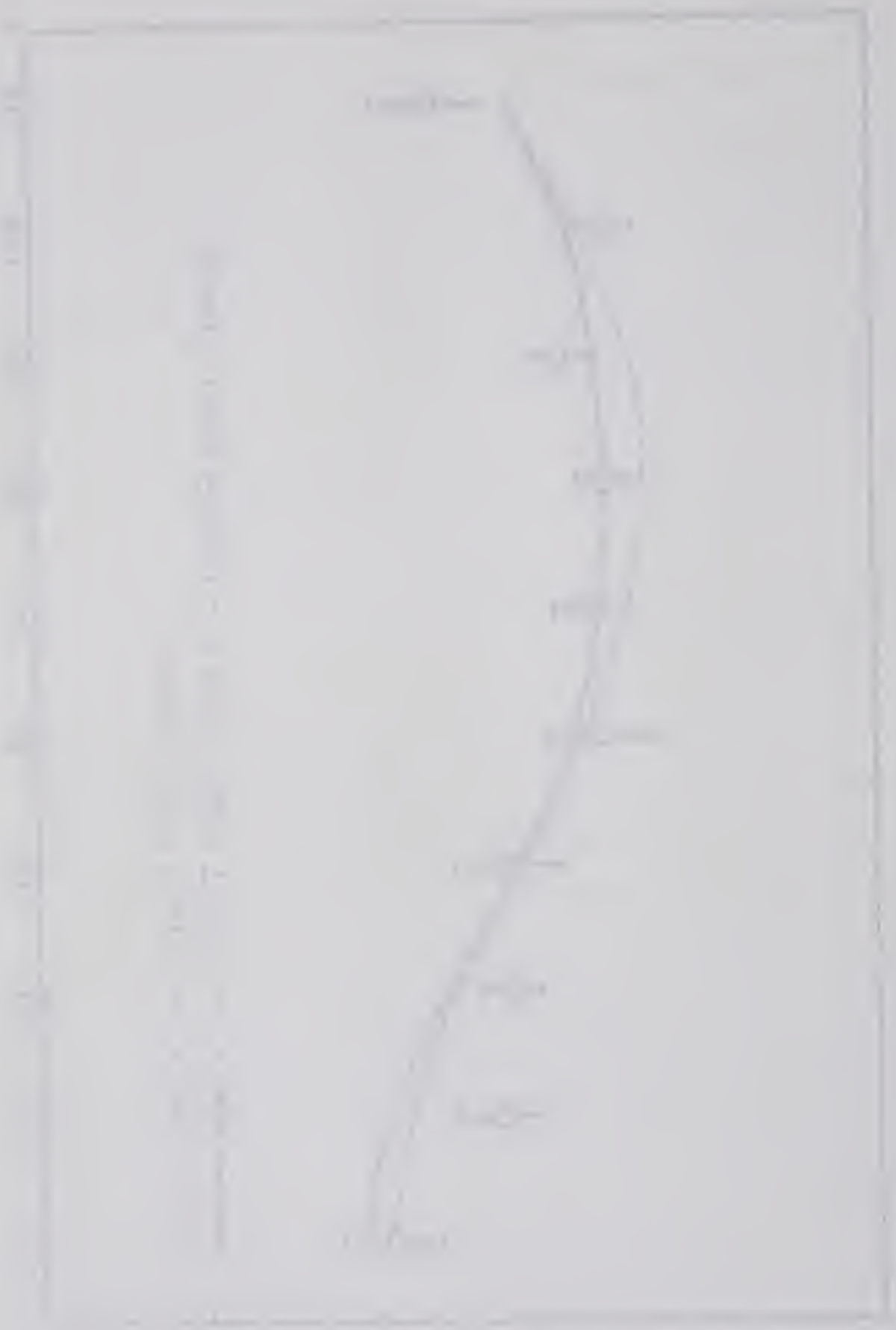

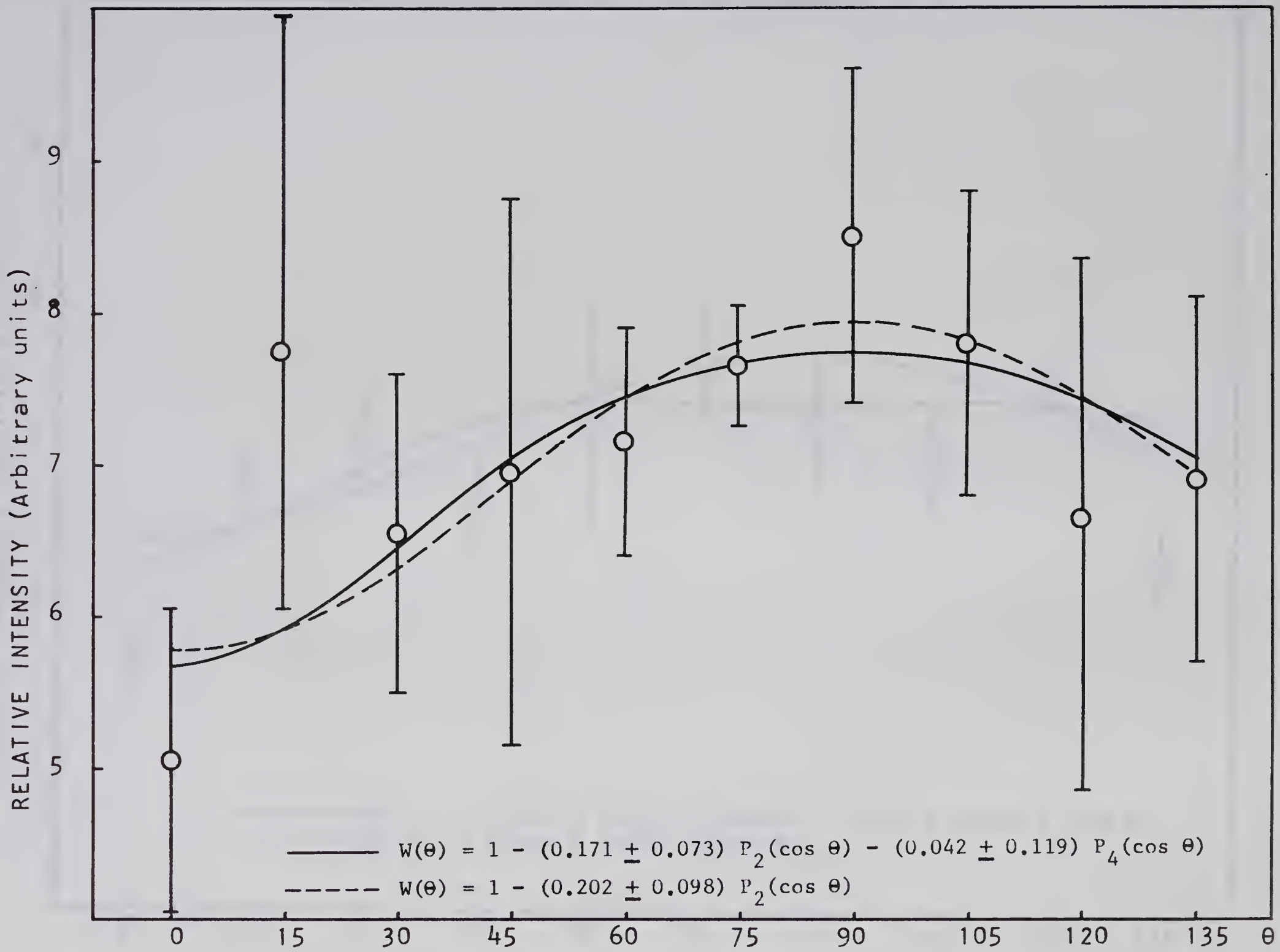

Fig 3.4: Measured neutron gamma-ray correlation of the 587 keV state
("Standard normalization")

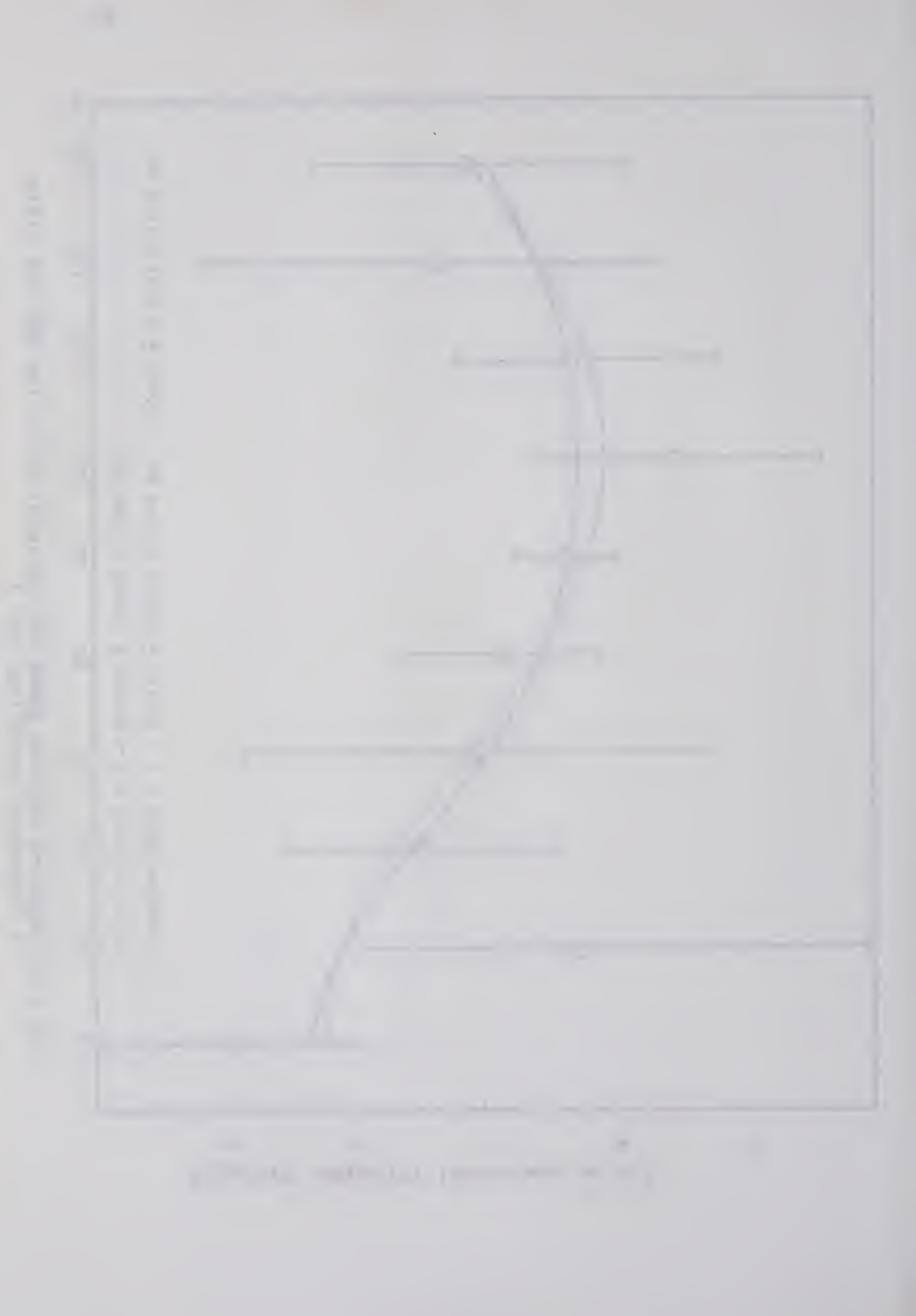

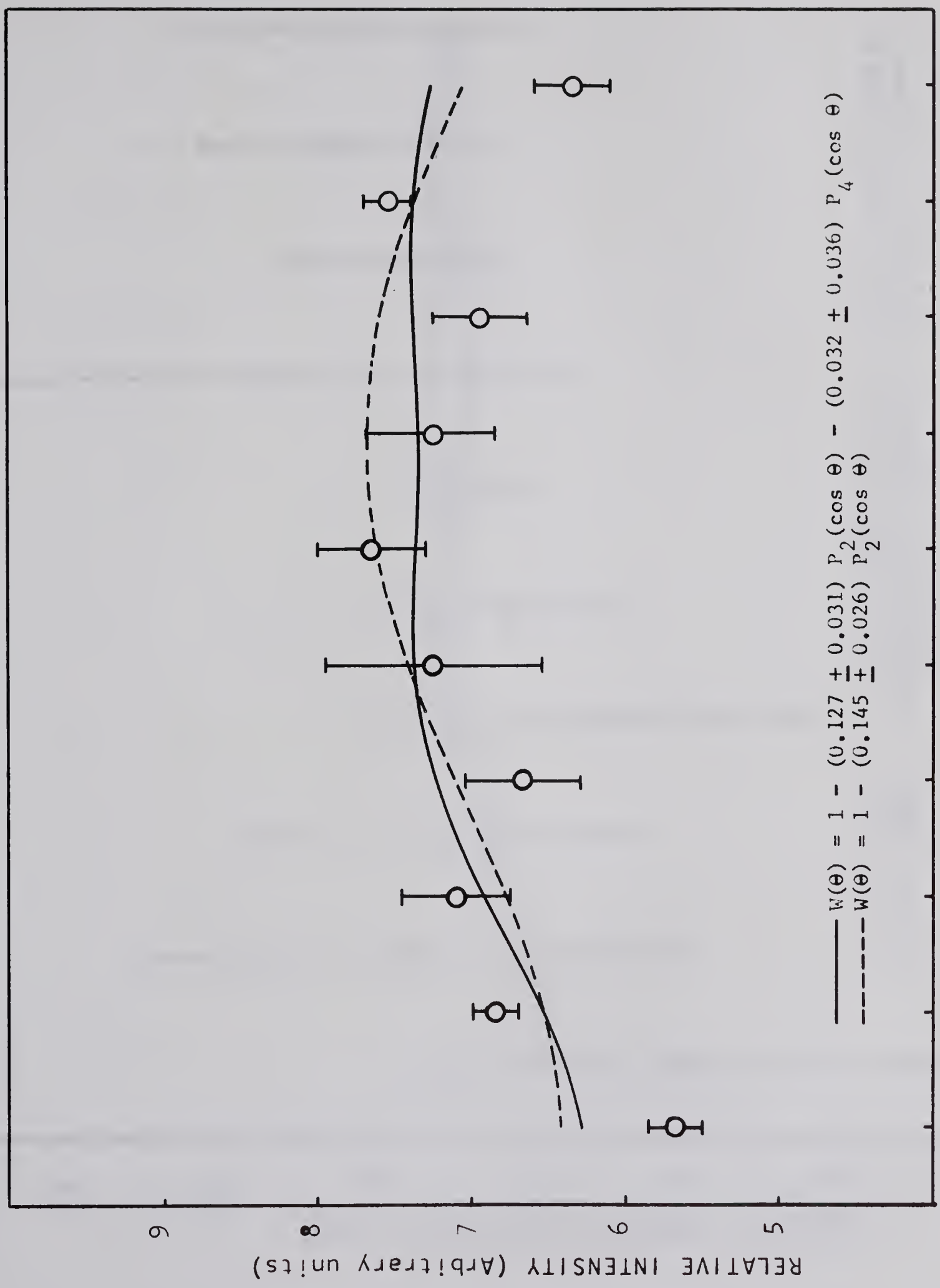

Fig 3.5: Measured gamma-ray distribution of the 587 keV state.
"corrections for variations at 90 degrees"

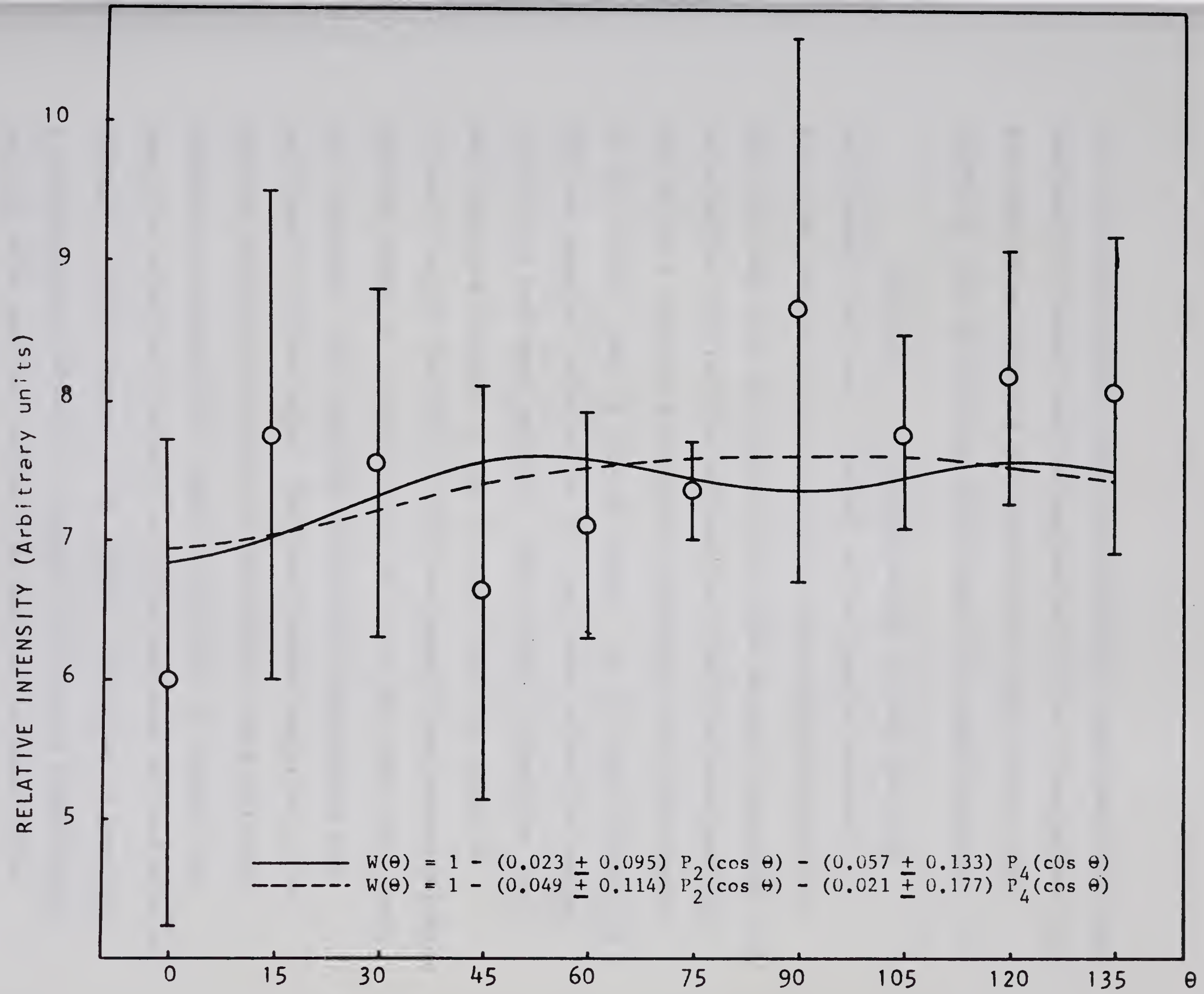

Fig 3.6: Measured neutron gamma-ray correlation of the 587 keV state. "corrections for variations at 90 degrees"

for the distribution than the correlation measurements, some systematic errors, such as assymetry of the correlation table, are much more revealed by distribution data and are the cause of this difference in the best fit coefficients.

Secondly, it is interesting to see how much improvement has been obtained by the second correction. From the various plots of angular distributions and from fig. 3.1 and 3.2, one can see that the second correction led to a better fit for the two angular distributions and for the 587 kev angular correlation, although the improvement in the latter case is not as large. On the other hand, the 892 kev angular correlation fit got worse after the second correction had been applied. This second correction has been applied because it was noticed that the relative intensities of the 587 and 892 kev peaks from non-coincidence spectra taken at a position of 90° from the beam axis, were not constant. The complete correlation experiment was performed in three days. For the longest day's run, the maximum absolute variation of the 892 kev peak relative intensity reached 13%. However, it must be pointed out that the relative intensity of this peak was defined with an average relative error of 4%. This correction is used as a normalization method in angular correlation experiments dealing with natural radioactive sources because finite

lifetimes are then involved. For induced reactions, where machine time may be limited, this method could hardly be applied if long runs are required for good statistics. Moreover, since the angle positions are taken at random this kind of error should cancel out after averaging all the data corresponding to one position.

As a conclusion for this first part, it can be said that the normalization with respect to the neutron monitor and the usual corrections (target thickness, finite solid angle of detector) are necessary and sufficient.

A second point which would have proved interesting to investigate was whether the results from the measurements of the 587 kev transition lead to the known 1^+ assignment.

Unfortunately, such a conclusion cannot be reached because of three reasons:

i) large errors of the experimental results

ii) multiple feeding of the 587 kev level

iii) long lifetime of the 660 kev and 587 kev levels.

These three causes will now be examined.

i) Large errors of the experimental results.

Fig 3.3, 3.4 and 3.5 show two different computed fits for the experimental data: one is limited to the fourth

order of even Legendre polynomials, the latter to the second order only. Because of the large errors, the value of the χ^2 best fit coefficient remained either much larger than one (for angular distribution) or much smaller than one (for angular correlation). From these different computations, the values of the a' coefficients are given with relative errors ranging from 20 to 120%. Such large errors would probably lead to ambiguous spin assignment even if no other corrections were to be applied.

ii) Multiple feeding of the 587 kev level.

It can be seen from diagram 2.1 that the 587 kev level is not only fed by neutrons but also by gamma-rays cascading via the 660 kev level from the 2.2 MeV state and the triplet at $\simeq$ 1.9 MeV. One should then consider the complete correlation and distribution formulae in which the unobserved transitions are taken into account. As shown by Devons and Goldfarb (De 57), the formulae can still be reduced to the form $W(\theta) = \sum_k a_k Q_k P_k(\cos\theta)$ but then, the a_k's also describe the unobserved radiations through various Racah and Clebsh-Gordon coefficients. It has been seen earlier (Chapter I) that if a state fed only by neutrons has spin 0 or 1, the coefficients of angular distributions and angular correlations are identical because no further restriction

on the number of magnetic substates which are fed is brought by the correlation. Since the 2.2 MeV level and the triplet levels may have spins different from 0 and 1, one should then expect different a coefficients for angular distribution and angular correlation. However, for a bombarding energy of 5.38 MeV, these levels are probably weakly excited. (It must be recalled that, in the last series of runs, no transition corresponding to an energy of more than 892 kev was observed on the n-γ coincidence spectra because the yield was too low for the running time). Consequently, some assumptions might be made if this were the only correction to apply. However, as will now be seen another perturbing condition is happening.

iii) Long lifetimes.

According to Temmer and Heydenburg (Te 58), the 660 kev level has a half-life $\tau_{\frac{1}{2}}$ equal to 14 nanoseconds and the 587 kev a $\tau_{\frac{1}{2}}$ equal to 266 nanoseconds. As seen earlier (section 2.1.b) the resolving time of the coincidence circuit is approximately 40 nanoseconds. As a result of the lifetime of the 587 kev excited state being much longer than the coincidence resolving time, the n-γ coincidence counting rate will be lowered. As a matter of fact, the problem is more complex because, as shown by Steffen and Frauenfelder (St 64), perturbations of the correlations are

possible when the lifetime of the intermediate state is longer than 10^{-11} seconds. Perturbed correlations have been studied extensively in the recent years and the most relevant papers on this topic can be found in (Ka 64). However, these studies have been mainly directed towards the study of radioisotopes and the influence of their physical and chemical environment.

If one considers a cascade $I_i \rightarrow I \rightarrow I_f$, the angular correlation of gamma rays will be altered if the nuclei in their intermediate state are subject to torque, due to the interaction of either the magnetic dipole moment with an extranuclear field B or the electric quadrupole moment Q with an electric field gradient $\frac{\partial^2 V}{\partial Z^2}$. These interactions produce a precession of the nuclei around the symmetry axis which results in a time dependence in the density matrix of the intermediate state. In solids, the magnetic interaction can usually be neglected in comparison with the quadrupole interaction (St 64). The magnitude of the quadrupole interaction is described by the precession frequency ω which is proportional to Q and $\frac{\partial^2 V}{\partial Z^2}$.

The correlation function is multiplied by an attenuation factor $G_k(f)$ which is a function of the parameters of the states involved and the precession frequency. Generally,

this attenuation factor is determined experimentally (interesting examples are given in (Fr 55)) and leads to the value of the electric quadrupole moment of the state which is studied.

In the present case, the situation is even more complex since two long lifetime states are involved and although it might be possible to assume some value for the electric field gradient due to surrounding electrons, the electric quadrupole moments are not known.

In conclusion, very little can be said about a possible assignment of the 587 kev level from the experimental results. Long calculations and many simplifying assumptions would be necessary and are not worthwhile because of the large errors of these results.

b. Spin assignment of the 892 kev level.

The situation for this level is fortunately clear cut: both values of a'_2 and a'_4 are well defined, no multiple feeding is involved. A question may be raised however concerning the half life of this level. No datum is actually given but compared with other nuclei [a table in (Ka 64) gives all the measured lifetimes for the levels of all nuclei] it is a good assumption that the half life of the

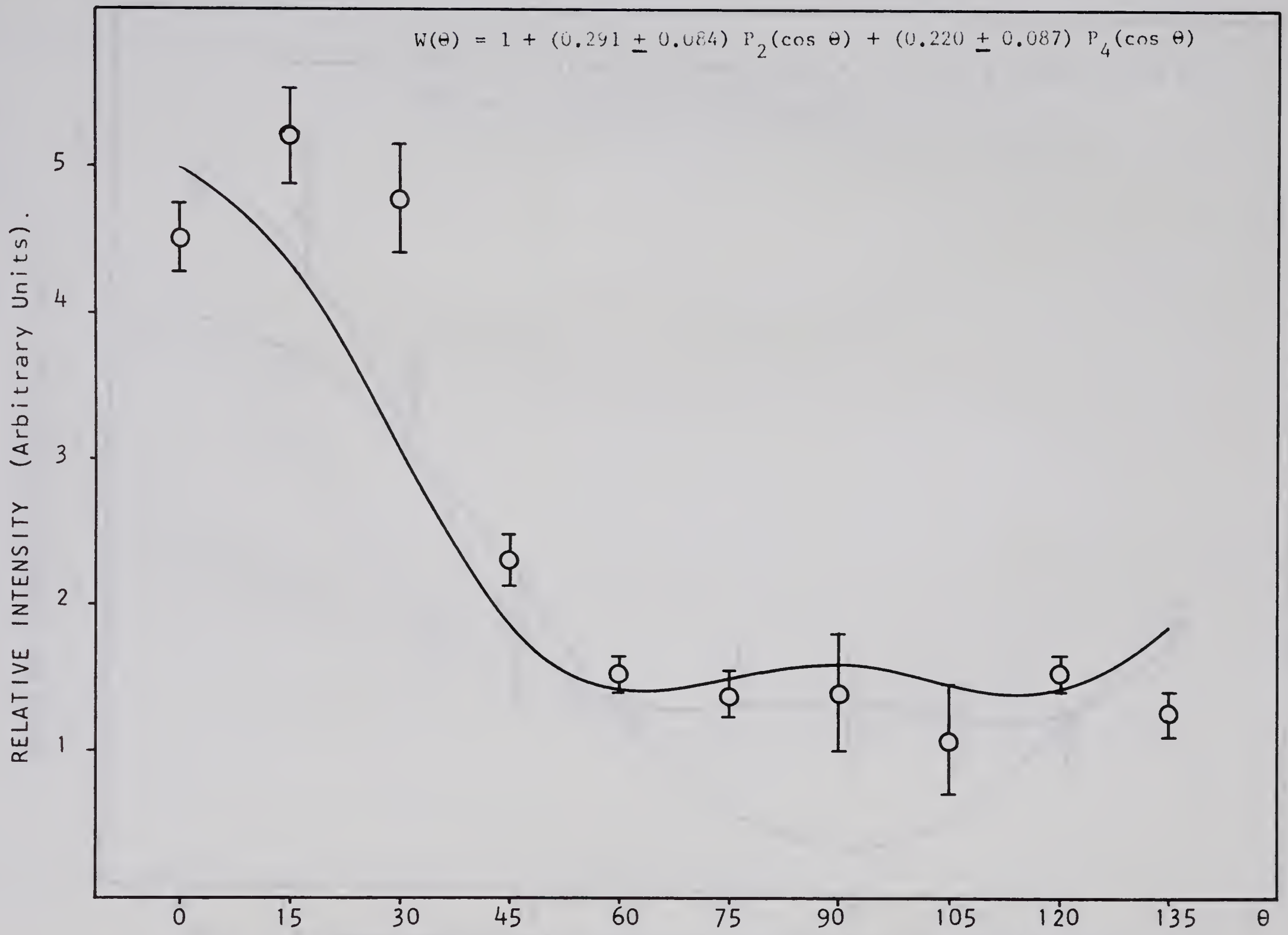

Fig. 3.7: Measured gamma-ray distribution of the 892 keV level. "Standard Normalization".

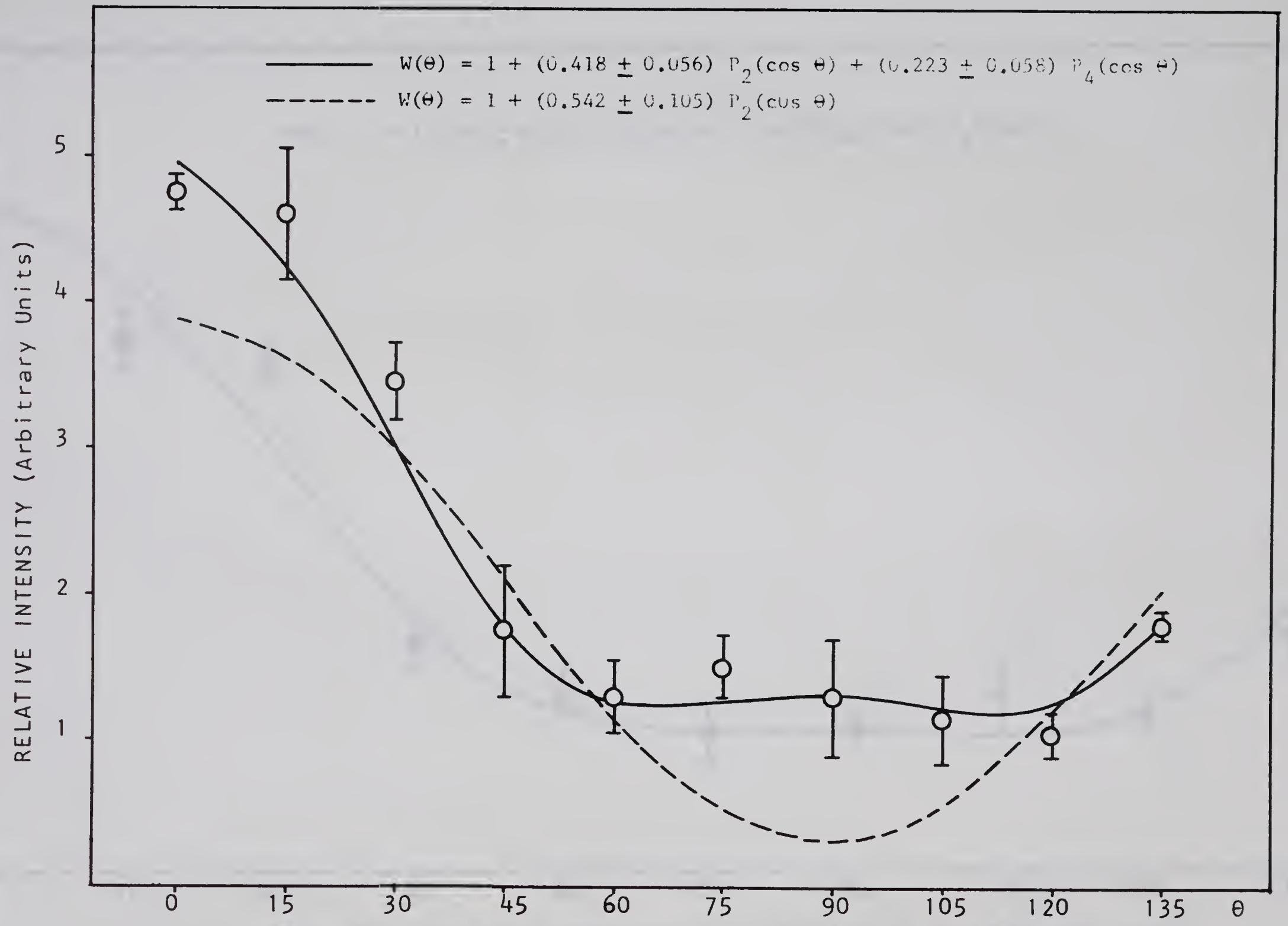

Fig. 3.8: Measured neutron gamma-ray correlation of the 892 keV level. "Standard normalization".

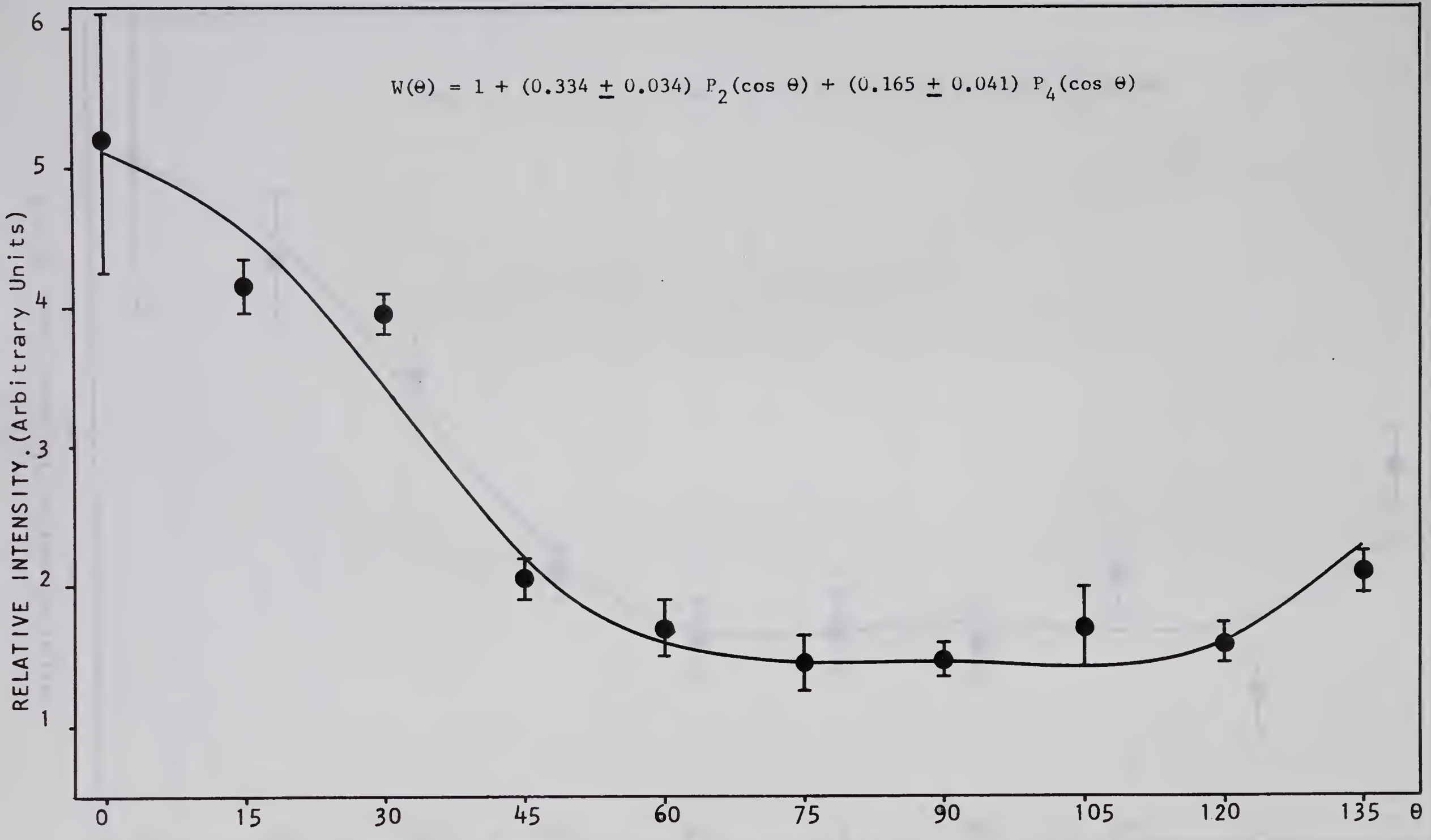

Fig. 3.9: Measured gamma-ray distribution of the 892 keV level. "corrections for variations at 90 degrees"

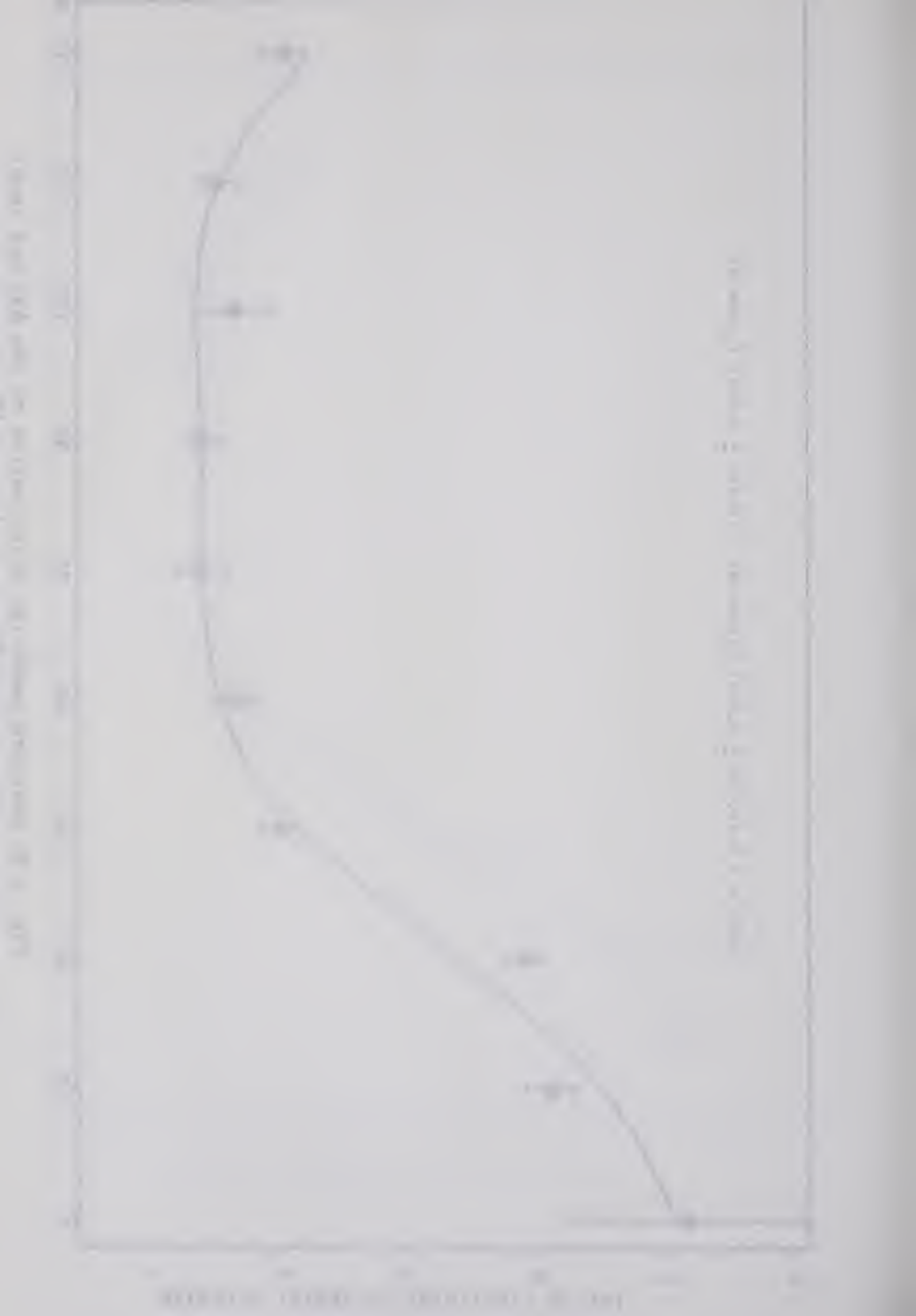

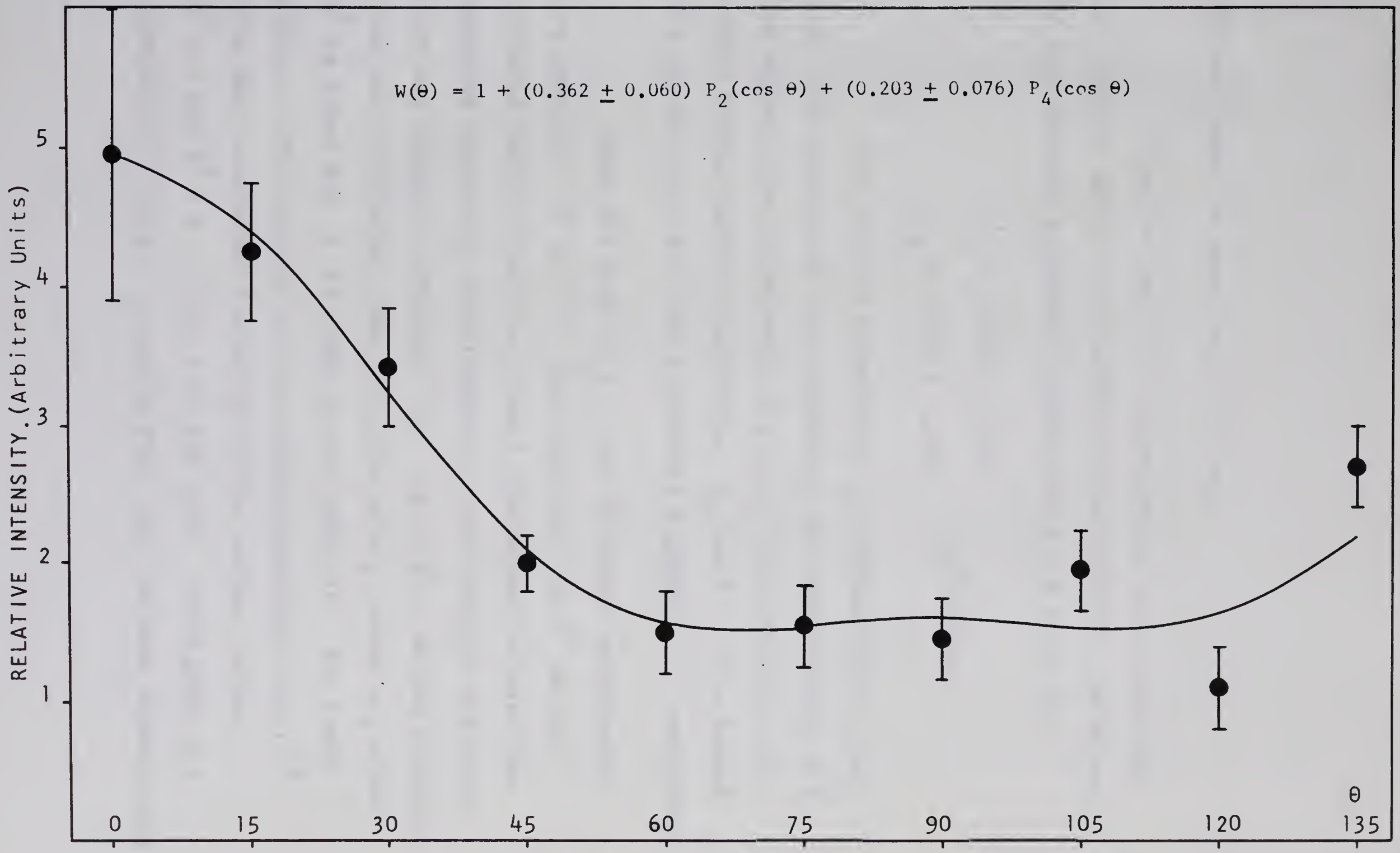

Fig. 3.10: Measured neutron gamma-ray correlation of the 892 keV level. "corrections for variations at 90 degrees"

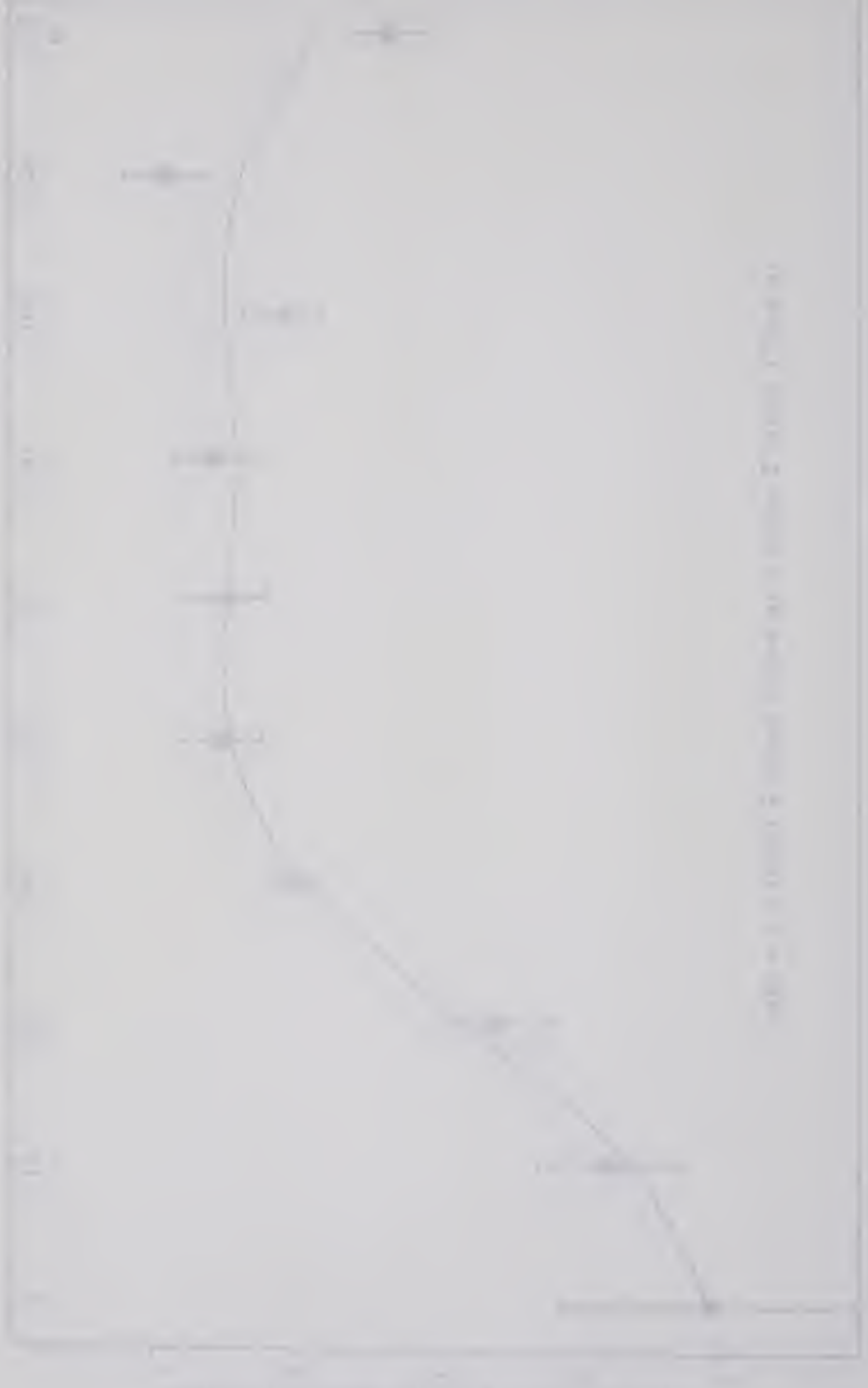

892 kev level is less than 10^{-11} sec.

From the best fit corresponding to the analysis of 7 angles using the "standard normalization", the values of the Legendre polynomial coefficients are given by:

$$a'_2 = 0.418 \pm 0.047$$
$$a'_4 = 0.223 \pm 0.048 \qquad (\chi^2 = 0.69)$$

This angular correlation is represented in graph 3.8. The continuous line represents the computed best fit. The dotted line corresponds to a best fit limited to the second degree Legendre polynomial $P_2(\cos\theta)$. This second fit is very poor and thus eliminates a priori a 1^+ assignment.

From the sign of a'_4, two different assignments are possible: 2^+ or 4^+. Qualitatively, the 2^+ is more probable because there is a small discrepancy between the Legendre polynomial coefficients for both angular distribution and angular correlation (cf. fig. 3.2). Better information can be obtained from the plots of a'_2 versus a'_4 where χ^2 is fixed and δ is taken as the variable. For these plots, a few values of the population parameter ratio, χ^2, have been considered including the two extreme values $\chi^2 = 0$ and $\chi^2 = \infty$, (fig. 3.11 and 3.12). From graph 3.11 (transition 4 to 3), it can be seen that the area representing

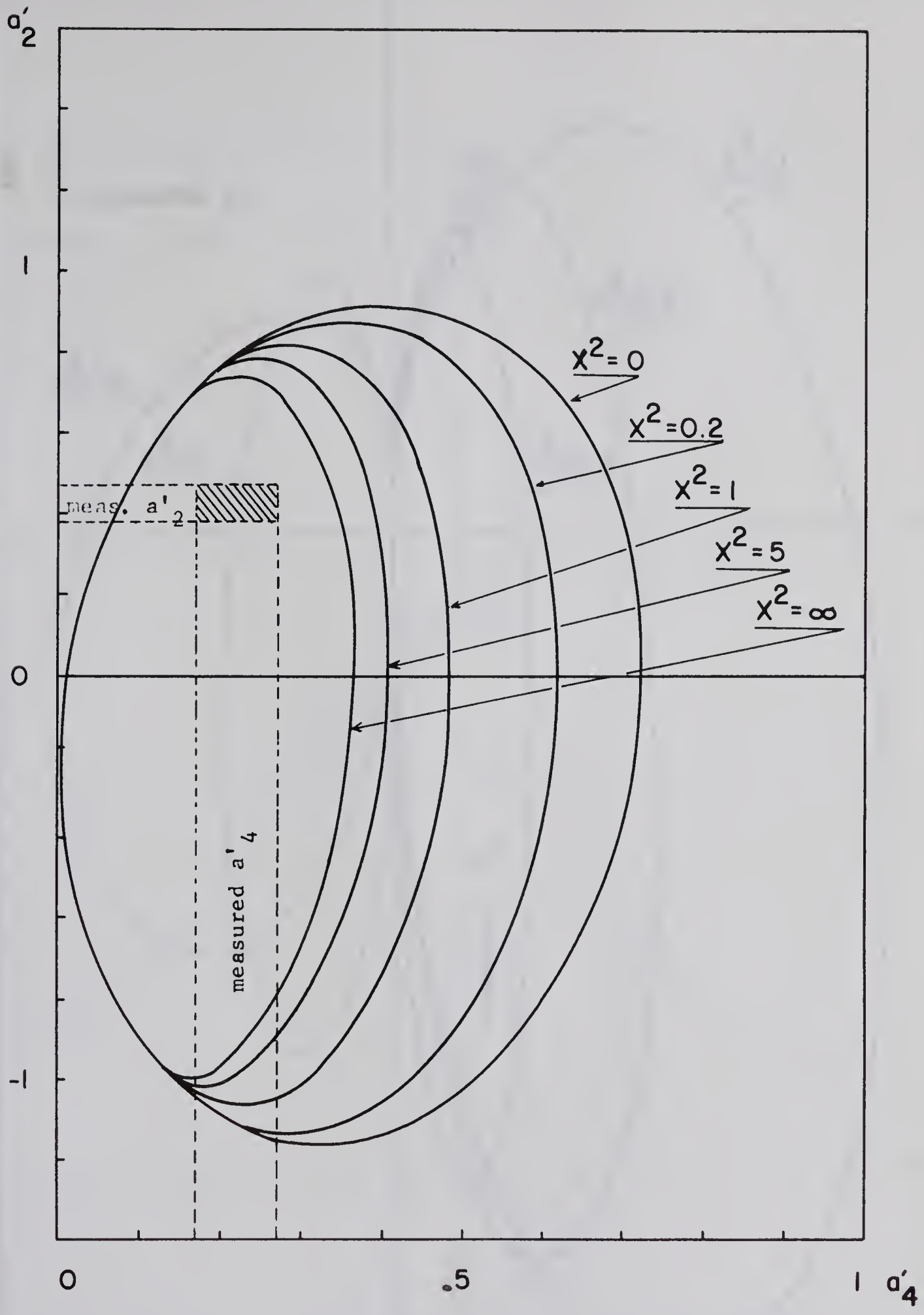

Fig 3.11: Plots of a'_2 versus a'_4 for all values of δ and for a 4 to 3 spin change, assuming s-wave neutrons only.
Different values of the population parameters ratio, x^2, are considered.

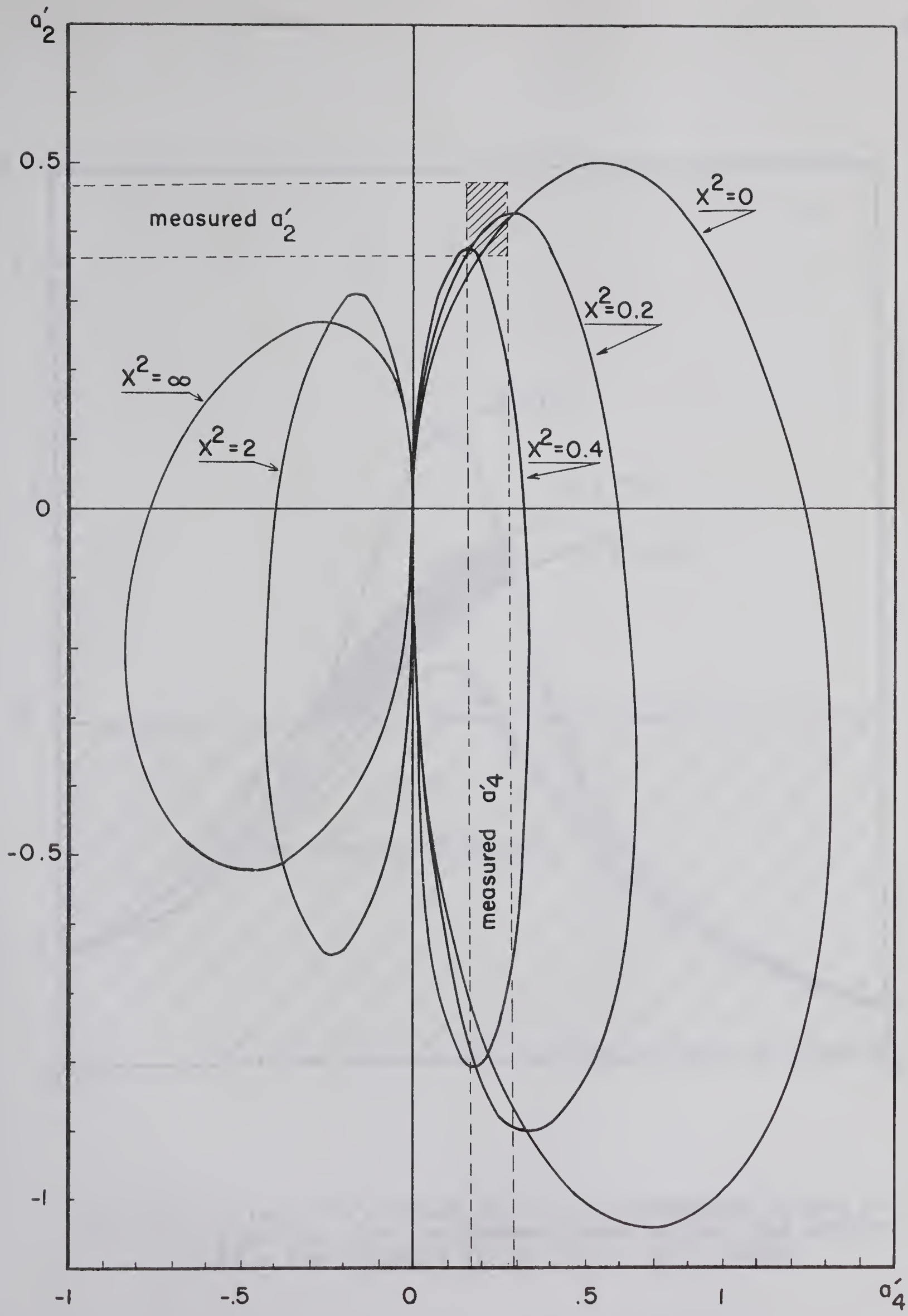

Fig 3.12: Plots of a'_2 versus a'_4 for all values of δ and for a 2 to 3 spin change assuming s-wave neutrons only. Different values of the population parameters are considered.

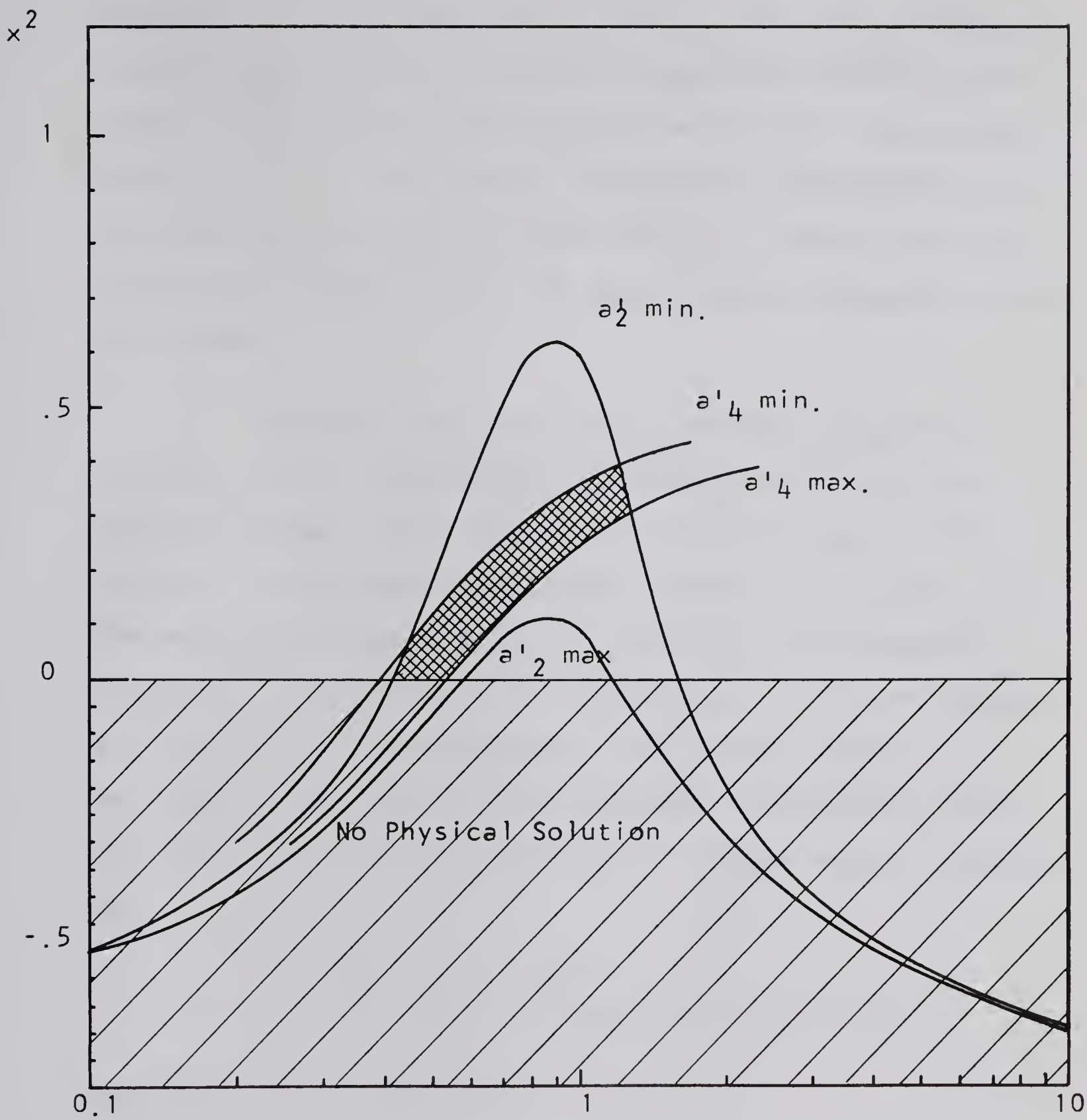

Fig 3.13: A plot of x^2 versus δ using the measured values of a_2' and a_4' for the 892keV gamma ray and the predicted a coefficients for a 2 to 3 spin change.

the experimental values of a'_2 and a'_4 does not correspond to any physical solution since it does not intersect the curves. From graph 3.12 (transition 2 to 3), one can see that for $X^2 = 0$ there is an intersection corresponding to an approximate value of δ equal to 0.5. One can then conclude that the spin 2^+ is the only possible assignment for this state.

Because there are two unquantized parameters involved in the correlation, the mixing ratio δ is not sharply defined. The figure 3.13 gives the plot of X^2 versus δ for the two experimental values of a'_2 and a'_4. The measured values a'_2 and a'_4 are put in the Legendre polynomial equations for the transition 2 to 3 (see Appendix A 1) and X^2 is then determined for a proper range of δ. Two regions are thus defined and their intersection gives the most probable range of X^2 and δ. These values are given by:

$$X^2 = 0 \text{ to } 0.40$$

$$\delta = 0.41 \text{ to } 1.03 \quad \text{or} \quad 0.72 \pm 0.31$$

They will now be discussed.

c. Discussion.

By considering the possible value of the ratio of the population parameters P(±1) and P(0), it may be assumed that $X^2 = 0$ is not likely, because this would correspond to the 0 substate being populated only. It must be recalled that all the calculations suppose that the neutron counter is at 0^o and that only S-wave neutrons are considered, thus limiting the magnetic substates populated to 0 and ±1. Actually, because of the finite size of the detector, the ±2 magnetic substates may be weakly populated. However, calculations show that the probability of populating these substates is small, a few percents generally. Assuming that the mean value of X^2, $X^2 = 0.2$, is more probable than the others and supposing that the ±2 magnetic substates are not populated, one can calculate the population parameters of the 0 and ±1 substates. Since $2\,P(1) + P(0) = 1$, one gets $P(0) = 71\%$ and $P(1) = 14.5\%$, if $X^2 = \frac{P(1)}{P(0)} = 0.2$. This result is reasonable compared to the equivalent data obtained from other experiments (see e.g. (Li 60)).

The value of δ which is the quadrupole to dipole mixing ratio is given by 0.72 ± 31 which corresponds to a relative error of 43%. As stated earlier (section 1.3.c), Morpurgo (Mo 63) has considered the Weisskopf estimates and showed that, in the case of self-mirrored nuclei, the

magnetic dipole transition with $\Delta T = 0$ should be reduced by a factor $\simeq 150$. It is also well known that compared to the Weisskopf estimates the electric quadrupole is generally enhanced. For the 892 kev transition, the Weisskopf estimate predicts a ratio $E2/M1 \simeq 3 \times 10^{-4}$. Despite its inaccuracy, the present result agrees with the fact stressed by Morpurgo that one should expect a strong M1 - E2 mixing even for rather low energy transitions.

The 2^+ spin assignment suggests that the 892 kev state is the first level of the $K = 2^+$ rotational band or the second level of the $K = 1^+$ band. The $K = 2^+$ rotational band is built on the transition of one odd-nucleon from the 3/2 + Nilsson level to the 1/2 + level. Using a value of $\frac{\hbar^2}{2J} = 0.23$ MeV, as proposed by Paul (op.cit.) would rule out the assumption that the 892 kev level is the second level of the $K = 1^+$ rotational band. This value of $\frac{\hbar^2}{2J}$ is similar to the value for Ne^{20} and Mg^{24}.

BIBLIOGRAPHY

Ar 65 S. E. Arnell and E. Wernbom-Selin. Arkiv för Fysik, Band 27, nr. 1, (1965).

Br 60 M. H. Brennan and A. M. Bernstein. Phys. Rev., 120, 927, (1960).

Da 52 C. M. Davisson and R. D. Evans. Rev. Mod. Phys., 24, 79, (1952).

Da 64 C. M. Davisson. Private communication to J. G. Pronko (cf. Pr 65).

De 57 S. Devons and L. J. B. Goldfarb. Handbuch der Fysik, 42 Julius Springer, Berlin (1957).

En 62 P. M. Endt and C. van der Leun. Nucl. Phys., 34, 1, (1962).

Es 64 M. A. Eswaran and C. Broude. Nucl. Phys., 42, 1311, (1964).

Fr 64 R. M. Freeman and G. S. Mani. Nucl. Phys., 51, 593, (1964).

Go 60 E. S. Goulding, R. W. Nicholson and J. B. Waugh. Nucl. Inst. and Meth., 8, 272, (1960).

Gov 60 H. E. Gove. Proc. Int. Conf. on Nucl. Structure, Univ. of Toronto Press, p. 438, (1960).

Ka 64 E. Karlsson, E. Matthias and K. Siegbahn. North Holland Publishing Company, Amsterdam, (1964).

Li 60 A. E. Litherland and G. J. McCallum. Can. J. Phys., 38, 927, (1960).

Li 61 A. E. Litherland and A. J. Ferguson. Can. J. Phys., 39, 788, (1961).

Li 64 A. E. Litherland. Scottish Univ. Summer School in Physics, (unpublished).

Mo 59 B. R. Mottelson and S. G. Nilsson. Mat. Fys. Skr. Dan. Vid. Selsk., 1, 8, (1959).

Mo 63 G. Morpurgo. Nuclear Spectroscopy. Proc. of the Int. School of Phys., "Enrico Fermi" XV Course, Academic Press, New York and London, p. 164, (1963).

Na 65 O. Nathan and S. G. Nilsson. In "Alpha, beta and gamma-ray spectroscopy" edited by K. Siegbahn, North Holland Publishing Company, p. 672, (1965).

Ne 60 G. C. Neilson, W. K. Dawson, F. A. Johnson, and J. T. Sample. Suffield Technical paper, No. 176, Defence Research Board of Canada, Department of Nat. Defence, (1960).

Ni 55 S. G. Nillson. K. Dansk. Vidensk. Selsk, Mat. Fys., 29, 16, (1955).

Pa 65 E. B. Paul. Private Communication.

Pe 61 F. Pellegrini. Nucl. Phys., 24, 372, (1961).

Pr 63 M. A. Preston. "Physics of the Nucleus." Addison-Wesley Publishing Company, Reading, Massachusetts, Palo Alto, London, (1963).

Pr 65 J. G. Pronko. Ph.D. Thesis, University of Alberta, (1965), (Unpublished).

Ra 57 G. Rakavy. Nucl. Phys., 4, 375, (1957).

Ro 53 M. E. Rose. Phys. Rev., 91, 610, (1953).

Sh 61 W. T. Sharp, et al. Report AECL No. 97, "Tables of coefficients for ang. distr. analysis." (Oct. 1961).

St 55 R. M. Steffen. Advances in Phys., 4, 293, (1955).

St 64 R. M. Steffen and Frauenfelder. Page 3 et seq. of "Ka 64." Also see alpha, beta and gamma-ray spectroscopy edited by K. Siegbahn. North-Holland Publishing Company, Amsterdam, (1965), p. 997, et seq.

Te 58 G. M. Temmer and N. P. Heydenburg. Phys. Rev., 111, 1303, (1958).

Va 64 D. A. Varshalovich. Izv. Ak. Nauk., S.S.S.R., Ser. Fiz., 28, 287, (1964).

Vo 58 W. F. Vogelsang and J. M. MacGruer. Phys. Rev., 109, 1663, (1958).

APPENDIX A-1

Angular correlation formulae assuming s-wave neutrons, for different possible spin assignments, in the case of the reaction $F^{19}(\alpha n\gamma)Na^{22}$.

δ is the mixing ratio.

x^2 the ratio of the population parameter of the magnetic sublevels ± 1 over the population parameter of the sublevel 0: $\left[x^2 = \frac{P(1)}{P(0)}\right]$.

It is reminded that the ground state is a 3+ and that the parity of the unknown states involved is positive.

Spin 1+ :

$$W(\theta) = 1 + \frac{0.144 + 1.170\,\delta - 0.250\,\delta^2}{1 + \delta^2} \; \frac{1-x^2}{1+2x^2} \; P_2(\cos\theta)$$

Spin 2+ :

$$W(\theta) = 1 - \frac{0.142 - 1.564\,\delta + 0.408\,\delta^2}{1 + \delta^2} \; \frac{1+x^2}{1+2x^2} \; P_2(\cos\theta)$$

$$+ \frac{1.219 - 1.626\,x^2}{(1+2x^2)\,(1+\delta^2)} \; P_4(\cos\theta)$$

Spin 3+ :

$$W(\theta) = 1 + \frac{(0.500-0.998\ \delta + 0.111\ \delta^2)+(0.748-1.496\ \delta-0.168\ \delta^2)x^2}{(1 + 2x^2)\ (1 + \delta^2)}$$

$$P_2(\cos\ \theta) - \frac{(0.533 + 0.180\ x^2)}{1 + 2x^2}\ \frac{\delta^2}{1 + \delta^2}\ P_4\ (\cos\ \theta)$$

Spin 4+ :

$$W(\theta) = 1 + \frac{-(0.537+0.608x^2)-(2.138+3.632x^2)\delta+(0.051+0.086x^2)\delta^2}{(1 + 2x^2)\ (1 + \delta^2)}$$

$$P_2\ (\cos\ \theta) + \frac{0.732(1+x^2)}{(1 + 2x^2)}\ \frac{\delta^2}{(1 + \delta^2)}\ P_4(\cos\ \theta)$$

The following five graphs represent the plots of some of the coefficients of the Legendre polynomials versus the mixing ratio for different population parameters ratios.

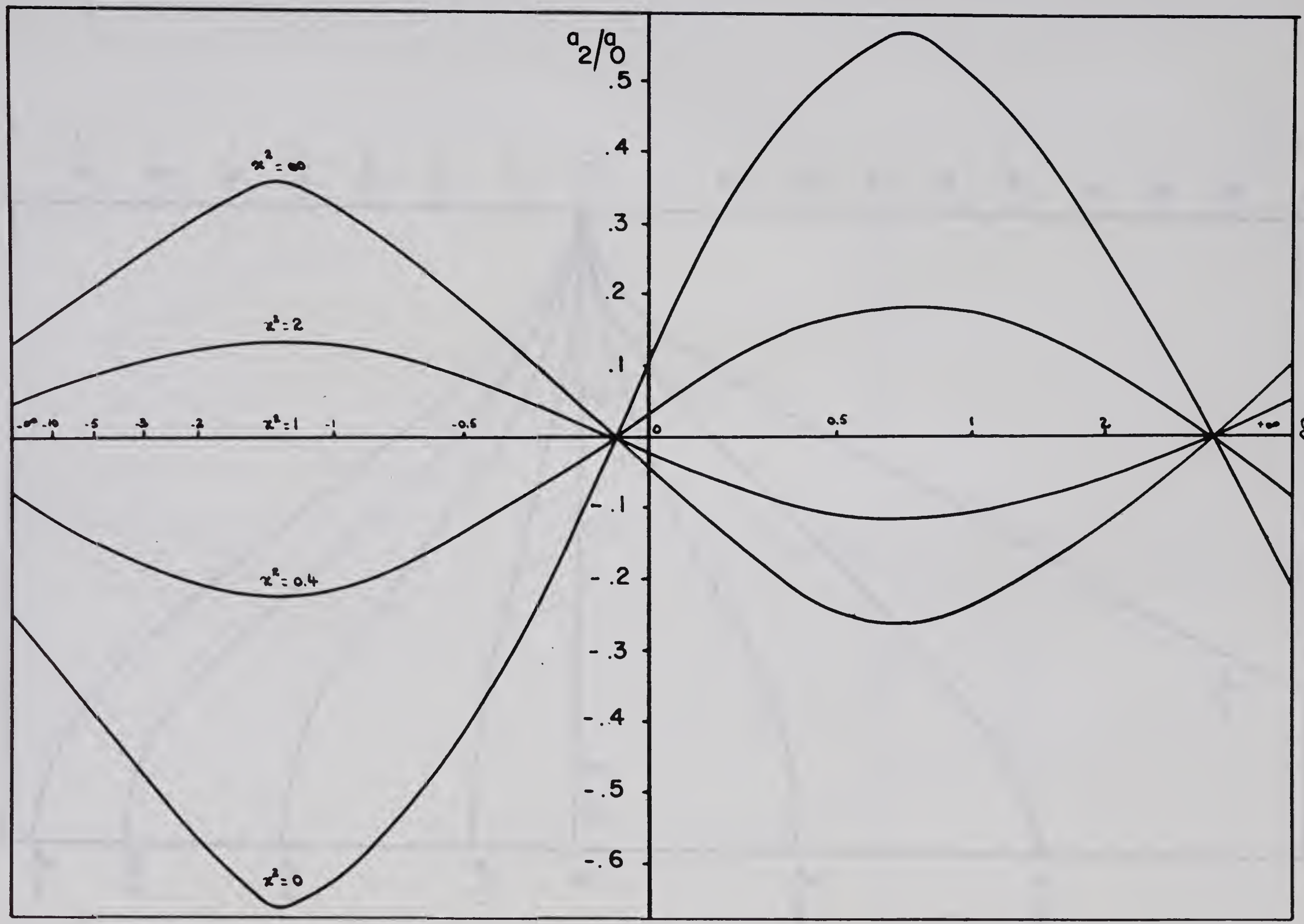

Fig. A.I.1: a_2/a_0 vs δ for a transition 1 to 3 (s-wave neutrons only)

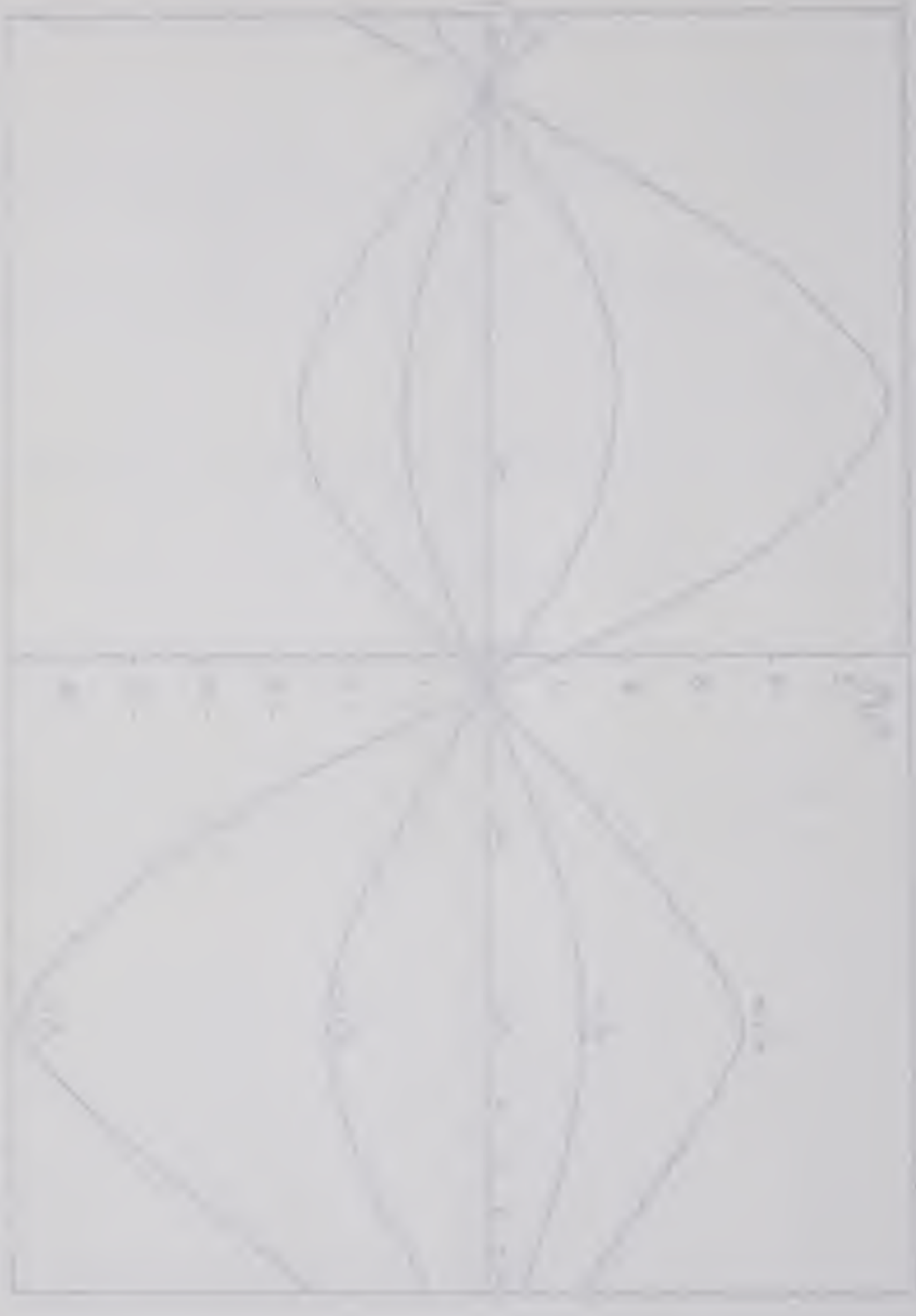

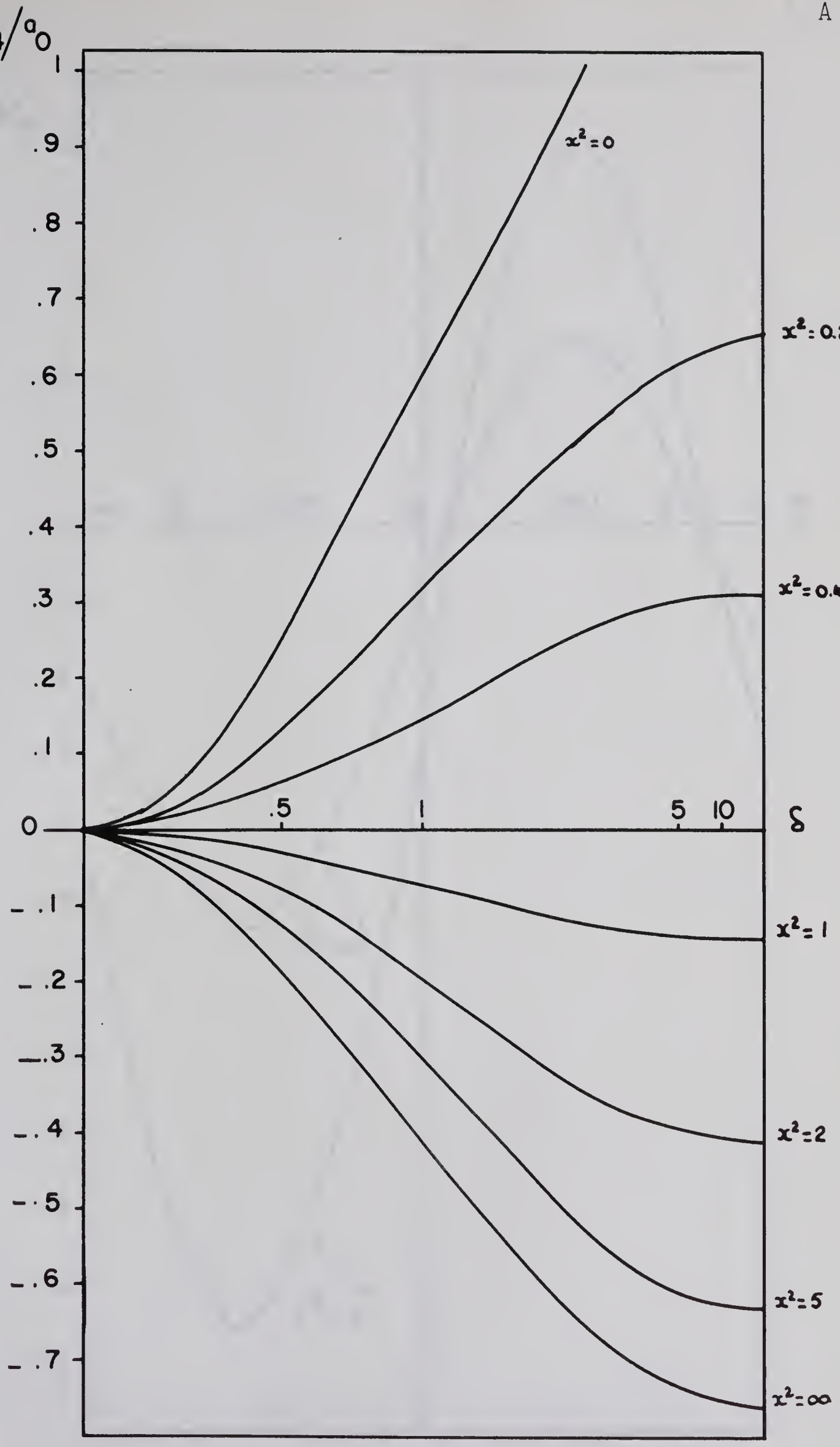

Fig: A.I.2 : a_4/a_0 vs δ for a transition 2 to 3
(s-wave neutrons only)

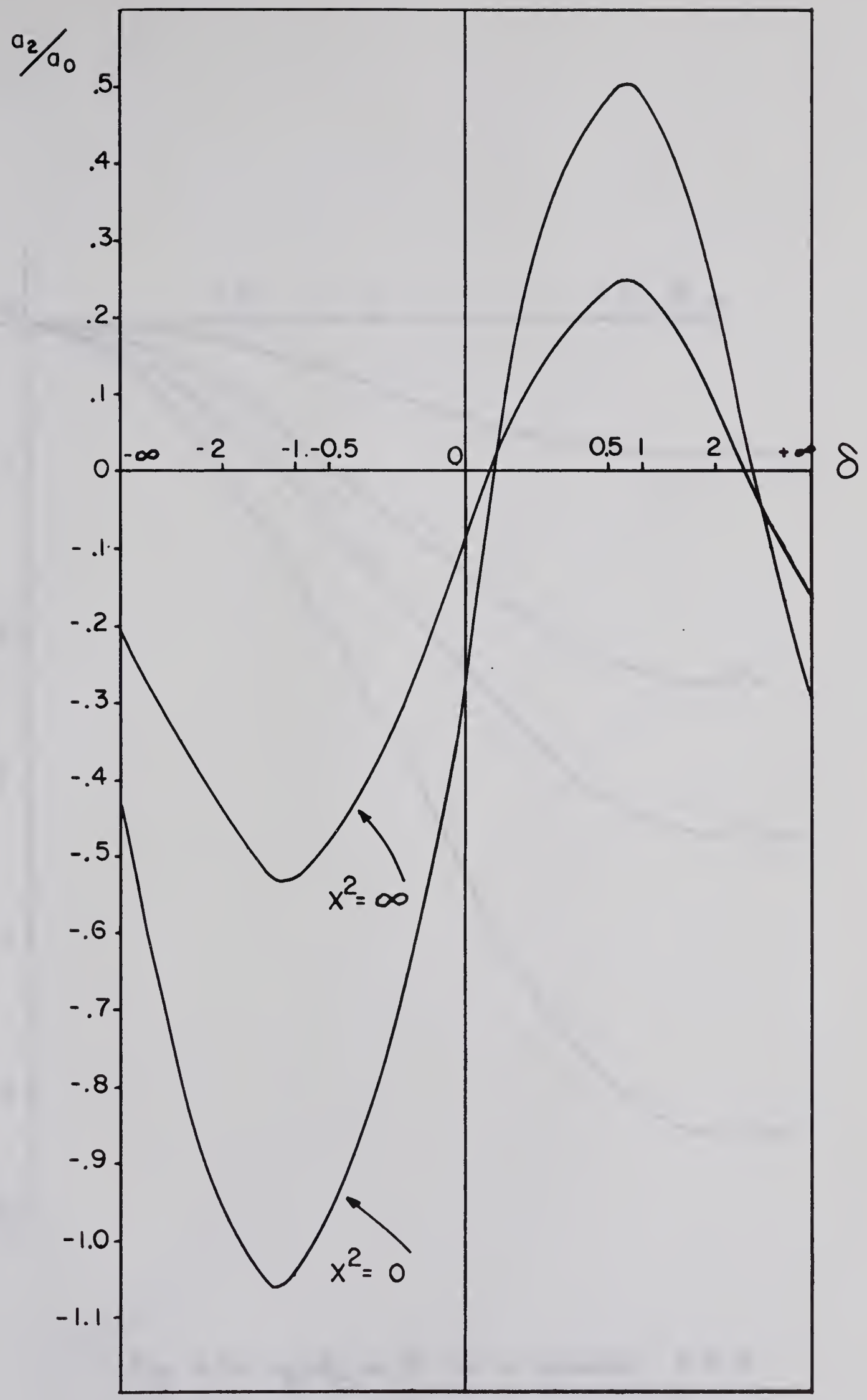

Fig. A.1.3 : a_2/a_0 vs δ for a transition 2 to 3
(s-wave neutrons only)

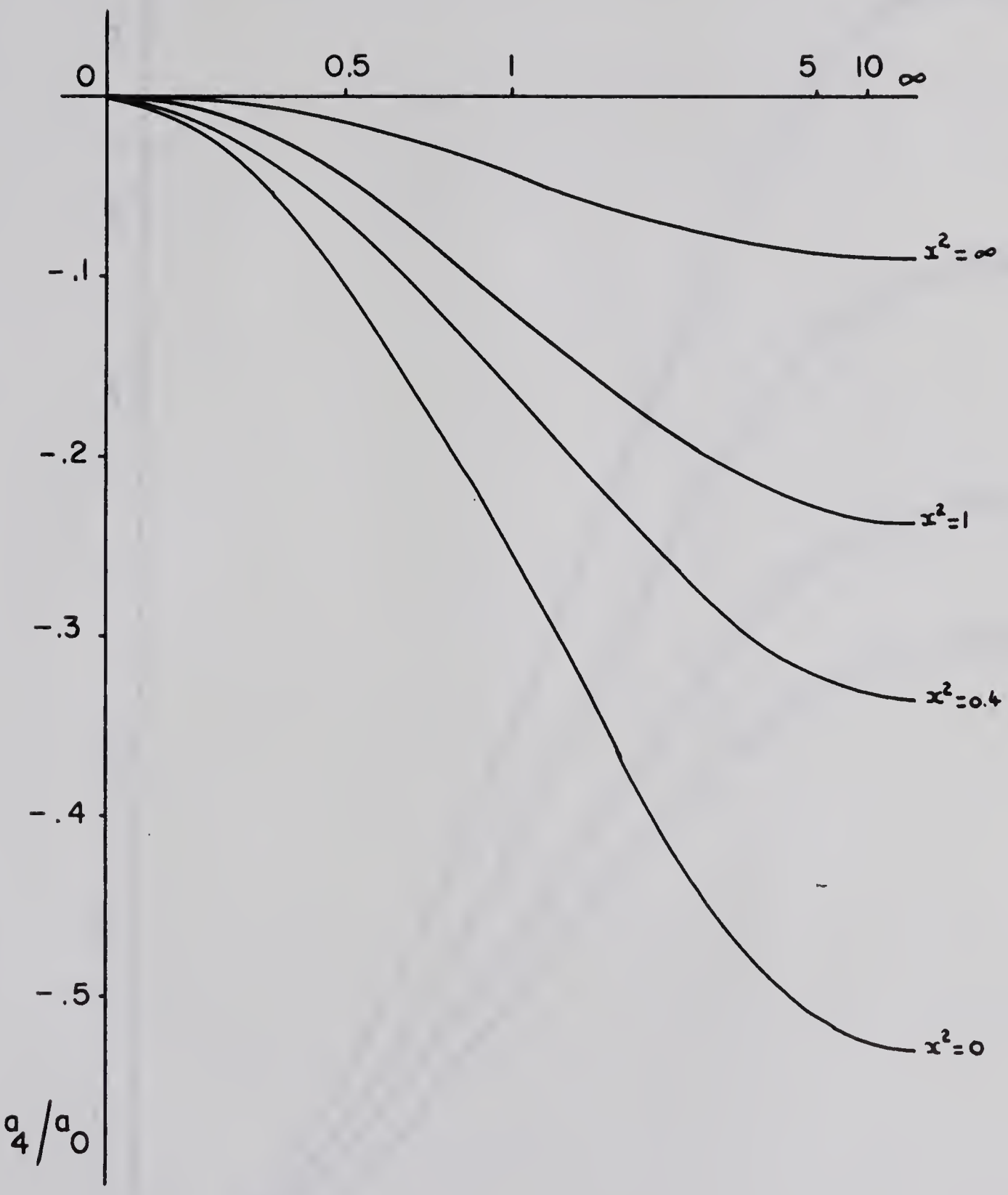

Fig. A.I.4 : a_4/a_0 vs. δ for a transition 3 to 3
(s wave neutrons only)

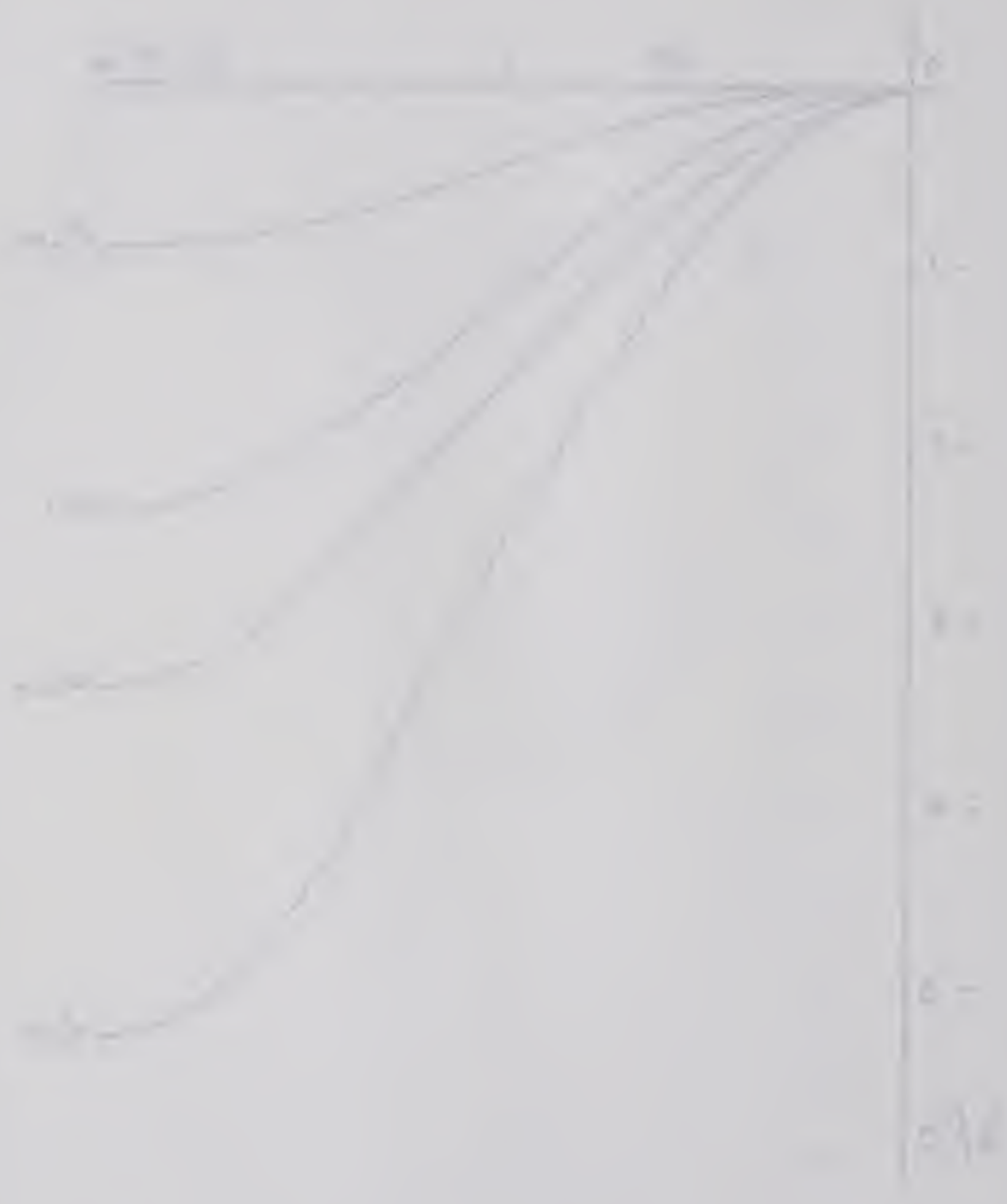

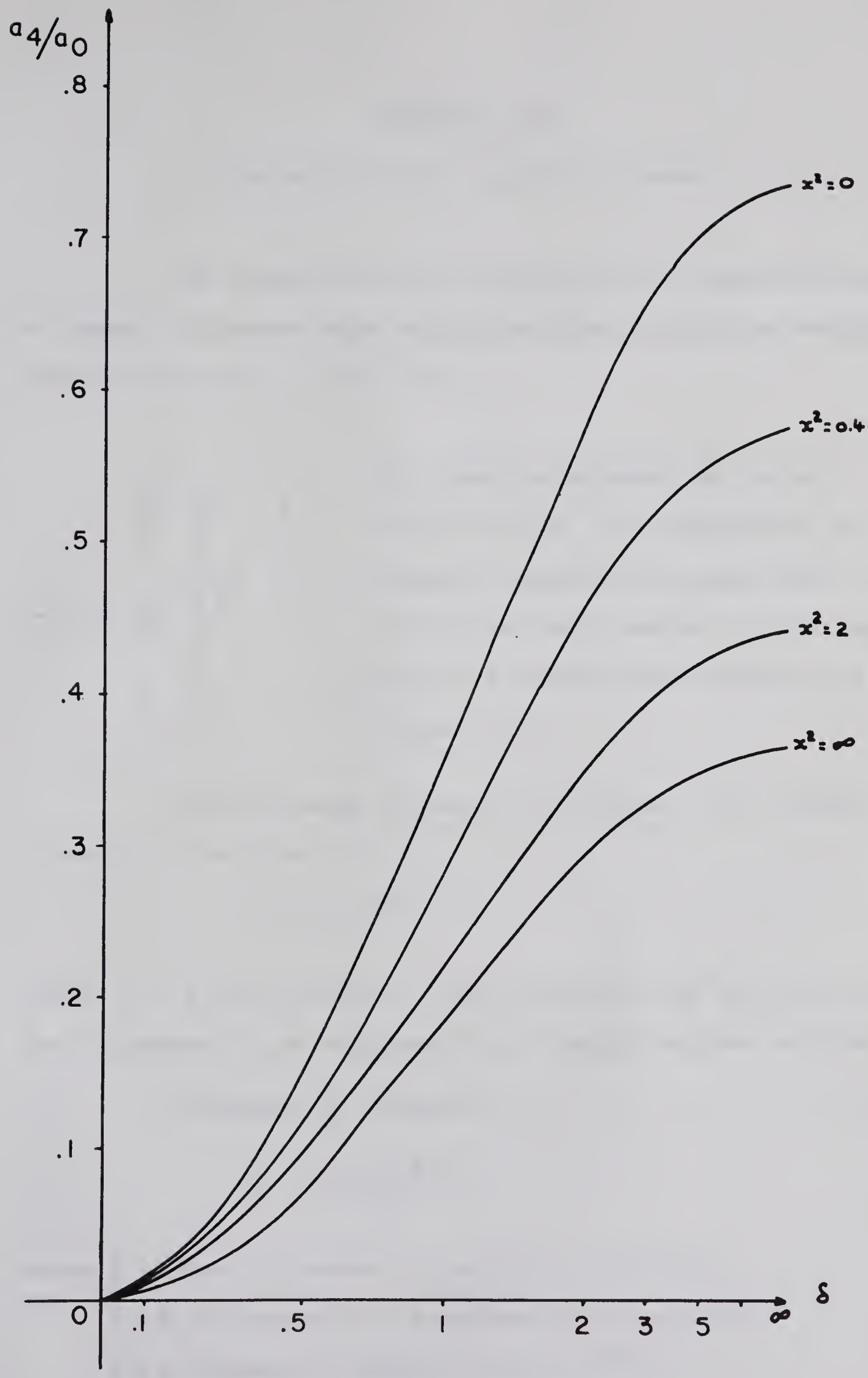

Fig. A.I.5: a_4/a_0 vs δ for a transition 4 to 3
(s-wave neutrons only)

APPENDIX A-2

Corrections for target thickness

The coefficients of correction for absorption due to target thickness were calculated for a platinum backing 0.002" thick (12.7×10^{-3} mm).

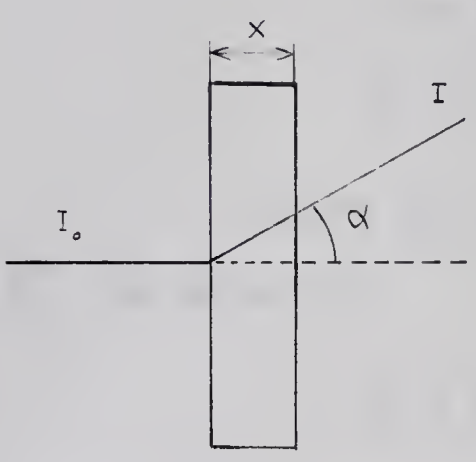

The beam is supposed to be well defined in O. The absorption of absolute intensity I_o has been calculated with respect to the angle α which is defined with respect to the normal in O.

After passage through a thickness X the reduced intensity I is given by:

$$I = I_o \, e^{-\mu x'}$$

where μ is the absorption coefficient in cm^2 per atom if the thickness X' is expressed in atoms per square centimeter.

Thickness in atoms/cm^2:

$$X' = \frac{X \times \rho \times N}{A}$$

where X is the thickness in cm (12.7×10^{-4} cm)

ρ is the density of platinum (21.37 g /cm^3)

N is Avogadro's Number (6.02×10^{23})

A is the atomic number of platinum (195.09).

These data yield a value of X' equal to 8.36×10^{19} atoms/cm^2.

The absorption coefficients, μ's, were determined by interpolation from the data published by Davisson (Da 52) and are given by:

$$\mu = 36.8 \text{ barns/atom for } E_\gamma = 587 \text{ kev}$$
$$\mu = 24.5 \text{ barns/atom for } E_\gamma = 892 \text{ kev.}$$

Since for each angle α the corresponding thickness X'_α is given by

$$X'_\alpha = \frac{X'}{\cos \alpha}$$

it was then possible to plot the ratio I/I_o versus α.

For a 3" x 3" detector whose crystal face is situated at a distance of 20.00 cm from the target axis, the half angle limited by the solid angle has a value of 10.8°.

Then for α varying from 0 to 90° by steps of 15°, integration was performed from $\alpha - 10.8^\circ$ to $\alpha + 10.8^\circ$ in order to determine the average target thickness correction. The results of these computations have been given in table 2.4 (section 2.4.c).